

LOSS OF NMP4 IMPROVES DIVERSE OSTEOPOROSIS THERAPIES IN A
PRE-CLINICAL MODEL: SKELETAL, CELLULAR, GENOMIC AND
TRANSCRIPTOMIC APPROACHES

Yu Shao

Submitted to the faculty of the University Graduate School
in partial fulfillment of the requirements
for the degree
Doctor of Philosophy
in the Department of Medical and Molecular Genetics,
Indiana University

August 2017

Accepted by the Graduate Faculty, Indiana University, in partial fulfillment of the requirements for the degree of Doctor of Philosophy.

Doctoral Committee

Joseph P. Bidwell, PhD. Co-Chair

Ronald C. Wek, PhD. Co-Chair

Amber L. Mosley, PhD.

Yunlong Liu, PhD.

Kenneth E. White, PhD.

June 22, 2017

Dedication

This thesis is dedicated to those most important in my life- first and foremost my wife Hongge Li. I would not have made such achievements without her understanding and tremendous support for me and my family. I would like to thank her for the sacrifice that she made when I could not stay with her and our baby, but focused on my work during the countless holidays and weekends. I also want to thank my 2-year old son Luke. The inmost part of my heart is filled with love, responsibility and courage each time I see him babble or toddle around. Finally, I would also like to dedicate this work to my parents. They live thousands of miles from me, but their love and support for my family can always reach me through phone and Internet, day and night.

Acknowledgements

The work presented in this dissertation would have been impossible without the help, advice and contribution by my mentor and colleagues. I would like to first convey my sincere gratitude to my mentor Dr. Joseph Bidwell. As an excellent mentor, he is so experienced in how to guide his students in each step of research. He taught me to pick the most biological-relevant questions in order to decide the direction of the next study, make careful plans for each experiment, reduce careless mistakes as much as possible, and analyze the data in a rigorous and unbiased way. Most importantly, he taught me how to think like a true scientist with necessary logic and creativity. The way he encouraged and spurred me kept me moving forward. I also want to give special thanks to Paul Childress, my ex-colleague and teacher. When I first stepped into Dr. Bidwell's lab, he offered important guidance to me. He helped me get familiarized with the lab quickly and taught me the necessary experimental techniques to thrive in this lab. I would also like to thank my current colleagues: Michele Klunk and Samuel Verga for their technical support during each of my experiment. I also want to thank all my committee members: Drs. Ronald Wek, Amber Mosley, Yunlong Liu, and Kenneth White for your invaluable advice for my research and career development. Finally, I want to thank Dr. Brittney Herbert. As the advisor of our graduate program, she takes serious responsibility for students. She is always ready to offer help, suggestion and guidance, especially when I had trouble being placed in a lab, registered for classes, or decided the details about my graduation.

LOSS OF NMP4 IMPROVES DIVERSE OSTEOPOROSIS THERAPIES IN A
PRE-CLINICAL MODEL: SKELETAL, CELLULAR, GENOMIC AND
TRANSCRIPTOMIC APPROACHES

We have previously demonstrated that disabling the transcription factor Nuclear Matrix Protein 4 (NMP4) improved parathyroid hormone (PTH)-induced trabecular bone gain in ovariectomized (OVX) and healthy mice. Here we evaluated whether loss of *Nmp4* enhanced bone restoration in OVX mice under concurrent PTH combination therapies and anti-catabolic mono-therapies. Wild type (WT) and *Nmp4*^{-/-} mice were OVX at 12wks of age followed by therapy regimens, administered from 16wks-24wks, and included individually or combined PTH, alendronate (ALN), zoledronate (ZOL), and raloxifene (RAL). Generally the PTH+RAL and PTH+ZOL therapies were more effective in restoring bone than the PTH mono-therapy. Loss of *Nmp4* further improved the restoration of femoral trabecular bone under these treatments. RAL and ZOL mono-therapies moderately increased bone volume but unexpectedly the *Nmp4*^{-/-} mice showed an enhanced RAL-induced increase in femoral trabecular bone. Immunohistochemical and flow cytometry analyses of the bone marrow and serum profiling for markers of bone formation and resorption indicated that the heightened osteoanabolism of the *Nmp4*^{-/-} mice under these diverse osteoporosis treatments was partially attributed to an expansion of the osteoprogenitor pool.

To address whether the enhanced bone formation observed in *Nmp4*^{-/-} mice produced structurally sound tissue, mechanical testing was conducted on the femurs of healthy mice treated with intermittent PTH, RAL mono-therapy, or PTH+RAL. *Nmp4*^{-/-} femurs showed modestly improved mechanical and material properties. At the cellular level, loss of *Nmp4* accelerated mineralization in differentiating mesenchymal stem/progenitor cells (MSPCs). Transcriptomic and biochemical analyses indicated that loss of *Nmp4* elevated ribosome biogenesis and expanded the capacity of the endoplasmic reticulum for processing protein.

Preliminary data showed that disabling *Nmp4* increased both aerobic glycolysis and oxidative phosphorylation in osteoprogenitors, which is an emerging hallmark of anabolic osteogenic cells. Transcriptomic analysis also suggested NMP4 targeted pathways driving bone formation. These included but not limited to BMP, IGF1, TGF β and Wnt signaling pathways. Finally, transcriptomic profiling revealed that *Nmp4*^{-/-} MSCs showed a significant perturbation in numerous immunomodulatory pathways, particularly in the interleukin system. The heightened osteoanabolism of the *Nmp4*^{-/-} skeleton enhances the effectiveness of diverse osteoporosis treatments, providing a promising target pathway for identifying barriers to pharmacologically-induced bone formation.

Joseph P. Bidwell, PhD., Co-Chair

Ronald C. Wek, PhD., Co-Chair

Table of Contents

ABBREVIATIONS	x
CHAPTER 1	1
BACKGROUND INTRODUCTION	1
<i>Basic bone biology</i>	1
<i>MSPC, an adult stem cell in controversy</i>	2
<i>Osteoporosis epidemic, cause and treatment</i>	7
<i>Combination therapy, a potential solution for osteoporosis?</i>	11
<i>NMP4, the structure, function and phenotype</i>	14
<i>The UPR pathway, guardian against ER stress</i>	17
<i>NMP4 regulates both ribosomal biogenesis and UPR pathways</i>	21
<i>Main research goals and significance</i>	21
CHAPTER 2	23
Improving Combination Osteoporosis Therapy In a Preclinical Model of Heightened Osteoanabolism	23
INTRODUCTION	23
MATERIALS AND METHODS	23
<i>Mice</i>	23
<i>Bilateral ovariectomy surgery</i>	24
<i>Therapies</i>	24
<i>Dual energy X-ray absorptiometry (DXA)</i>	27
<i>Micro-computed tomography (μCT)</i>	27
<i>Serum biochemistry</i>	27
<i>Immunohistochemistry</i>	28
<i>Flow cytometry</i>	29
<i>Statistical analysis</i>	30
RESULTS	30
<i>Effect of Combination Treatments Using Anabolic Agents On Bone</i>	30
<i>Effects of Anti-Catabolic Treatments On Bone</i>	46

<i>The Effects of Combination Treatments using Anabolic Agents on Osteoprogenitor Cells</i>	46
<i>Effects of Anti-Catabolic Treatments on Osteoprogenitor Cells</i>	53
<i>Effects of Treatments on Bone Turnover Markers</i>	53
DISCUSSION	57
CONTRIBUTIONS	62
CHAPTER 3	63
MAPPING THE Nmp4 ANTI-ANABOLIC BONE TRANSCRIPTOME	63
INTRODUCTION	63
MATERIALS AND METHODS	63
<i>Cell culture</i>	63
<i>Alizarin red staining for mineralization</i>	64
<i>RNA-Seq</i>	64
<i>Bioinformatics profiling</i>	65
<i>Seahorse Assay for mitochondria stress test</i>	66
<i>Mice</i>	67
<i>Therapies</i>	67
<i>Bone Storage</i>	68
<i>Microcomputed tomography (μCT)</i>	69
<i>Three-point bending</i>	69
<i>Influenza infection</i>	70
<i>Statistical analysis (for bone mechanical study and Seahorse Assay)</i>	70
RESULTS	71
<i>Differentiating Nmp4^{-/-} MSPCs mineralize earlier than WT MSPCs</i>	71
<i>Loss of Nmp4 significantly alters extracellular matrix/mineralization transcriptome</i>	73
<i>Loss of Nmp4 improved trabecular bone gain in healthy mice treated with PTH and PTH+RAL therapies</i>	76
<i>Loss of Nmp4 improves bone structural and estimated material properties</i>	80
<i>Loss of Nmp4 biased MSPCs towards osteogenesis</i>	87

<i>Loss of Nmp4 promotes pathways that directly regulate osteoblast function and bone formation</i>	90
<i>Loss of Nmp4 affects unfolded protein response (UPR) and ribosomal biogenesis</i>	95
<i>Loss of Nmp4 alters glycolysis and enhances mitochondrial respiration capacity</i>	100
<i>Loss of Nmp4 impacts immunomodulation</i>	103
DISCUSSION	107
CONTRIBUTIONS	112
CHAPTER 4	113
SUMMARY	113
REFERENCES	118
CURRICULUM VITAE	

ABBREVIATIONS

aBMD	Areal bone mineral density
ALN	Alendronate
ANOVA	Analysis of variance
AP	Anterior-posterior
AT2	Aleovar type 2
ATF4	Activating transcription factor 4
ATF6	Activating transcription factor 6
ATP	Adenosine triphosphate
BCL2L11	BCL2 like 11
BGP	Glycerol 2-phosphate disodium salt hydrate
BM	Bone marrow
BMC	Bone mineral content
BMD	Bone mineral density
BMMNCs	Bone marrow mononuclear cells
BMP	Bone morphogenetic proteins
BMSCs	Bone marrow stromal cells
BMU	Basic multicellular unit
BRU	Bone remodeling unit
BV/TV	Bone volume/Total volume
cAMP	Cyclic adenosine monophosphate
CFU-F	Colony-forming unit fibroblast
ChIP-Seq	chromatin immunoprecipitation-Sequencing
CHOP	transcription factor C/EBP homologous protein
Ciz	Cas-interacting zinc finger protein
Col1 α 1	Type I collagen α 1 polypeptide chain
cpm	Counts per million
CSA	Cortical surface area
CTX	C-terminal telopeptide
CXCL12	C-X-C motif chemokine ligand 12

DMSO	Dimethyl sulfoxide
DNA	Deoxyribonucleic acid
DR5	Death receptor 5
DXA	Dual energy X-ray absorptiometry
ECM	Extracellular matrix
eIF2	Eukaryotic translation initiation factor 2
eIF2 α	Eukaryotic translation initiation factor 2 α
ER	Endoplasmic reticulum
ERAD	ER-associated degradation
ETC	Electron transfer complex
EWSR1	EWS RNA binding protein 1
FC	Fold change
FCCP	Carbonyl cyanide-p-trifluoromethoxyphenylhydrazone
G x T	Genotype x Treatment
GADD34	Growth arrest and DNA damage-inducible 34
GDP	Guanosine diphosphate
GI	Gastrointestinal
GRP94	Glucose-regulated protein 94
HBSS	Hank's balanced salt solution
hPTH	Human PTH
HSCs	Hematopoietic stem cells
IDO	Indoleamine 2,3-dioxygenase
IFN γ	Interferon γ
IGF1	Insulin-like growth factor 1
IGFBPs	IGF binding proteins
IL	Interleukin
ip	Intraperitoneal
IQR	Interquartile range
IRE1	Inositol-requiring enzyme 1
KEGG	Kyoto Encyclopedia of Genes and Genomes
LepR	Leptin receptor

Imin	Minimum moment of inertia
logFC	log fold change
Ip	Polar moment of inertia
ML	Medial-lateral
Mmp	Matrix metalloproteinase
mRNA	Messenger ribonucleic acid
MSCs	Mesenchymal stem cells
MSPCs	Mesenchymal stem/progenitor cells
NaF	Sodium fluoride
NCPs	non-collagenous proteins
NMP4	Nuclear Matrix Protein 4
NO	Nitric oxide
OCN	Osteocalcin
OCR	Oxygen consumption rate
OPG	Osteoprotegerin
ORFs	Open reading frames
Osterix	OSX
OVX	Ovariectomy
p130CAS	Crk-associated substrate
PERK	PRKR-like ER kinase
pfu	Plaque-forming unit
PKA	Protein kinase A
PMNs	Apoptotic neutrophils
PP1	Protein phosphatase 1
PTH	Parathyroid hormone
PTHR1	PTH receptor 1
QCT	Quantitative computed tomography
RAL	Raloxifene
RANKL	Receptor activator of nuclear factor kappa-B ligand
RIDD	Ire1-dependent decay
RIN	RNA integrity number

RIP	Intramembrane proteolysis
RNA-Seq	RNA sequencing
RUNX2	Runt-related transcription factor 2
sc	Subcutaneous
SCF	Stem cell factor
SERM	Selective estrogen modulator
SH3	SRC homology 3
Tb.N	Trabecular number
Tb.Sp	Trabecular spacing
Tb.Th	Trabecular thickness
TCA	Tricarboxylic acid
TF	Transcription factor
TGF β	Transforming growth factor beta
TLDA	TaqMan Low Density Array
TLRs	Toll-like receptors
TRAP	Tartrate-resistant acid phosphatase
TRAP+ S/BS	TRAP+ surface/bone surface
TRB3	telomere repeat binding factor 3
UPR	Unfolded protein response
VCAM-1	Vascular cell adhesion molecule-1
WB	Whole body
WT	Wild type
XBP1	x-box binding protein 1
Zfp384	or
Znf384	Zinc finger protein 384
ZOL	Zoledronate
μ CT	Micro-computed tomography

CHAPTER 1

BACKGROUND INTRODUCTION

Basic bone biology

Human skeleton is comprised of two types of bones: 80% cortical bone and 20% trabecular bone. Cortical bone forms the dense protective cortex outside the bone cavity. It is mechanically stronger and plays a major role in weight bearing due to its high resistance to torsion, bending and other external forces (Figure 1-1A). Trabecular bone is highly porous and interconnected yet also fully mature bone. It is less dense and mostly found in the ends of the long bone or interior of vertebrae (Figure 1-1B).

There are several types of bone cells that contribute to the bone homeostasis. Osteoblast is a direct descendent from the mesenchymal lineage. It adopts the cubic morphology and is responsible for new bone formation via secreting collagen matrix and depositing inorganic bone mineral. After the high peak of bone formation, osteoblast gradually becomes flattened, inactive and turns into the bone lining cells. Upon fully buried inside the bone matrix, osteoblast is transformed into osteocyte, which possesses long processes to allow it in contact with other osteocytes or bone lining cells. On the other hand, osteoclast is multi-nuclei cell descending from the myeloid lineage. The cell attaches to the bone and degrades the bone matrix via secreting acid through the proton pumps.

Bone remodeling (or bone turnover) is a necessary physiological process to maintain healthy homeostasis. The first resorption phase of bone remodeling involves landing of osteoclasts onto the bone in a bone-remodeling unit (BRU) (Figure 1-1C). The osteoclasts then start degrading bone matrix under the cells, creating a pit. The next phase is reversal, which has not been fully understood yet but may involve mononuclear cells clearing the matrix remnants (Raggatt and Partridge, 2010). The osteoblasts then take over, secreting non-mineralized matrix “osteoid” into the pit. The osteoid mineralizes eventually and the new bone

is formed (Figure 1-1C). Bone remodeling requires delicate balancing and loss of balance usually leads to diseases such as osteoporosis.

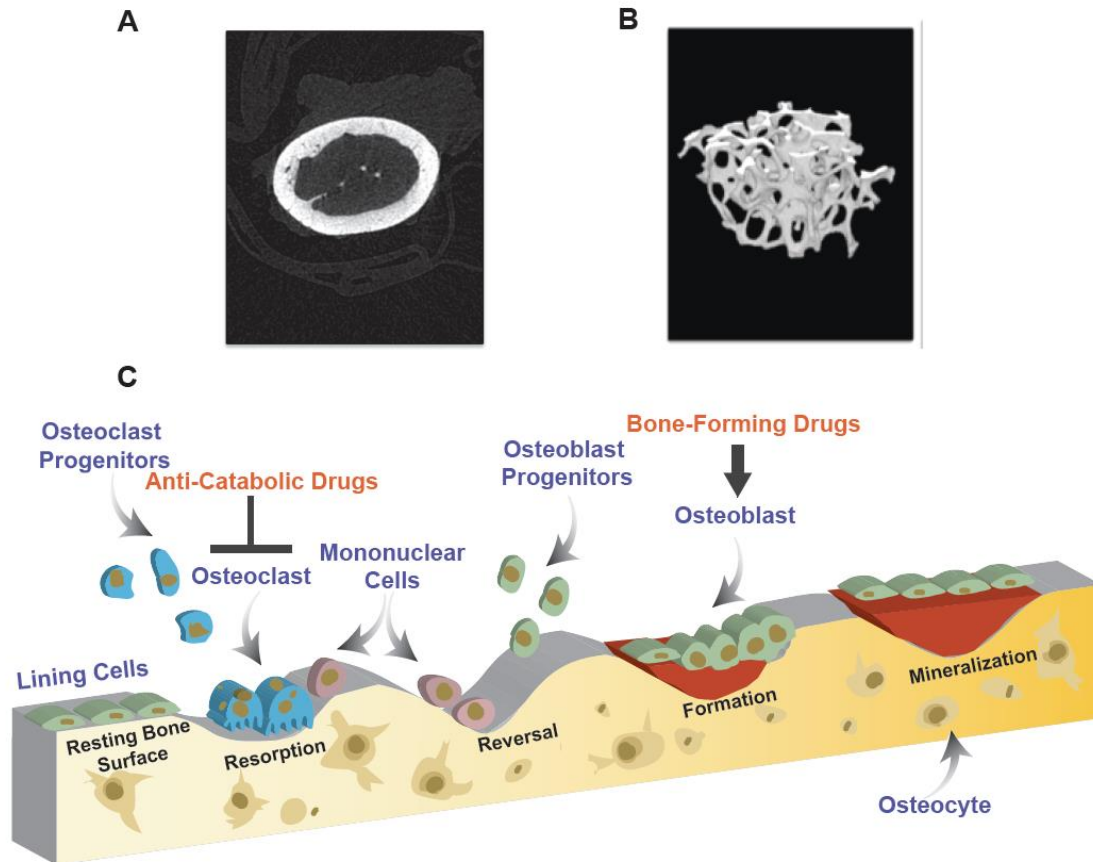


Figure 1-1: Basic bone biology [A] Cortical bone structure [B] Trabecular bone structure [C] bone remodeling can be divided into four phases-resorption, reversal, formation and mineralization (see text for details). Some of the key cell players include osteoclast and its progenitor, mononuclear cell, osteoblast and its progenitor, bone lining cell and osteocyte. To treat osteoporosis, osteoclast is targeted by anti-catabolic drugs whereas osteoblast activity is targeted by bone-forming drugs. Modified based on illustration published by Kapinas and Delany, (Kapinas and Delany, 2011).

MSPC, an adult stem cell in controversy

Mesenchymal stem/progenitor cells (MSPCs) are more commonly known as mesenchymal stem cells (MSCs), which by definition can undergo self-

renewal and give rise to three mature cell types: osteoblast, adipocyte and chondrocyte (Figure 1-2). MSC is a historical term and is often used inappropriately. The genuine MSCs are rare in our body and in cell culture more committed progenitor cells are abundant; “MSPCs” is therefore the more appropriate name (Frenette et al., 2013). Stringent functional assays for MSPC identification involve serial transplantation of these cells into allogenic recipients; if each time after the transplantation, heterotopic bone can be found in the recipient then it is concluded that the cells transplanted can self-renew and differentiate into osteogenic lineage (Mendez-Ferrer et al., 2010; Sacchetti et al., 2007). *In vitro* identification of MSPCs relies heavily on cell surface markers and colony-forming unit fibroblast (CFU-F) assay.

Unfortunately there is no single combination of markers for MSPCs that can be uniformly accepted by all the researchers. MSPCs harvested from different species express different markers. The International Society of Cellular Therapy proposed a minimal set of human surface markers that include CD105, CD73 and CD90 and the cells must also be negative for CD45, CD34, CD14, CD11b, CD79a, CD19 and HLA-DR. Additionally, the cells must also be able to adhere to the plastic surface and differentiate into all the three cell types (Dominici et al., 2006). However, these criteria are out-of-date, because many more surface markers have been identified since then, including markers CD146, CD271 and STRO-1 (Sacchetti et al., 2007; Shi and Gronthos, 2003; Tormin et al., 2011).

At least one group of researchers has found MSPCs in non-adherent population (Zhang et al., 2009). Mouse MSPCs can be defined via different sets of markers as well such as Nestin⁺CD45⁻CD31⁻, CD51⁺CD105⁺CD90⁻CD45⁻Tie2⁻ and PDGFR α ⁺Sca1⁺CD45⁻Ter119⁻ (Chan et al., 2009; Mendez-Ferrer et al., 2010; Morikawa et al., 2009). Some other markers include Osterix (OSX) and Leptin Receptor (LepR) (Matsuzaki et al., 2014; Mizoguchi et al., 2014). None of these markers are unique to MSPCs and therefore multiple markers have to be used for identification and sorting purposes. Moreover, several markers mentioned above are artificial and only appear in cell culturing environment such as CD44

and CD146 (Blocki et al., 2013; Qian et al., 2012), whereas SP7 (Osterix or OSX) appears to be an *in vivo* marker for MSCs (Mizoguchi et al., 2014).

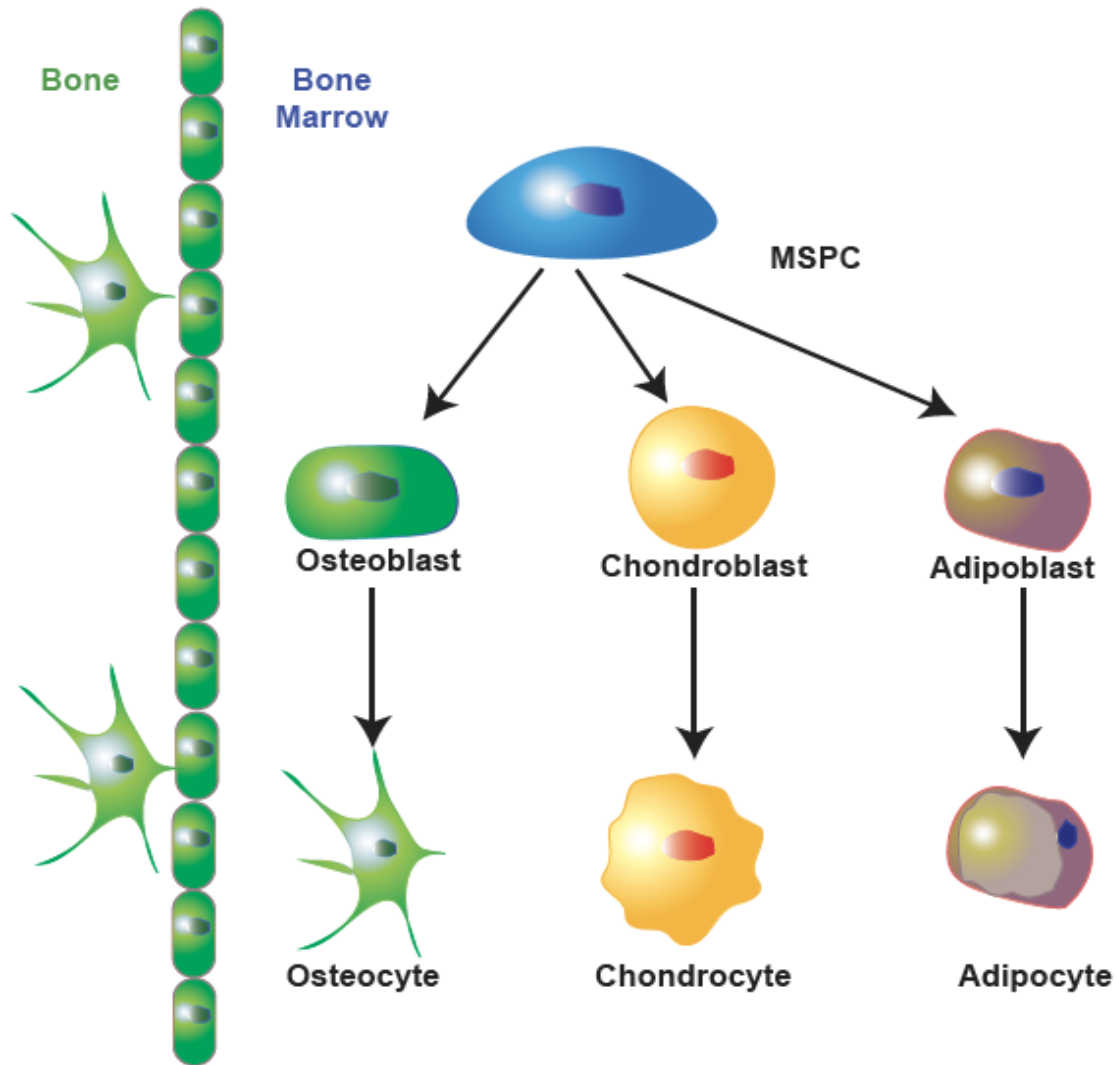


Figure 1-2: BM MSC differentiation. MSCs can become committed to osteogenic (osteoblast-osteocyte), chondrogenic (chondroblast-chondrocyte) and adipogenic (adipoblast-adipocyte) lineages. Modified based on illustration published by Frenette *et al.*, (Frenette et al., 2013).

A major problem with using surface markers to define MSCs is that MSCs are highly heterogeneous. In the bone marrow, they occupy three different niches: endosteal, perivascular and stromal and it is still unclear whether

these cells can migrate between different niches (da Silva Meirelles et al., 2008; Mendez-Ferrer et al., 2010; Rasini et al., 2013). Upon isolation, MSCs also exhibit distinct morphologies: some are extremely small and proliferative; some are medium-sized, spindle-shaped and modestly proliferative while others are larger, flattened and grow at a much slower pace (Digirolamo et al., 1999; Muraglia et al., 2000). Some markers such as Nestin and LepR are not universally expressed in all MSCs. Nestin⁺ MSCs play a role in supporting hematopoiesis and neurogenesis (Mendez-Ferrer et al., 2010; Wislet-Gendebien et al., 2004); LepR⁺ MSCs are important contributor of osteogenesis and adipogenesis in the BM (Zhou et al., 2014). MSCs can be isolated from all kinds of mesenchymal tissues besides BM such as fat, muscle, lung, skin, umbilical cord blood and fetal tissues (Mosna et al., 2010). Although these cells harvested from different sources can differentiate into all the three cell types but they express different surface markers. For instance, CD49d is expressed in MSCs harvested from human adipose tissues but not those from BM; whilst CD106 found in human BM MSCs is not expressed in cells from the adipose tissue (De Ugarte et al., 2003). Different techniques used in MSC isolation (e.g. BM flushing vs. compact bone grinding) may also result in different subpopulations of MSCs being isolated (Bara et al., 2014).

The current MSC culturing techniques remain to be further developed and optimized. One study conducted by Sacchetti *et al.*, showed 50% isolated CD146⁺ MSCs from human gave rise to compact bone but not bone marrow, suggesting that isolated MSCs from marrow tend to become more committed towards the osteogenic lineage (Sacchetti et al., 2007). Furthermore, phenotypic shift is often observed during long-term MSCs culturing and expansion. On one hand, multipotency was found to be gradually lost and more cells became committed to the osteogenic lineage (Banfi et al., 2002; Bruder et al., 1997; Wagner et al., 2008). On the other hand, there are reports showing that MSCs expanded under normoxia condition are under stress from the high oxygen level; only cells that lose P53 and acquire immortality are more proliferative and more likely to form colonies. It is therefore recommended that MSCs isolated from

BM be expanded under hypoxic condition to avoid spontaneous transformation (Boregowda et al., 2012). Generally speaking, MSCs past p10 tend to become more granular with shortened telomeres and eventually lose the multipotency (Bonab et al., 2006). Some researchers have proposed to culture MSCs in the three-dimensional environment, such as mesosphere. Just like neural stem cell and embryonic stem cell, MSCs are also able to form “sphere” structures when grown under non-adherent condition, and both *in vivo* and *in vitro* evidences showed mesospheres could maintain the stemness (i.e. self-renewal and multipotency) of MSCs better and longer than the traditional monolayer culturing (Mendez-Ferrer et al., 2010).

There is intimate crosstalk among MSCs, osteoblasts and hematopoietic stem cells (HSCs) inside the BM. MSCs were found to be in physical contact with HSCs in endosteal and perivascular niches and MSCs play supportive role in HSC maintenance (Mendez-Ferrer et al., 2010). For instance, C-X-C motif chemokine ligand 12 (CXCL12) secreted from osteoblasts and MSCs in endosteal niche and MSCs in perivascular niche is a crucial factor in maintaining the HSC pool; selectively disabling this gene in these cell types disrupted the self-renewal of HSCs and soon depleted the HSC pool (Calvi et al., 2003; Greenbaum et al., 2013). Similarly, Notch signaling was also found to support *ex vivo* HSC persistence and expansion via CD146⁺ but not CD146⁻ MSCs (Corselli et al., 2013). Other factors secreted by MSCs that help maintain the HSC pool include 1) stem cell factor (SCF) that regulates HSC quiescence and adhesion (Kent et al., 2008), 2) Osteopontin, Angiopoietin-1 and Thrombopoietin-1 that also contribute to HSC quiescence (Arai et al., 2004; Nilsson et al., 2005; Qian et al., 2007; Yoshihara et al., 2007), and 3) vascular cell adhesion molecule-1 (VCAM-1) that regulate HSC adhesion as well (Papayannopoulou et al., 1995; Simmons et al., 1992). Conversely, HSCs may promote osteogenesis of MSCs via inducers like bone morphogenetic proteins (BMPs) such as BMP2 and BMP6 (Jung et al., 2008).

MSCs also impact the immune system in our bodies. In general, a good number of studies showed that MSCs inhibited proliferation, differentiation and

activation of vast different types of immune cells such as B cells, T cells, dendritic cells, neutrophils and natural killer cells (Abomaray et al., 2015; Cassatella et al., 2011; Gerdoni et al., 2007; Jiang et al., 2016; Selmani et al., 2008). *In vitro* proliferation studies indicated human MSCs could effectively inhibit the proliferation of CD2⁺, CD4⁺ and CD8⁺ T lymphocytes through certain soluble factors and direct contact is not necessary (Di Nicola et al., 2002; Duffy et al., 2011). However, some researchers suggested physical contact with immune cells could enhance the immunomodulation activity of MSCs (English et al., 2010). One clinical study showed that the symptoms of patients suffering from chronic graft-versus-host disease were greatly alleviated after receiving MSC infusion (Le Blanc et al., 2008). The molecular mechanism of MSC's immunosuppressive activity remains to be elucidated but seemingly upon activation by interferon γ (IFN γ), MSCs can release factors such as nitric oxide (NO) and indoleamine 2,3-dioxygenase (IDO) that inhibit immune cell proliferation and exert anti-inflammatory effect (François et al., 2012; Sato et al., 2007; Schena et al., 2010).

MSCs and mature osteoblasts are professional secretory cells that can release different factors into the BM stroma and bone matrix; these factors contribute to bone homeostasis, angiogenesis, hematopoiesis and neurogenesis (Chuang et al., 2012; Estrada et al., 2009; Giunti et al., 2012; Greenbaum et al., 2013; Kim et al., 2013).

Finally, MSCs may also have clinical value in regenerative medicine and tissue engineering (Caplan, 2007; Tae et al., 2006). The soluble factors secreted by MSCs exert beneficial paracrine effect on multiple tissues and may be used to treat various diseases such as intestinal ischemia, diabetic retinopathy and lung injury caused by cigarette smoking (Jensen et al., 2016; Rajashekhar et al., 2014; Schweitzer et al., 2011).

Osteoporosis epidemic, cause and treatment

Osteoporosis is a chronic disease characterized by gradual and continuous bone loss, decreased bone strength, increased risk of bone fracture,

chronic pain, and decreased mobility (Glaser and Kaplan, 1997). Osteoporosis causes more than 9 million of fracture incidences worldwide every year and currently in the US around 14 million people are affected by osteoporosis, and this number is still increasing (Borrelli, 2012). Bone fractures caused by osteoporosis can occur anywhere across the skeleton, but most likely in the hip, wrist, and spine. At the tissue level, osteoporosis is mainly caused by loss of balance in bone formation and remodeling. In other words, bone resorption surpasses bone formation in each basic multicellular unit (BMU) in osteoporosis patients.

Several risk factors can contribute to this pathological characteristic of osteoporosis, including age, gender, race, smoking, Vitamin D deficiency, inactive life style, and medications (e.g. glucocorticoid) (Stevenson et al., 1989). Typically, post-menopausal women are a major population susceptible to this disease due to the sharp decline of estrogen levels. Estrogen can induce osteogenesis, inhibit adipogenesis, and promote osteoclast apoptosis (Dang et al., 2002; Hughes et al., 1996). Estrogen deficiency is the most common risk factor of osteoporosis and estrogen itself is used to treat the disease, although its use is heavily limited due to its severe side effects, which will be discussed later.

Current treatments of osteoporosis can be classified into three categories: nutritional supplement, anti-catabolic drugs, and anabolic drugs. Nutritional supplement mainly refers to repeated uptake of calcium and Vitamin D beyond dietary uptake; however, calcium deficiency is not the only cause of postmenopausal osteoporosis and this treatment is only supplemental to other therapies (Tucker, 2009). Anti-catabolic drugs inhibit bone resorption and are used most often in osteoporotic treatment. Estrogen replacement therapy used to be widely used to treat osteoporosis until its side effects, such as increased risks for breast cancer, endometrial cancer, and stroke (Bath and Gray, 2005; Grady et al., 1995; Shah and Wong, 2006). Today the use of estrogen is largely restricted to acute, short-term use, which is not consistent with treating chronic osteoporosis.

Selective estrogen receptor modulators (SERM) were developed to replace the estrogen therapy. SERMs are capable of activating the estrogen receptors in certain tissues while inhibiting estrogen receptors in other tissues. Raloxifene (RAL) is a type of SERM that is used to treat osteoporosis and reduce the risk of invasive breast cancer (Cauley et al., 2001; Ettinger et al., 1999; Martino et al., 2004). Several clinical studies have shown that raloxifene can significantly reduce fracture frequency although the underlying mechanism remains to be determined (Delmas et al., 2002; Ettinger et al., 1999). Bisphosphonates are the largest group of anti-catabolic drugs, which can be absorbed by osteoclasts in the bone matrix during the resorption process and induce osteoclast apoptosis either by creating nonhydrolyzable ATP analogs or by disrupting protein prenylation. Bone resorption activity can be drastically suppressed by bisphosphonate and previous studies have shown bisphosphonate, such as alendronate (ALN) and zoledronate (ZOL), can maintain long-term increase of bone mineral density (BMD) (Adachi et al., 2001; Bolland et al., 2008; Michaelson et al., 2007). Several side effects are associated with the long-term use of bisphosphonate, such as gastrointestinal (GI) tract irritation and osteonecrosis of the jaw (Cryer and Bauer, 2002; Ruggiero et al., 2004).

Denosumab is another type of anti-catabolic drug that targets receptor activator of nuclear factor kappa-B ligand (RANKL), which is a critical stimulator of osteoclast differentiation, activation and survival. Denosumab has been found to be able to potently reduce osteoclast number (Reid et al., 2010). Previous studies have shown that denosumab can significantly increase BMD and reduce the relative risk of bone fracture (Lewiecki et al., 2007; Papapoulos et al., 2012). As an anti-catabolic drug slightly more potent than bisphosphonate, denosumab can also cause different side effects such as hypocalcaemia and osteonecrosis of the jaw (Diz et al., 2012; McCormick et al., 2012; Okada et al., 2013; Olate et al., 2014).

Parathyroid hormone (PTH) and the PTH-related protein analog, abaloparatide, are the only FDA-approved bone anabolic drugs that can add new

bone to the skeleton. Clinical application of PTH involves teriparatide, which is the recombinant form of PTH consisting of the first 34 N-terminal amino acids of endogenous PTH but capable of binding to and activating the PTH receptor as well. Unlike bisphosphonate, intermittent PTH injection has been proven to accelerate the bone turnover rate. The bone formed during each remodeling cycle is always more than the bone resorbed and this creates a positive BMU balance.

At the cellular level, intermittent PTH is able to increase osteoblast development, inhibit osteoblast apoptosis and reactivate the matrix secretion activity of bone lining cells via molecular mechanisms that have not been fully elucidated (Bellido et al., 2003; Jilka et al., 1998; Kim et al., 2012; Kostenuik et al., 1999; Pettway et al., 2005). PTH binds to the PTH receptor 1 (PTH1R), a 7-transmembrane receptor that activates the cyclic adenosine monophosphate (cAMP)/protein kinase A (PKA) pathway. Via its direct or indirect effects, PTH targets a broad spectrum of genes that in turn impact different aspects of bone formation. For instance, Runx-related transcription factor 2 (RUNX2) is a master regulator of osteoblast development and differentiation and insulin-like growth factor 1 (IGF1) exhibits pro-differentiating and pro-survival effect on osteoblasts. Studies have shown that PTH directly activates the expression of RUNX2 and IGF1; this activation was blocked by the use of PKA inhibitor (Wang et al., 2006). Interestingly, IGF1 is also an important mediator for PTH action and the anabolic effect of PTH disappeared in IGF1 *null* mice (Bikle et al., 2002). Furthermore, intermittent administration of PTH transiently suppressed sclerostin mRNA expression (Silvestrini et al., 2007), which is an inhibitor of Wnt signaling pathway that plays important roles in bone anabolism. Additionally, PTH induced transient production of RANKL (Dai et al., 2006; Huang et al., 2004), which in turn boosted osteoclastogenesis. PTH was shown to be able to attenuate adipogenesis by inhibiting PPAR γ (Rickard et al., 2006). Finally, the anti-apoptotic effect of PTH was acting mainly through its impact on pro- or anti-apoptotic genes such as *Bcl2* and *Bad* (Bellido et al., 2003)

All of aforementioned signaling events directly or indirectly contribute to accelerated bone turnover and positive bone formation under PTH treatment. The period during which the bone formation activity surpasses bone resorption activity under PTH treatment is known as the anabolic window of PTH. Unfortunately this anabolic window can only last for 1-2 years and eventually both bone formation and resorption activities decline back to the pre-treatment level (Cusano et al., 2011). The exact reason for this limited efficacy is still unclear. Furthermore, a potential adverse effect for PTH treatment is increased risk of osteosarcoma and the high price of this therapy severely limits the use of PTH in clinic. Numerous animal and clinical studies have been conducted to further expand the anabolic window of PTH and one potential strategy is to combine the hormone with anti-catabolic drugs (Bilezikian, 2008).

Combination therapy, a potential solution for osteoporosis?

The basic rationale for combination therapy is that PTH stimulates bone formation and accelerates the remodeling rate, whereas the anti-catabolic drugs "freeze" the existing bone and prevent its further loss (Cusano and Bilezikian, 2013; Pinkerton and Dalkin, 2007). However, previous studies of combination therapy often led to controversial or underwhelming conclusions (Finkelstein et al., 2010; Keaveny et al., 2008; Wu et al., 2010). For instance, a clinical study conducted by Finkelstein *et al.*, recruited 93 postmenopausal women with low BMD; PTH, ALN or concurrent PTH+ALN therapies were given for 30 months; Higher spine and neck BMDs under PTH treatment than RAL and PTH+RAL were observed; patients under PTH treatment also showed higher level of bone formation markers: osteocalcin and type 1 collagen than patients receiving PTH+ALN treatment (Finkelstein et al., 2010). Another study conducted by Samadfam *et al.*, pretreated ovariectomized (OVX) mice with either alendronate or osteoprotegerin (OPG, an inhibitor of RANKL) for 30 days and then continued the treatment for an additional 30 days in combination with PTH; It was reported that both of these two anti-catabolic drugs blunt the anabolic effect of PTH-induced increases in BMD and bone volume (BV/TV) (Samadfam et al., 2007).

Indeed a meta-analysis performed by Zhang *et al.*, involving a comprehensive literature search revealed the addition of alendronate to PTH therapy reduces the BMD at several skeletal sites (Wang et al., 2015). By contrast, the use of another bisphosphonate zoledronate in combination with PTH tends to yield more promising results. Cosman *et al.*, conducted a randomized clinical study by giving 412 osteoporotic women a single infusion of zoledronate followed by daily injection of PTH; the study lasted for a year and revealed significantly more increase in spine and hip BMD than patients who received PTH or zoledronate alone (Cosman et al., 2011). An animal study using OVX rat showed similar result as PTH+ZOL provoked strongest response in terms of bone architecture and biomechanical strength (Li et al., 2012). Similarly, combination studies involving PTH and RAL also in general showed a trend of additive or synergistic effect. For example, a clinical study conducted by Deal *et al.*, revealed a significant increase in hip BMD in osteoporotic patients receiving concurrent PTH+RAL compared to PTH alone; unlike most studies on PTH+bisphosphonate therapies, the addition of RAL to PTH treatment did not blunt the increase in serum bone formation marker (Deal et al., 2005). A recent sequential combination study by Amugongo *et al.*, using OVX rat showed both RAL and ALN could preserve the increase in bone area, thickness and strength after the 3-month PTH treatment had been withdrawn (Amugongo et al., 2014).

The major debate for combination therapy is whether the addition of anti-catabolic drug to PTH anabolic treatment is beneficial or harmful. Some suggest that the newly formed bone can be quickly lost after PTH treatment is withdrawn and anti-catabolic drugs can help preserve the bone for months or years (Cusano and Bilezikian, 2013; Pinkerton and Dalkin, 2007); this outcome may result when concurrent therapies or sequential treatment with PTH followed by an anti-catabolic drugs were given. Alternatively, it has been proposed that the anabolic effect of PTH relies on the fast remodeling process on the bone surface and the use of anti-catabolic drug heavily reduces the space available for remodeling (Eriksen and Brown, 2016).

There are several explanations for the conflicting results from previous animal and clinical studies. One variable is whether patients had been previously treated or not with any anti-catabolic drugs. Naïve untreated patients versus previously treated patients have major differences in active bone surface as well as effects of previous treatment on osteoblast/osteoclast function (e.g. altered osteoblast proliferation and differentiation, impaired osteoclast activity) and parathyroid dynamics (Cosman, 2014). The treatment sequence of the anabolic and anti-catabolic therapies may also play a role (Cosman et al., 2016b). It is clinically more common to give patients PTH treatment when the initial anti-catabolic treatment becomes inadequate (e.g. effect wanes or side effect starts to show); during the ongoing PTH treatment, the initial anti-catabolic treatment may cease or continue; however as PTH becomes more popular in clinical use, doctors may also give naïve untreated patients PTH first followed by anti-catabolic drugs to maintain the PTH-induced increase in bone.

Several studies have been conducted to explore all these potential sequences of drug combinations for osteoporosis therapy. It was noticed that when switching from anti-catabolic drugs to PTH, the patients might suffer a transient decrease in hip BMD below baseline for 1-2 years, whereas adding PTH to ongoing anti-catabolic treatment did not cause such a problem (Boonen et al., 2008; Cosman et al., 2013; Cosman et al., 2009; Ettinger et al., 2004). Switching from PTH to anti-catabolic drugs such as bisphosphonate could be beneficial in treating osteoporotic patients who had not been treated before, as studies have shown that their hip and femoral BMDs can be maintained and further improved after the switching (Leder et al., 2015; Prince et al., 2005). Some other factors that might influence the outcome of combination study include the type of anti-catabolic drug used, the length of the study, the gender of the patients or animal, the type of response assessment (e.g. BMD, BV/TV, biomechanical properties, histomorphometry data and serum markers) and skeletal sites of interest.

In conclusion, the use of combination therapy to treat osteoporosis is a potential solution to overcome the limited anabolic window of PTH but there are still a lot of controversies over this therapy and further therapeutic improvement

is required to maximize its benefit before it can be used widely among clinics. Fortunately, the discovery of an anti-anabolic axis regulated by a transcription factor known as nuclear matrix protein 4 (NMP4) may shed light on improving the efficacy of combination therapy.

NMP4, the structure, function and phenotype

The official name of NMP4 is zinc finger protein 384 (Zfp384 for rodent and Znf384 for human) and some researchers also named it Ciz (Cas-interacting zinc finger protein). NMP4 is an architectural transcription factor that is suggested to bind a homopolymeric deoxyribonucleic acid (DNA) consensus sequence (dA.dT) in the minor groove (Childress et al., 2015; Torrungruang et al., 2002). It is expressed in almost all tissues. NMP4 possesses several functional domains, including a strong trans-activating domain at the N' terminal, an overlapping SRC homology 3 (SH3) binding and AT-hook motif that can mediate interaction with proteins such as Crk-associated substrate (p130Cas), 5-8 Cys₂His₂ zinc fingers that directly interact with the DNA consensus sequence and a weak trans-activating domain consisting of a poly(QA) tail at the C' terminus (Figure 1-3). NMP4 protein shuttles between cytosol and the nucleus. In the cytoplasm, NMP4 binds to p130Cas directly in rat and indirectly through the focal plaque protein Zyxin (Janssen and Marynen, 2006). The protein p130Cas plays a role in focal adhesion and cell migration (Cary et al., 1998) but the involvement of NMP4 in this function remains to be elucidated. NMP4 primarily accumulates in the nucleus; it binds to AT-rich binding-site and bends the DNA (Alvarez et al., 1998; Nakamoto et al., 2000). NMP4 is a context-dependent transcription factor that may either upregulate or downregulate its targets (Torrungruang et al., 2002). At least 7 isoforms of NMP4 with 5-8 zinc fingers exist as a result of alternative splicing (Thunyakitpisal et al., 2001).

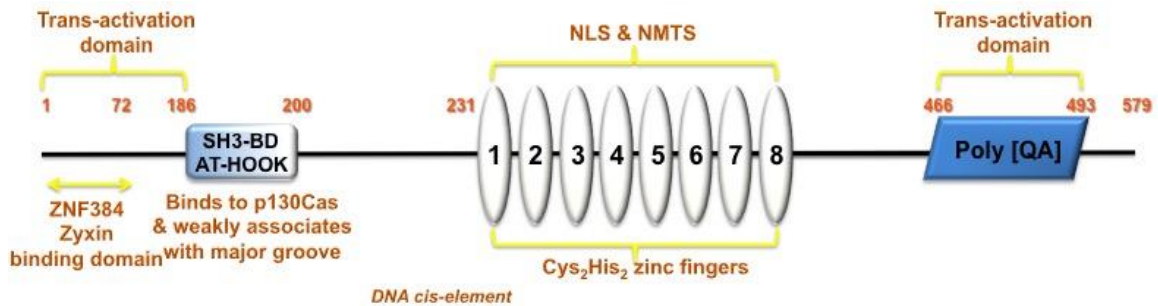


Figure 1-3: Structure of NMP4 (see text for details)

The *NMP4* gene itself is highly conserved across mammals. However, *NMP4* is not essential as studies showed no major defects in *Nmp4*^{-/-} mice but only some minor phenotypes (Robling et al., 2009). Nakamoto *et al.*, showed impaired spermatogenesis in *Nmp4*^{-/-} mice (Nakamoto et al., 2004). Fusion between NMP4 and another gene EWS RNA binding protein 1 (EWSR1) has been implicated in the development of acute leukemia, suggesting a role of NMP4 in lymphoid and myeloid development (Martini et al., 2002). Of interest, a recent report demonstrates that loss of *Nmp4* suppresses the induction of serum transfer-induced arthritis (Nakamoto et al., 2016). Other than these, no obvious defects have been reported for *Nmp4*^{-/-} mice when receiving no drug or chemical challenges. However, the *Nmp4*^{-/-} mice exhibited enhanced response to bone anabolic agents such as PTH and BMP2 (Childress et al., 2015; Morinobu et al., 2005; Robling et al., 2009). A most recent study conducted by Childress *et al.*, showed significant enhancement of bone gain response to 4-week and 8-week PTH therapy in OVX *Nmp4*^{-/-} mice (Childress et al., 2015). *Nmp4*^{-/-} mice also exhibited enhanced recovery from bone marrow ablation as well as enhanced resistance to disuse-induced bone loss (Hino et al., 2007; Morinobu et al., 2005). All of these studies suggested NMP4 is a critical regulator in bone anabolism.

At the cellular level, MSCs harvested from *Nmp4*^{-/-} mice exhibited modest but significant increase in proliferation rate compared to their WT counterpart (Childress et al., 2015). Moreover, under osteogenic stimuli, the *Nmp4*^{-/-} MSCs showed accelerated mineralization rate, on average one week ahead of the WT MSCs (Childress et al., 2015). In fact, the untreated *Nmp4*^{-/-} mice exhibited

elevated number of BM CD45⁻/CD105⁺/CD146⁺/Nestin⁺ osteoprogenitors and BM CD8⁺ T cells, both of which contribute significantly to osteogenesis (Bedi et al., 2012; Childress et al., 2015; He et al., 2013; Terauchi et al., 2009).

Early studies showed NMP4 regulates several genes that are important during osteogenesis, such as type I collagen α 1 polypeptide chain (*Col1a1*) and matrix metalloproteinase (*Mmp*) genes (Shah et al., 2004; Torrungruang et al., 2002). Most recently, chromatin immunoprecipitation sequencing (ChIP-Seq) analysis was used to identify genes that are directly targeted by NMP4 in MC3T3-E1 cells (pre-osteoblasts), murine embryonic stem cells and two blood cell lines (Childress et al., 2015). A total of 2114 NMP4 candidate target genes were found in these 4 cell lines. Bioinformatics analysis of the ChIP-seq data showed that the top five biological functions of genes associated with Nmp4 binding included control of transcription, chromosome organization, protein catabolic process, chromatin modification and cell cycle. A custom TaqMan Low Density Array (TLDA) system was then used to further examine the expression profiles of some of these NMP4-target genes in undifferentiated and osteogenic-differentiating MSCs. Several pro-osteogenic genes including *Igfbp2*, *Pdk1* and *Plaur* were found upregulated in *Nmp4*^{-/-} cells; whereas some anti-osteogenic genes such as *Igfbp4* and *Cxcl12* were downregulated in the null cells (Calleja et al., 2014; Childress et al., 2015; Hamidouche et al., 2010; Kalbasi Anaraki et al., 2013). These studies implied that NMP4 is an apex regulator of multiple pathways and impacts different aspects of cellular and biological functions, directly or indirectly. All of these pathways and functions are part of an anti-anabolic bone axis of NMP4 (Childress et al., 2015).

As mentioned above, NMP4 is ubiquitously expressed in almost all kinds of cell types but its phenotype in bone anabolism is mainly manifested through MSCs. At the molecular level, NMP4 was also found to impact the unfolded protein response (UPR) (Young et al., 2016).

The UPR pathway, guardian against ER stress

Endoplasmic reticulum (ER) stress occurs when misfolded or unfolded proteins accumulate in the ER lumen, detrimental to the normal cell function. Cells cope with ER stress by activating a transcriptional and translational gene expression program referred to as the UPR. The UPR pathway serves to expand the processing capacity of the ER to better manage increases in the secretory load. The UPR also adjusts cell metabolism and homeostasis level in the following ways: 1) the global protein translation is dampened; 2) lipid synthesis is elevated and ER capacity is expanded; and 3) cell apoptosis is induced if UPR continues to be activated (Walter and Ron, 2011). Recognition of ER stress and implementation of the UPR is achieved via three sensory proteins that are associated with the ER. These sensory proteins are activating transcription factor 6 (ATF6), PRKR-like ER kinase (PERK) and inositol-requiring enzyme 1 (IRE1) (Figure 1-4) (Walter and Ron, 2011), which monitor by distinct mechanisms the perturbations in the lumen and membrane of the ER. Collectively, these three sensory UPR proteins trigger gene expression programs that are integrated to restore protein homeostasis.

ATF6 is a transcription factor that spans across the ER membrane. ATF6 is mainly responsible for proper protein folding, secretion and degradation upon ER stress. Once ATF6 senses the accumulation of unfolded proteins in the ER lumen, the protein is packaged into vesicle and released from ER; the protein is then delivered to Golgi apparatus where it is cleaved by two proteases: S1P and S1P; the N-terminal domain, which is a CREB/ATF bZIP transcription factor is subsequently released and transported to the nucleus (Haze et al., 1999; Okada et al., 2003; Schindler and Schekman, 2009). Upon entering the nucleus, ATF6 activates different UPR target genes including genes involved in protein folding: *BiP (Hspa5)*, *glucose-regulated protein 94 (GRP94)* and *protein disulfide isomerase* (Shen et al., 2002). This whole process of activation of ATF6 is known as regulated intramembrane proteolysis (RIP). ATF6 is crucial for early development, as disabling both isoforms of *Atf6*: *Atf6 α* and *Atf6 β* in mice is lethal at early embryonic stage (Wu et al., 2007; Yamamoto et al., 2007).

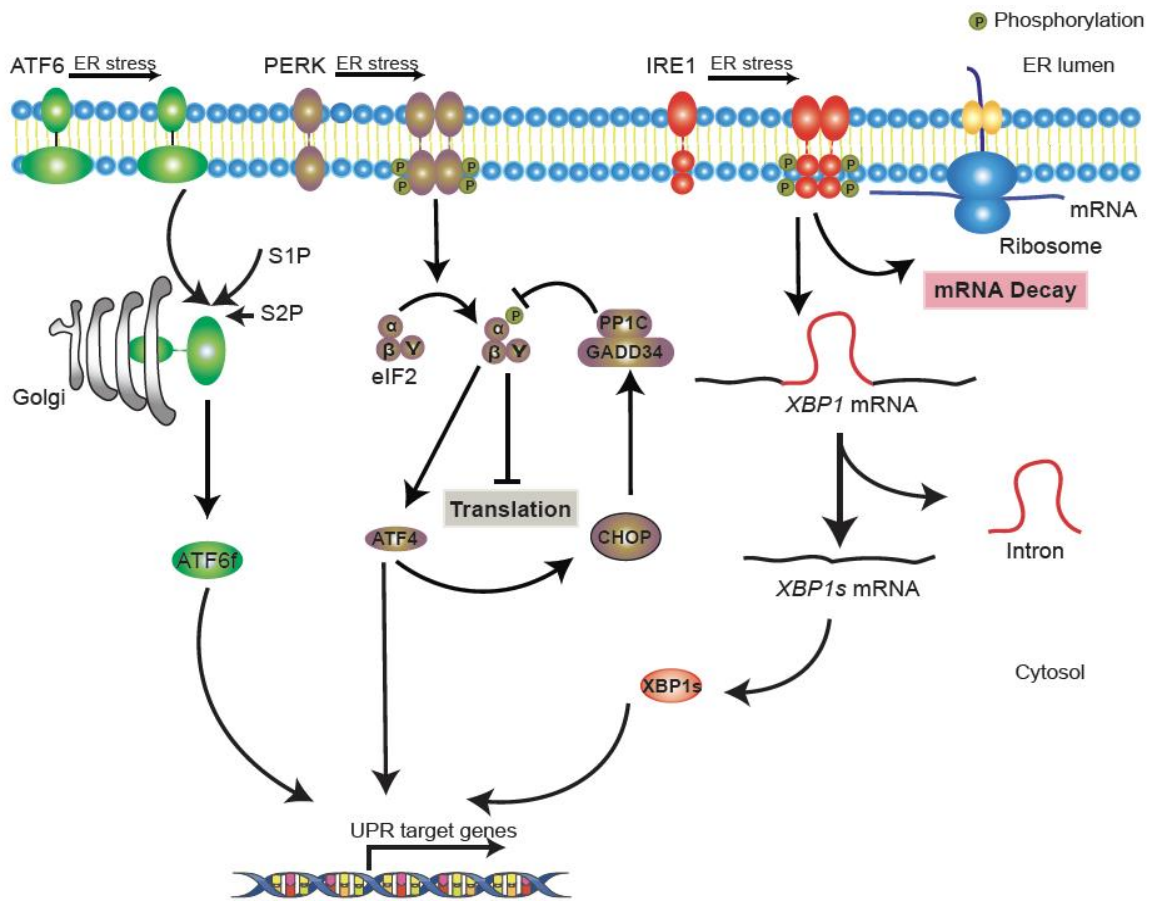


Figure 1-4: Unfolded protein response is initiated via three branches-ATF6, PERK and IRE1 (see text for details). Modified based on illustration published by Hetz *et al.*, (Hetz *et al.*, 2013).

PERK initiates the second branch of the UPR response. It also resides on the ER membrane and possesses a serine/threonine kinase domain in the cytoplasm. Upon sensing the accumulation of the unfolded proteins in the ER lumen, PERK undergoes oligomerization and autophosphorylation; the kinase also phosphorylates the α subunit of eukaryotic translation initiation factor 2 (eIF2) (Iurlaro and Muñoz-Pinedo, 2016). This translation factor combines with GTP and functions to deliver initiator tRNA to the translation apparatus during the initiation phase of protein synthesis. During ER stress, phosphorylation of eIF2 α by the protein kinase PERK inhibits the activity of this translation initiation by

stabilizing the eIF2/GDP complex and thus lowers the formation of eIF2/GDP/Met-tRNA^{iMet} that is required for global translation (Hinnebusch, 2014); the influx of nascent proteins into ER is therefore reduced to mitigate the ER stress. On the other hand, activation of PERK-eIF2 α pathway also selectively promotes the translation of several select UPR genes through bypass of inhibitor upstream open reading frames (ORFs) in these target mRNAs. One of UPR target genes is activating transcription factor 4 (ATF4). ATF4 promotes osteogenesis from MSPCs via β -catenin and RUNX2 (Lin et al., 2010; Yu et al., 2013). ATF4 also targets and upregulates two specific genes: *growth arrest and DNA damage-inducible 34 (Gadd34 or Ppp1r15a)* and *transcription factor C/EBP homologous protein (Chop or Ddit3)*. *Gadd34* encodes a regulatory subunit of protein phosphatase 1 (PP1) that dephosphorylates eIF2 α and therefore acts as a negative regulator of PERK (Brush et al., 2003; Connor et al., 2001). This negative feedback loop is essential to keep the UPR translational control under check and prevent prolonged UPR responses once the ER stress has been mitigated. CHOP is a pro-apoptotic transcription factor that activates pro-apoptotic genes including *BCL2 like 11 (BCL2L11)*, *Death receptor 5 (DR5)* and *telomere repeat binding factor 3 (TRB3)*; CHOP can also inhibit anti-apoptotic gene *Bcl-2* (McCullough et al., 2001; Ohoka et al., 2005; Puthalakath et al., 2007; Yamaguchi and Wang, 2004). This mechanism ensures that if ER stress cannot be alleviated, the cell undergoes apoptosis before producing too many unfolded proteins.

IRE1 possesses both transmembrane kinase and endoribonuclease activities. It is the most conservative pathway among the three branches of UPR responses and actually the only UPR pathway in lower organisms such as yeast. Upon activation by unfolded proteins, the monomers of this endoribonuclease can form dimers and further become active oligomers. IRE1 can then cleave transcripts of a specific gene *x-box binding protein 1 (Xbp1)*, which is subsequently ligated by a tRNA ligase RTCB (Jurkin et al., 2014). The spliced form of *Xbp1* is then translated and become an active CREB/ATF basic leucine zipper (bZIP)-containing transcription factor (Walter and Ron, 2011). XBP1

upregulates a wide range of UPR-specific genes that in turn contribute to ER protein folding & secretion, ER expansion and ER-associated degradation (ERAD) (Reimold et al., 2001). Previous studies have shown a chaperon protein BiP binds to ATF6, PERK and IRE1 and keeps all of these three UPR signaling transducers inactive; the dissociation of BiP activates these three proteins and initiates the UPR response (Bertolotti et al., 2000; Shen et al., 2002); however, some other studies suggest that IRE1 can directly sense and respond to the unfolded proteins in ER and BiP is not necessarily required in this process (Credle et al., 2005; Pincus et al., 2010). Interestingly, in some specific professional secretory cells such as B cells, IRE1 can be activated by developmental cues rather than the ER stress (van Anken et al., 2003). The endoribonuclease function of IRE1 can also degrade mRNAs in proximity of the ER to selectively lower portions of the transcriptome through a process referred to as Ire1-dependent decay (RIDD) (Hollien et al., 2009). Hence the UPR can repress, as well as enhance, selective portions of the transcriptome.

MSPCs and osteoblasts are professional secretory cells that rely heavily on the ER to properly fold the growth factors and signaling molecules that are to be released to the bone matrix. Multiple genes in the UPR pathway were found to play critical role in osteoblast differentiation and development. For instance, in one earlier study *Perk* was found to be critical for osteoblast differentiation and *Perk*^{-/-} mice suffered severe osteopenia; Loss of *Perk* also impaired the secretion of collagen I; meanwhile collagen I was abnormally accumulated in the ER lumen (Wei et al., 2008). ATF4 is highly abundant in osteoblasts and one study confirmed ATF4 enhanced osteoblast function via crosstalk with BMP2 pathway (Saito et al., 2011). A most recent study has shown the UPR pathways may have profound contributions to the NMP4 phenotype in MSPCs derived from mouse BM (Young et al., 2016). The unfolded protein response (UPR) pathway is critical in protein synthesis and secretion; Previous CHIP-Seq analyses revealed that this pathway is the major target of NMP4 in pre-osteoblasts (Childress et al., 2015) and therefore the UPR may be an important molecular mechanism underlying the NMP4 phenotype in bone and other tissues.

NMP4 regulates both ribosomal biogenesis and UPR pathways

In this study (Young et al., 2016), Young and her colleagues first examined *Gadd34* expression in *Nmp4*^{-/-} MSPCs and mice respectively and found *Gadd34* was significantly upregulated in the *null* cells and multiple tissues from the *null* animal. This is consistent with what Childress *et al.*, reported in a NMP4 ChIP-Seq study that *Gadd34* is a candidate target of NMP4. Treatment with tunicamycin, an ER stress inducer further enhanced the upregulation of *Gadd34* in *Nmp4*^{-/-} MSPCs. Similarly c-MYC, which is an important ribosomal biogenesis activator, was also found upregulated in *Nmp4*^{-/-} MSPCs. Further polysome profiling revealed that there was higher level of mRNA translation in *Nmp4*^{-/-} MSPCs and this was accomplished by elevated level of ribosomal subunits. This phenotype could be reversed by the addition of salubrinal, an inhibitor of GADD34. The elevated *Gadd34* level was found highly correlated with reduced induction of eIF2 α and ATF4 in *Nmp4*^{-/-} MSPCs under ER stress. Meanwhile, downstream targets of C-MYC including *Rpl11*, 45S rRNA and *Rps6* were all upregulated in *Nmp4*^{-/-} MSPCs, supporting the idea that c-MYC is responsible for the upregulation of ribosomal biogenesis in the *Nmp4*-deficient cells. Finally, *Nmp4*^{-/-} MSPCs were more sensitive to tunicamycin-induced ER stress. The general idea is that by disabling *Nmp4*, both *c-Myc* and *Gadd34* are upregulated. Consequently, the protein synthesis machinery is induced and the PERK-eIF2 α arm of the UPR pathway is inhibited; therefore global protein synthesis is high in *Nmp4*^{-/-} MSPCs, supporting the super secretion in the cells, but any further ER stress may induce apoptosis (Young et al., 2016).

Main research goals and significance

Three major questions are to be addressed for the projects described in this dissertation: 1) Does loss of *Nmp4* improve the efficacies of PTH/anti-catabolic combination therapies; 2) Does NMP4 interfere with the efficacies of anti-catabolic mono therapies and 3) What are the cellular/molecular mechanisms driving the *Nmp4*^{-/-} hyper-anabolism phenotype?

Previous studies have shown loss of *Nmp4* improves the response of mice to PTH mono therapy (Childress et al., 2011; Childress et al., 2015). Meanwhile PTH combination therapies have not become a viable clinical option yet (Finkelstein et al., 2010; Keaveny et al., 2008; Wu et al., 2010). Studies aiming at the first two aforementioned research questions may facilitate the clinical use of different osteoporosis therapies in the future; Meanwhile it may also help us gain deeper understanding to the role of NMP4 in the resorption arm of the bone remodeling. Better understanding of the cellular/molecular mechanisms mediating the *Nmp4*^{-/-} hyper-anabolism phenotype may lead to the identification of feasible pharmacological targets, translating the current animal experiment to clinical application. In fact, we recently found BM MSCs and UPR pathway as the central part of the anti-anabolic axis governed by NMP4. We also extended our research from osteoporosis to influenza and type II diabetes. Preliminary data suggested *Nmp4*^{-/-} mice exhibited improved survival rate upon infection with influenza and we proposed MSCs and UPR pathways are critical in altering the immunomodulation process in the *null* mice (See Chapter 3 for details). Furthermore, the β cells from *Nmp4*^{-/-} mice appeared to produce less insulin than the WT. More studies are required to better understand the mechanisms driving these phenotypes but NMP4 has proven to be a promising target for future clinical application in treating different diseases.

CHAPTER 2

Improving Combination Osteoporosis Therapy In a Preclinical Model of Heightened Osteoanabolism

INTRODUCTION

Our previous studies have revealed that *Nmp4* inhibition represents an attractive strategy to enhance anabolic therapy in bone. However, it remains to be determined whether *Nmp4* inhibition can enhance the efficacy of anti-catabolic therapies in the skeleton. Therefore, the goal of this study was twofold: (1) to test the hypothesis that combining a sustained anabolic response to PTH with an anti-catabolic agent results in superior bone acquisition compared to PTH mono-therapy alone and (2) to test the hypothesis that *Nmp4* does not interfere with the efficacy of anti-resorptive agents. To test these hypotheses we evaluated the efficacy of combining PTH therapies in ovariectomized mice (normal and *Nmp4-null*) with one of three anti-catabolic drugs: the nitrogen-containing bisphosphonates alendronate and zoledronate and the selective estrogen receptor modulator (SERM) raloxifene. Our findings demonstrate that loss of *Nmp4* significantly enhances the response of combining PTH with anti-catabolics and intriguingly improves the skeletal effects of the RAL mono-therapy, but not the bisphosphonate mono-therapies. The sustained anabolic effect may be driven, in part, by an expansion in the bone marrow pool of hyper-anabolic osteoprogenitors. Nevertheless, disabling the *Nmp4* anti-anabolic bone axis provides a novel potential strategy for improving diverse existing osteoporosis treatments.

MATERIALS AND METHODS

Mice

WT and *Nmp4^{-/-}* mice were generated as previously described (Childress et al., 2015; Robling et al., 2009). Mice were maintained in our colony at Indiana University Bioresearch Facility, Indiana University School of Dentistry. Animals

for these experiments were randomly selected from litters produced by heterozygous x heterozygous, *Nmp4*^{-/-} x WT, WT x WT, and *Nmp4*^{-/-} x *Nmp4*^{-/-} breeding pairs. Local Institute Animal Care and Use Committee have approved all husbandry practices and experimental procedures described in the present study.

Bilateral ovariectomy surgery

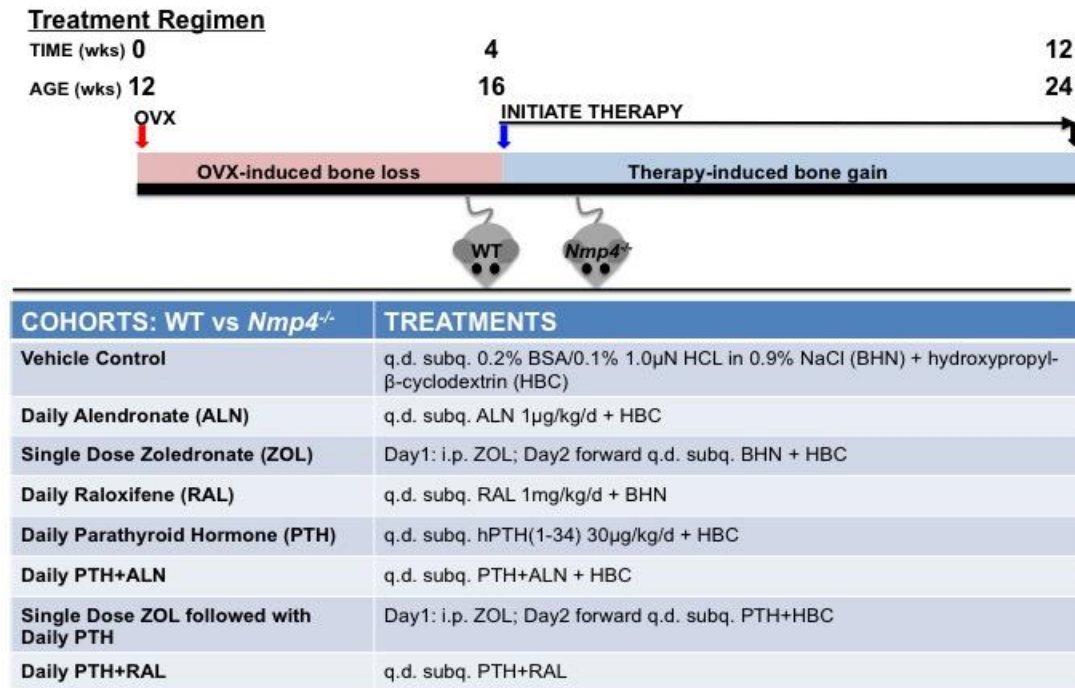
The surgeries on 12 week-old virgin mice were performed as previously described in detail (Childress et al., 2015). To keep the study to 16 treatment groups we did not perform sham surgeries since we have previously shown ovariectomy induces significant bone loss in both genotypes and there is no difference between the baseline skeletal phenotypes in healthy and ovariectomized mice (Childress et al., 2015; Robling et al., 2009).

Therapies

At 16 weeks of age the ovariectomized mice were sorted into 16 treatment groups by weight and genotype. All mice were housed typically 2-4 per cage under standard conditions with ad libitum access to water and regular chow (Laboratory Rodent Diet 5001, LabDiet St. Louis, MO, USA). Each mouse received two sequential 100 µl injections/day containing the drugs or vehicle(s) 7 days/week for 8 weeks (see Figure 2-1 for full details). Zoledronate and alendronate were synthesized by the IUPUI Chemistry core facility, verified by NMR spectroscopy, and have been previously shown to produce the expected effects on bone remodeling (Burr et al., 2015; Newman et al., 2015). Mice receiving PTH were injected subcutaneously (sc) with synthetic human PTH (hPTH) 1–34 acetate salt (Bachem Bioscience, Inc) at 30 µg/kg/d, daily, a dose frequently used in mice to study PTH bone anabolic action *in vivo*. Doses of anti-catabolic agents were based on human clinical doses. The standard ALN dose for treatment of osteoporosis is typically given as either a daily (10 mg) or weekly (70 mg) dose. Based on a 60 kg individual this is roughly 1.17 mg/kg/wk. The human dose is oral and has an estimated bioavailability of around 0.6%, meaning

that the absorbed dose is approximately 7 µg/kg/wk. We dosed via injection, assuming 100% absorption, thus we delivered ALN at 1 µg/kg/day (Ettinger et al., 2004; Lui et al., 2013; Muschitz et al., 2013). RAL is typically given clinically as a 60 mg daily dose. Based on a 60 kg patient, the dose would be 1 mg/kg/day. The assumption is 100% absorption thus the full dose is used when injecting (Cano et al., 2008; Ettinger et al., 2004). ZOL is typically given yearly at a dose of 5 mg. Based on a 60 kg patient, the dose is 0.083 mg/kg. Our single dose of 80 µg/kg approximates this amount (Cosman et al., 2011; Sheng et al., 2009).

Figure 2-1: WT and *Nmp4^{-/-}* mice were ovariectomized (ovx'd) at 12wks of age. At 16wks of age the mice were sorted into 16 treatment groups by weight and genotype. Each mouse received two sequential 100 µl injections/day containing the drugs or vehicle(s) as shown for 8wks. Mice were euthanized and the bones processed for analysis at 24wks of age.



WT and *Nmp4^{-/-}* mice were administered the following treatments:

- Vehicle-control: inject subcutaneously (sc) 100 µl 0.2% Bovine serum albumin/0.1% 1.0 µN HCl in 0.9% NaCl (abbreviation BHN diluent for

PTH/alendronate (ALN)) + 100 μ l 20% Hydroxypropyl- β -Cyclodextrin (abbreviation HBC diluent for raloxifene (RAL) diluent)

- Daily alendronate (ALN): inject sc 100 μ l ALN at 1 μ g/kg/d + 100 μ l HBC
- Daily zoledronate (ZOL): on Day 1 of treatment inject intraperitoneal (ip) 100 μ l ZOL at 80 μ g/kg in PBS. On Day 2 forward inject sc 100 μ l BHN + 100 μ l HBC
- Daily raloxifene (RAL): inject sc 100 μ l RAL at 1mg/kg/d +100 μ l BHN
- Daily parathyroid hormone (PTH): inject sc 100 μ l synthetic human PTH 1–34 acetate salt, Bachem Bioscience Inc, PA, at 30 μ g/kg/d + 100 μ l HBC
- Daily PTH+ALN: inject sc 100 μ l PTH/ALN +100 μ l HBC
- Single dose ZOL followed by daily PTH: on Day 1 of treatment inject ip 100 μ l ZOL. On Day 2 forward inject sc 100 μ l PTH + 100 μ l HBC

Daily PTH+RAL: inject sc 100 μ l RAL +100 μ l PTH.

Dual energy X-ray absorptiometry (DXA)

The postcranial skeleton and spine (L3-L5) areal bone mineral density (aBMD; mg/cm²) and bone mineral content (BMC; g) were evaluated *in vivo* using a PIXImus II densitometer as previously described (Childress et al., 2011; Robling et al., 2009).

Micro-computed tomography (μ CT)

Trabecular and cortical bone architectures were analyzed as we have previously described in detail (Childress et al., 2011; Childress et al., 2015). Briefly, after tissue preparation the distal femur metaphysis and the L5 vertebral body were scanned using a Skyscan 1172. All scans were conducted at a 6 μ m scan resolution. Three-dimensional reconstructions using Skyscan software provided the following parameters: trabecular bone volume per total volume (BV/TV, %), trabecular number (Tb.N, mm⁻¹), trabecular thickness (Tb.Th, mm), and trabecular spacing (Tb.Sp, mm). Additionally, the Skyscan software provided the following data for femoral diaphysis cortical bone: periosteal perimeter (mm), endocortical perimeter (mm), total area (mm²), bone area (mm²), marrow area (mm²), cortical porosity (%), cortical thickness (mm), minimum moment of inertia (I_{min}, mm⁴), maximum moment of inertia (I_{max}, mm⁴), and polar moment of inertia (I_p, mm⁴).

Serum biochemistry

Serum osteocalcin (OCN) was evaluated as a bone formation marker using ELISA BTI Mouse Osteocalcin EIA kit (Biomedical Technologies, Inc., Stoughton MA). Serum C-terminal telopeptides (CTX) was assessed as an indicator for resorption using the RatLapsTM ELISA (Immunodiagnostic System Inc., Scottsdale, AZ). Serum osteoprotegerin and serum receptor activator of nuclear factor- κ B ligand (RANKL) were determined using Mouse Osteoprotegerin/TNFRSF11B Immunoassay kit and the Mouse TRANCE/RANK L/TNFSF11 Immunoassay kit, respectively (R&D Systems, Inc., Minneapolis, MN).

Immunohistochemistry

Osterix was detected on formalin-fixed, paraffin-embedded sections by using primary antibodies from AbCam (human anti-SP7/osterix, #ab 94744). We followed the protocol described by Nissenson and colleagues with some modifications (Hsiao et al., 2008; Wattanachanya et al., 2015). Briefly, slides were de-paraffinized at room temperature in Coplin jars in three washes of xylene, and rehydrated in a decreasing ethanol gradient. Endogenous peroxidases were deactivated with 3% H₂O₂ for 5 min, and sections were blocked in PBS supplemented with 1.5% goat serum (Gibco BRL) for 30 min at room temperature. Sections were incubated with primary antibody (1:25 dilution) in blocking solution overnight at 4°C. Sections were then washed in PBS and incubated with the biotinylated goat anti-rabbit IgG (VectaStain® Elite ABC Kit, Vector Laboratories, Inc. Burlingame, CA) for 45 min at room temperature. After washing with PBS, sections were incubated with VECTASTAIN® ABC Reagent for 30 minutes at room temperature, followed by washing in buffer for 5 minutes. Incubating sections in peroxidase substrate solution according to the manufacturer's instructions achieved color development. Finally, counterstaining was accomplished by staining with 0.2% methyl green for 60-90 seconds, followed by dehydration in a series of ethanol and xylene changes and mounted using coverslips with xylene-based mounting media.

Tartrate-resistant acid phosphatase (TRAP) staining was performed using a modified protocol based on the method of Erlebacher and Derynck (Erlebacher and Derynck, 1996). In brief, formalin-fixed, paraffin-embedded sections were de-paraffinized followed by rehydration via a sequential ethanol wash. Subsequently, slides were transferred to 0.2M acetate buffer (pH 5.0) for 20 minutes at room temperature and then placed in medium containing naphthol AS-MX phosphate (0.5mg/ml, Sigma-Aldrich, N4875) and fast red TR salt (1.1mg/ml, Sigma-Aldrich, E6760) in acetate buffer for 60 minutes at 37°C before counterstaining with Toluidine Blue. Slides dried for 24 hrs Aqueous-base mounting media was added on top of the sample and coverslip was applied.

Adipocytes were stained in de-paraffinized slides that had been rehydrated using a sequential ethanol wash. Sections were then incubated in Sudan Black B solution for 3 hours. Subsequently, the slides were rinsed thoroughly in two changes of 70% isopropyl alcohol followed by six changes of distilled water. The slides were counterstained in nuclear fast red solution for 10 minutes and rinsed again with two changes of distilled water. Slides were coverslipped with an aqueous based mounting medium.

The stained bone marrow cells were counted using the Bioquant imaging software (Nashville Tennessee, USA). Bone marrow osteoprogenitors were counted within a 0.75-1 mm² area approximately 1mm below the growth plate of the distal femur. Small, round cells within the marrow exhibiting a brown nucleus indicating positive staining for osterix, were counted as osteoprogenitors and then the count normalized to the tissue area selected. Adipocytes were counted within a 1.75-2 mm² area adjacent to the growth plate at the distal femur. Empty-appearing cells >30µm in diameter and exhibiting a membrane positively stained with Sudan Black were counted and then normalized to tissue area. Finally, to determine the osteoclast surface, a 1.75-2 mm² area adjacent to the growth plate at the distal femur was selected; the surface of all TRAP+ cells and the total trabecular surface in this region were measured. The ratio of the two was then calculated (TRAP+ S/BS, %).

Flow cytometry

Cellular marker profiles from bone marrow were assessed using the antibodies CD45, CD146, CD105, and nestin (BD Biosciences) as previously described (Childress et al., 2015; He et al., 2013). Stained cells were analyzed on a FACSCalibur (BD Biosciences) and results were quantified using FlowJo Version 8.8.6 software (TreeStar, Inc).

Statistical analysis

Statistical packages JMP version 7.0.1 (SAS Institute, Cary, NC) and the Statistical Analysis System version 9.4 (SAS, SAS Institute, Cary, NC) were used for analyses.

To test the hypothesis that combining a sustained anabolic response with an anti-catabolic agent results in superior bone acquisition compared to PTH mono-therapy we compared the anabolic therapies PTH+RAL, PTH+ZOL, PTH+ALN, and PTH to each other and to VEH. To test our second hypothesis that *Nmp4* does not interfere with the efficacy of anti-resorptive agents we compared the anti-catabolic treatments ALN, ZOL, RAL to each other and to VEH. All data were first analyzed for outliers using the interquartile range (IQR) method to evaluate statistical dispersion (Moore DS, 2003). Data were then analyzed with a 2-way analysis of variance (ANOVA) for effects of genotype and treatment followed by a Tukey-Kramer post hoc test for comparison of more than two groups or Student t post hoc test for comparing WT and *Nmp4*^{-/-} parameters as two groups. Statistical significance was set at $p \leq 0.05$. In these analyses all experimental data were grouped by either genotype or treatment to determine whether either or both impacted the value of the endpoint parameter as well as whether genotype influenced the response to treatment (genotype x treatment interaction). Finally, to determine if there was an interaction between PTH and any of the anti-catabolic drugs we performed a series of 2-way ANOVAs using PTH and the anti-resorptive drug in question as the independent variables.

RESULTS

Effect of Combination Treatments Using Anabolic Agents On Bone

PTH+RAL and PTH+ZOL synergistically enhanced therapeutic bone restoration; loss of Nmp4 further improved the actions of these treatments on femoral trabecular bone

We have previously shown that loss of *Nmp4* improves femoral trabecular bone response to PTH in both healthy and ovariectomized mice without compromising gains in cortical bone (Childress et al., 2011; Childress et al.,

2015; He et al., 2013; Robling et al., 2009). To address the contribution of *Nmp4* in regulating the response of trabecular bone to concurrent PTH combination therapies we evaluated the distal femoral BV/TV of mice under these treatments. Mice administered the PTH+RAL and PTH+ZOL treatments yielded the highest femoral BV/TV in both WT and *null* mice and these combination therapies surpassed femoral BV/TV obtained with the PTH mono-therapy (Figures 2-2A&B, treatment effect $p < 0.0001$). Moreover, PTH showed a greater-than-additive (synergistic) interaction with RAL and ZOL at this site (Table 2-1A). In contrast the femoral BV/TV values of mice under the PTH+ALN treatment were equivalent to those values of the PTH mono-therapy cohorts (Figure 2-2A and Table 2-1A).

Loss of *Nmp4* improved the gains in femoral BV/TV of PTH+RAL, PTH+ZOL, and PTH treatments (genotype x treatment interaction $p = 0.0038$, Figures 2-2A&B). The 3-D μ CT images of the distal femur illustrate the differences in trabecular bone between the WT and *Nmp4*^{-/-} VEH cohorts and various treatments (Figures 2-3A~D). Similarly, the 2-D μ CT images show the more extensive bone formation in the *Nmp4*^{-/-} mice treated with PTH or PTH+RAL compared to the WT animals (Figures 2-6A~D).

Loss of *Nmp4* had similar effects on femoral trabecular architecture (Tb.N, Tb.Th, Tb.Sp) as observed for BV/TV. *Null* mice showed significantly higher Tb.N under the PTH+RAL, PTH+ZOL, and PTH therapies compared to the WT cohorts (Table 2-2A). Similarly, the *Nmp4*^{-/-} mice exhibited a lower Tb.Sp under PTH+RAL, and PTH+ZOL compared to WT mice (Table 2-2A). Finally, loss of *Nmp4* enhanced increases in Tb.Th under PTH+ZOL and PTH.

We next interrogated the impact of the therapies on vertebral trabecular bone. As we observed with the femoral BV/TV, the comparative efficacies of the anabolic treatment groups were PTH+RAL=PTH+ZOL>PTH+ALN=PTH>VEH (treatment effect $p < 0.0001$, Figures 2-2D&E). PTH exhibited a greater-than-additive (synergistic) interaction with RAL and ZOL at this site (Figure 2-2B and Table 2-1B).

The loss of *Nmp4* did not further enhance the efficacy of the anabolic treatments for restoring L5 BV/TV (Figures 2-2D&E). However, the *null* mice

showed an enhanced increase in Tb.Th under PTH+RAL, PTH+ZOL, and the PTH mono-therapy (Table 2-3A). The 3-D μ CT images (Figures 2-4A~D) and 2-D μ CT (Figures 2-7A-D) of the L5 vertebrae show comparative improvements we observed in the trabecular architecture with various treatments.

Over stimulation of the PTH receptor has been reported to increase trabecular bone but decrease cortical bone formation in transgenic mice (Calvi et al., 2001). Therefore, to address whether the cortical bone gains in the *Nmp4*^{-/-} mice were compromised under the present experimental therapies we evaluated post-cranial whole body (WB) BMD and femoral cortical geometry. Both WT and *Nmp4*^{-/-} mice administered PTH+RAL yielded the highest WB BMD exhibiting a strong treatment effect ($p < 0.0001$) but without a genotype x treatment interaction (Figures 2-5A&B). The PTH+RAL and PTH+ZOL cohorts exceeded the WB BMD observed in the PTH mono-therapy cohorts but only the PTH and RAL drugs showed a synergistic interaction and only for the WT mice (Table 2-1C). Furthermore, PTH+RAL was the only combination treatment that significantly improved femoral cortical area over the PTH mono-therapy (Figures 2-5D&E) and the drugs showed a significant interaction in the WT animals for this parameter (Table 2-1D). Finally, the anabolic treatments were equally efficacious for improving other aspects of cortical geometry (Table 2-4A). Therefore, although the loss of *Nmp4* did not further improve the combination treatments restorative efficacy, the gain in trabecular bone (Figures 2-2A&B) did not compromise the improved gains in the cortical compartment.

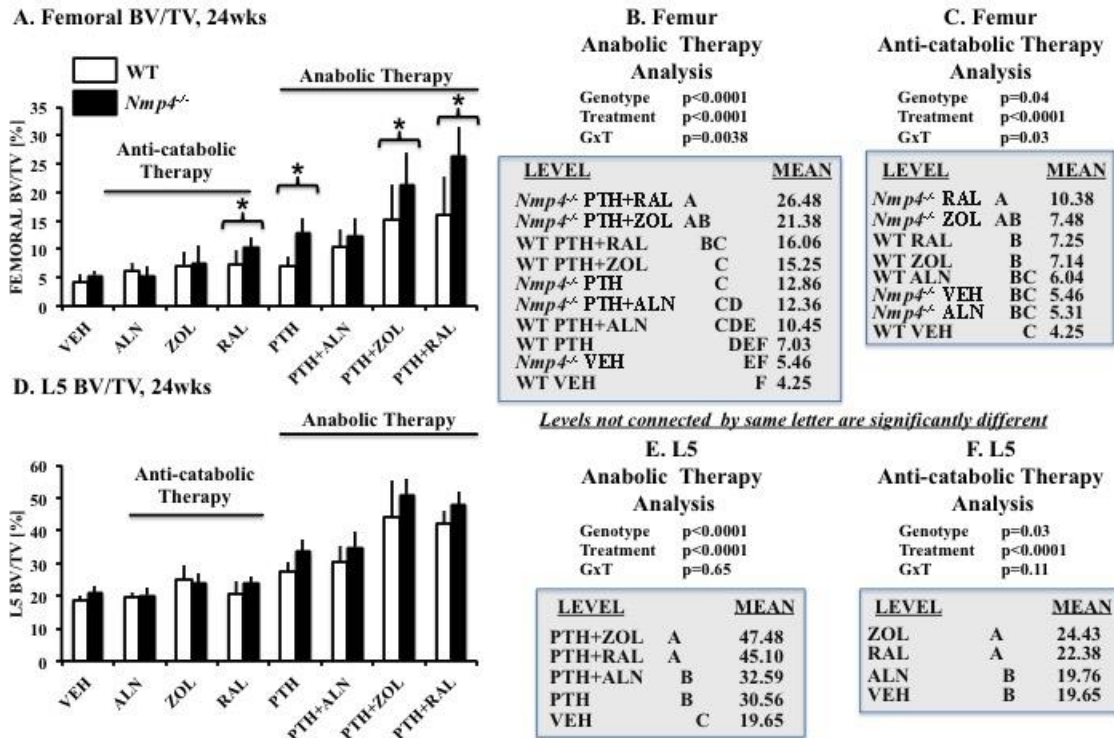


Figure 2-2: [A-C] Femoral BV/TV and [D-F] L5 BV/TV for all the experimental cohorts (age 24wks) comparing ovx'd WT and *Nmp4*^{-/-} mice. [B, E] We compared the anabolic therapies PTH+RAL, PTH+ZOL, PTH+ALN, and PTH to each other and to VEH. [C, F] we compared the anti-catabolic treatments ALN, ZOL, RAL to each other and to VEH. Statistical analyses were performed using 2W ANOVAs setting genotype and treatment as the independent variables. Statistical significance was set at p≤0.05. The asterisk denotes genotype x treatment interaction. The data represents average ± SD, n=7-12 mice/group. See text for explanation of results.

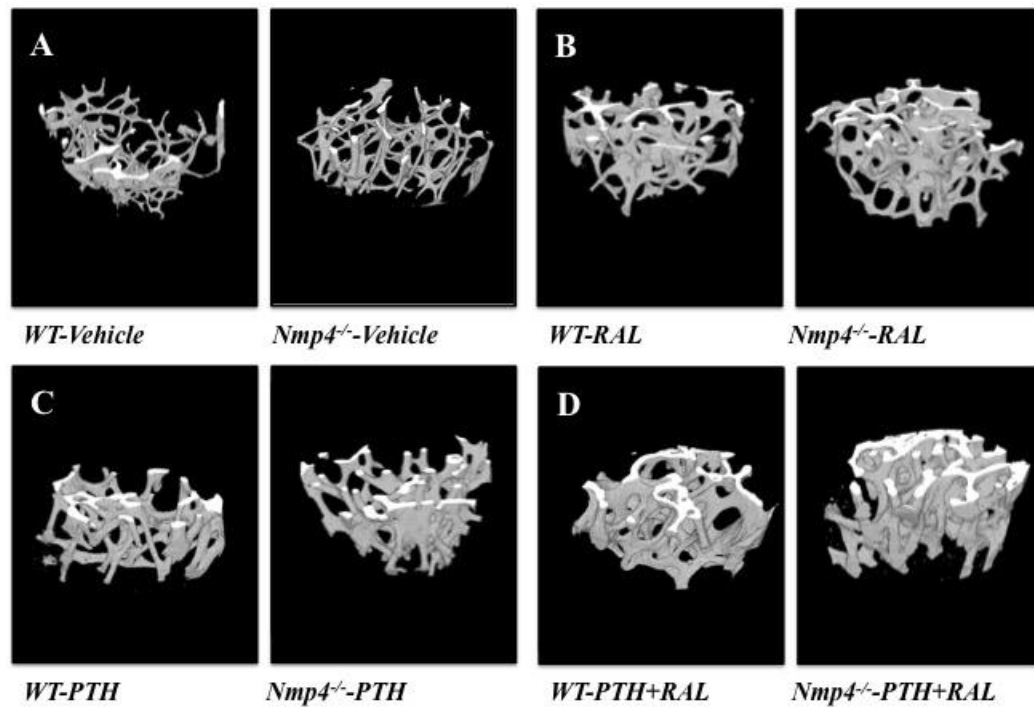


Figure 2-3: The 3-D μ CT images of the femoral distal femur from WT and *Nmp4*^{-/-} mice (24wks of age). Mice were ovx'ed at 12wks of age and treated with the indicated therapies from 16wks to 24wks [A] Vehicle control; [B] RAL monotherapy; [C] PTH mono-therapy; [D] PTH+RAL combination therapy.

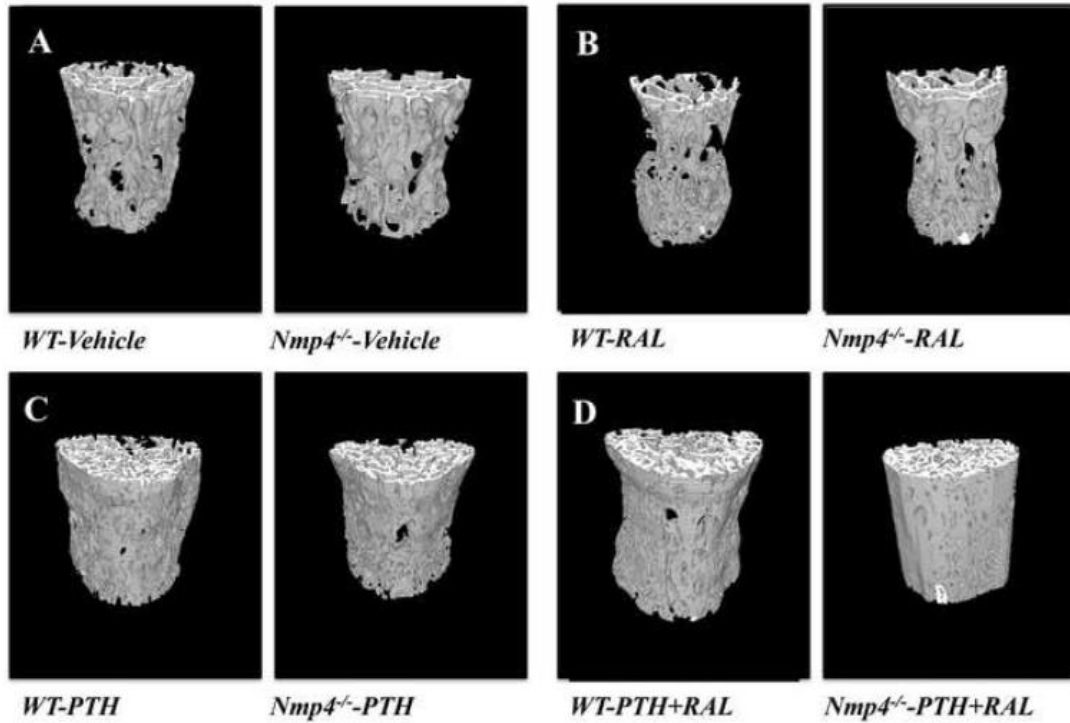


Figure 2-4: 3-D μ CT images of the L5 vertebra from from WT and *Nmp4*^{-/-} mice (24wks of age). Mice ovx'ed at 12wks of age and treated with the indicated therapies from 16wks to 24wks [A] Vehicle control; [B] RAL mono-therapy; [C] PTH mono-therapy; [D] PTH+RAL combination therapy.

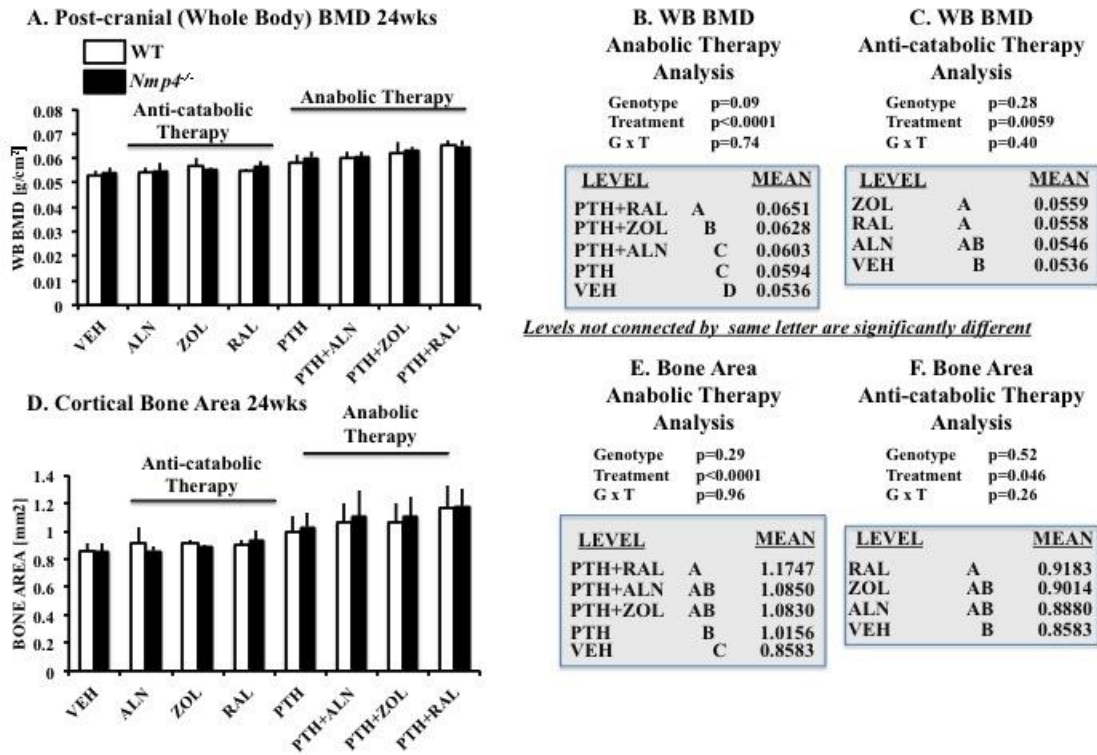


Figure 2-5: [A-C] Post-cranial (Whole Body) BMD and [D-F] Cortical bone area of femoral diaphysis for all the experimental cohorts comparing ovx'd WT and *Nmp4*^{-/-} mice (age 24wks). [B, E] We compared the anabolic therapies PTH+RAL, PTH+ZOL, PTH+ALN, and PTH to each other and to VEH. [C, F] we compared the anti-catabolic treatments ALN, ZOL, RAL to each other and to VEH. Statistical analyses were performed using 2W ANOVAs setting genotype and treatment as the independent variables. Statistical significance was set at $p \leq 0.05$. The data represents average \pm SD, n=5-12 mice/group. See text for explanation of results.

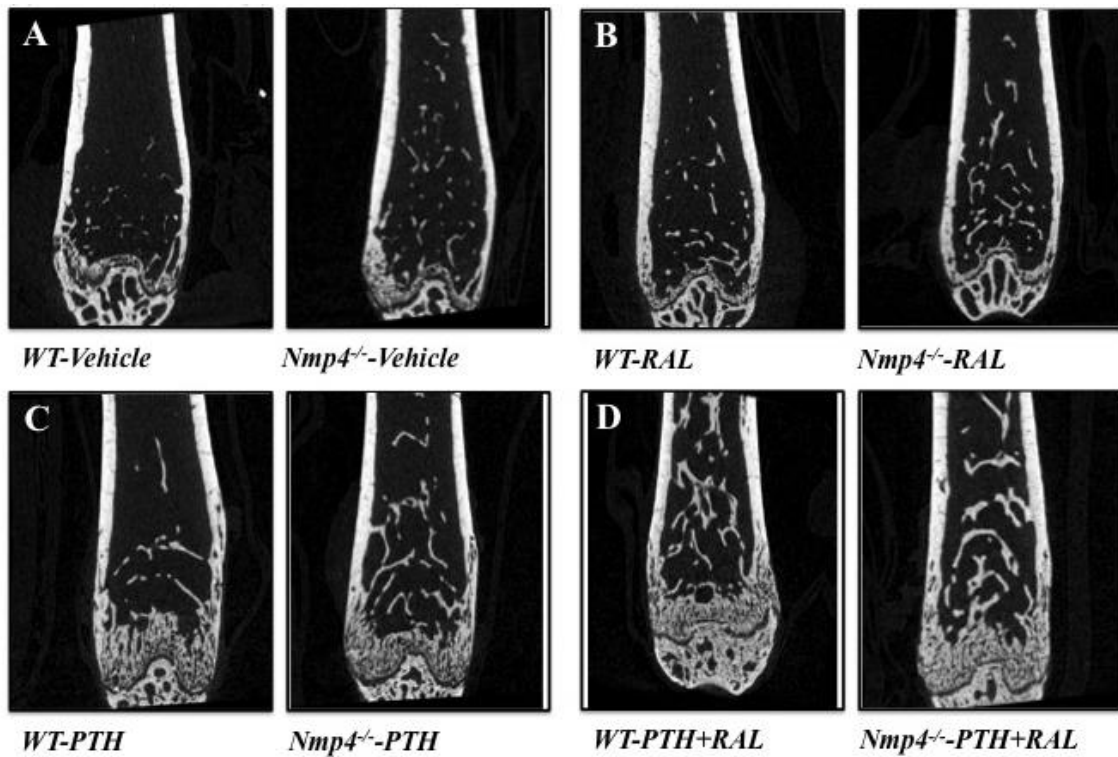


Figure 2-6: The 2-D μ CT images of the femoral distal femur from WT and *Nmp4*^{-/-} mice ovx'ed at 12wks of age and treated with the indicated therapies from 16wks to 24wks [A] Vehicle control; [B] RAL mono-therapy; [C] PTH mono-therapy; [D] PTH+RAL combination therapy.

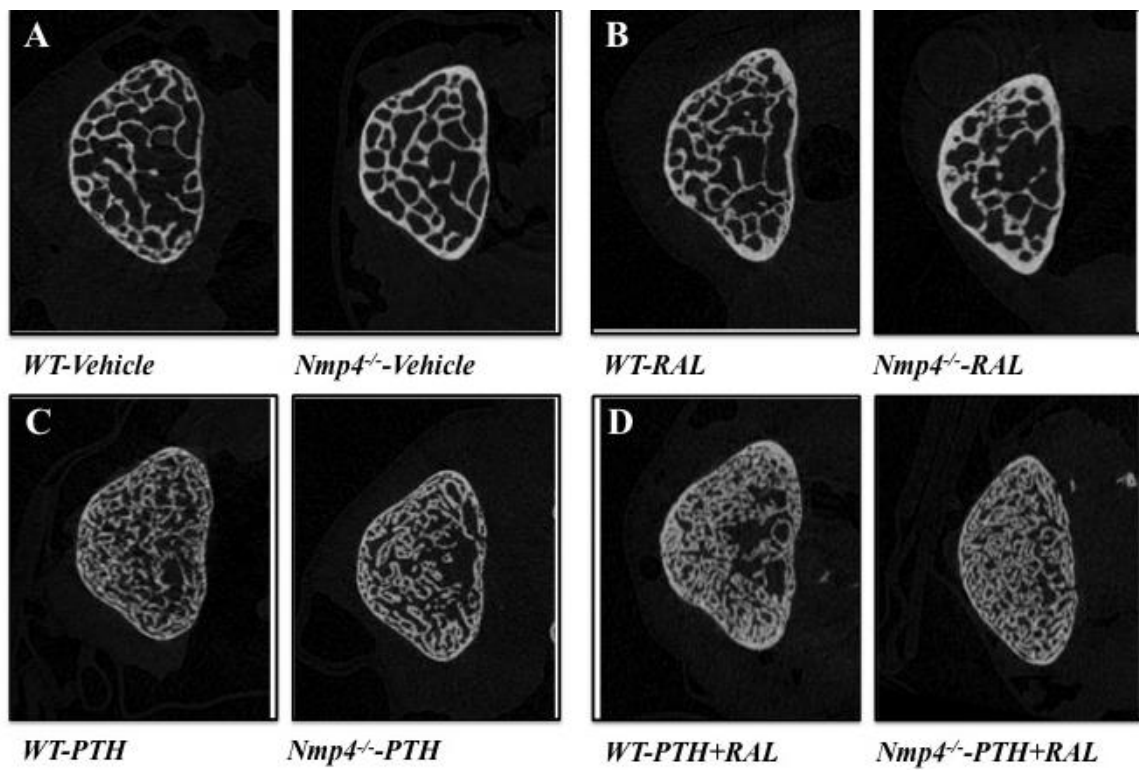


Figure 2-7: 2-D μ CT images of the L5 vertebra from mice ovx'ed at 12wks of age and treated with the indicated therapies from 16wks to 24wks [A] Vehicle control; [B] RAL mono-therapy; [C] PTH mono-therapy; [D] PTH+RAL combination therapy.

THERAPY	p-value PTH Treatment	p-value Anti-catabolic Treatment	p-value PTH x Anti-catabolic interaction
Table 2-1A: FEMUR BV/TV			
PTH+ALN [WT]	p<0.0001	p=0.0001	p=0.19
PTH+ALN [<i>Nmp4^{-/-}</i>]	p<0.0001	p=0.55	p=0.91
PTH+ZOL [WT]	p<0.0001	p<0.0001	p=0.02
PTH+ZOL [<i>Nmp4^{-/-}</i>]	p<0.0001	p<0.0001	p=0.01
PTH+RAL [WT]	p<0.0001	p<0.0001	p=0.0139
PTH+RAL [<i>Nmp4^{-/-}</i>]	p<0.0001	p<0.0001	p=0.001
Table 2-1B: L5 BV/TV			
PTH+ALN [WT]	p<0.0001	p=0.05	p=0.31
PTH+ALN [<i>Nmp4^{-/-}</i>]	p<0.0001	p=0.84	p=0.38
PTH+ZOL [WT]	p<0.0001	p<0.0001	p=0.02
PTH+ZOL [<i>Nmp4^{-/-}</i>]	p<0.0001	p<0.0001	p<0.0001
PTH+RAL [WT]	p<0.0001	p<0.0001	p=0.0002
PTH+RAL [<i>Nmp4^{-/-}</i>]	p<0.0001	p<0.0001	p<0.0001
Table 2-1C: WB BMD			
PTH+ALN [WT]	<0.0001	0.04	0.65
PTH+ALN [<i>Nmp4^{-/-}</i>]	<0.0001	0.50	0.64
PTH+ZOL [WT]	<0.0001	0.0003	0.8258
PTH+ZOL [<i>Nmp4^{-/-}</i>]	<0.0001	0.0034	0.3620
PTH+RAL [WT]	<0.0001	<0.0001	0.0007
PTH+RAL [<i>Nmp4^{-/-}</i>]	<0.0001	<0.0001	0.1807
Table 2-1D: CORTICAL BONE AREA			
PTH+ALN [WT]	0.0001	0.0867	0.9113
PTH+ALN [<i>Nmp4^{-/-}</i>]	<0.0001	0.2717	0.3244
PTH+ZOL [WT]	<0.0001	0.0663	0.8497
PTH+ZOL [<i>Nmp4^{-/-}</i>]	<0.0001	0.1095	0.5698
PTH+RAL [WT]	<0.0001	0.0081	0.0407
PTH+RAL [<i>Nmp4^{-/-}</i>]	0.0009	<0.0001	0.1487

Table 2-1: Identification of synergy between PTH and anti-catabolic drugs using a series of 2 way ANOVAs comparing the efficacy of the PTH mono-therapy, a specific anti-catabolic mono-therapy and the combination of the two drugs. Statistical significance was set at p≤0.05.

Table 2-2A: femoral trabecular parameters anabolic therapies

GROUP	FEMORAL Tb.N	FEMORAL Tb.Th	FEMORAL Tb.Sp
VEH: WT/ <i>Nmp4</i> ^{-/-}	0.91±0.23/1.18±0.09	0.046±0.006/0.045±0.003	0.331±0.023/0.285±0.011
PTH: WT/ <i>Nmp4</i> ^{-/-}	1.27±0.17/1.99±0.21	0.058±0.002/0.065±0.002	0.345±0.038/0.264±0.023
PTH+ALN: WT/ <i>Nmp4</i> ^{-/-}	1.71±0.43/1.96±0.45	0.059±0.004/0.063±0.004	0.275±0.020/0.263±0.029
PTH+ZOL: WT/ <i>Nmp4</i> ^{-/-}	2.07±0.65/2.74±0.47	0.072±0.008/0.081±0.006	0.282±0.039/0.235±0.034
PTH+RAL: WT/ <i>Nmp4</i> ^{-/-}	2.16±0.78/3.23±0.49	0.075±0.005/0.081±0.008	0.263±0.041/0.202±0.032
Anabolic Therapy	G: p<0.0001 T: p<0.0001 GxT: p=0.02 <i>Nmp4</i> ^{-/-} PTH+RAL A <i>Nmp4</i> ^{-/-} PTH+ZOL AB WT PTH+RAL BC WT PTH+ZOL C <i>Nmp4</i> ^{-/-} PTH C <i>Nmp4</i> ^{-/-} PTH+ALN C WT PTH+ALN CD WT PTH DE <i>Nmp4</i> ^{-/-} VEH DE WT VEH E	G: p<0.0001 T: p<0.0001 GxT: p=0.0427 <i>Nmp4</i> ^{-/-} PTH+RAL A <i>Nmp4</i> ^{-/-} PTH+ZOL A WT PTH+RAL AB WT PTH+ZOL BC <i>Nmp4</i> ^{-/-} PTH CD <i>Nmp4</i> ^{-/-} PTH+ALN DE WT PTH+ALN DE WT PTH E <i>Nmp4</i> ^{-/-} VEH F WT VEH F	G: p<0.0001 T: p<0.0001 GxT: p=0.0123 WT PTH A WT VEH A <i>Nmp4</i> ^{-/-} VEH B WT PTH+ZOL B WT PTH+ALN BC <i>Nmp4</i> ^{-/-} PTH BC WT PTH+RAL BC <i>Nmp4</i> ^{-/-} PTH+ALN BC <i>Nmp4</i> ^{-/-} PTH+ZOL CD <i>Nmp4</i> ^{-/-} PTH+RAL D

Table 2-2B: femoral trabecular parameters anti-catabolic therapies

GROUP	FEMORAL Tb.N	FEMORAL Tb.Th	FEMORAL Tb.Sp
VEH: WT/ <i>Nmp4</i> ^{-/-}	0.91±0.23/1.18±0.09	0.046±0.006/0.045±0.003	0.331±0.023/0.285±0.011
ALN: WT/ <i>Nmp4</i> ^{-/-}	1.17±0.25/1.14±0.29	0.051±0.006/0.046±0.004	0.302±0.007/0.294±0.023
ZOL: WT/ <i>Nmp4</i> ^{-/-}	1.38±0.38/1.47±0.47	0.052±0.003/0.049±0.007	0.316±0.032/0.282±0.029
RAL: WT/ <i>Nmp4</i> ^{-/-}	1.21±0.36/1.74±0.13	0.060±0.003/0.059±0.005	0.313±0.023/0.274±0.011
Anti-Catabolic Therapy	G: p=0.0024 T: p<0.0001 GxT: p=0.0306 <i>Nmp4</i> ^{-/-} RAL A <i>Nmp4</i> ^{-/-} ZOL AB WT ZOL AB WT RAL BC <i>Nmp4</i> ^{-/-} VEH BC WT ALN BC <i>Nmp4</i> ^{-/-} ALN BC WT VEH C	G: p=0.0701 T: p<0.0001 RAL A ZOL B ALN B VEH B GxT: p=0.22	G: p<0.0001 T: p<0.2017 GxT: p=0.04 WT VEH A WT ZOL AB WT RAL AB WT ALN ABC <i>Nmp4</i> ^{-/-} ALN BC <i>Nmp4</i> ^{-/-} VEH BC <i>Nmp4</i> ^{-/-} ZOL BC <i>Nmp4</i> ^{-/-} RAL C

Table 2-2: The μ CT analyses of the femoral architecture in mice treated with [A] the anabolic therapies and [B] mice treated with the anti-catabolic therapies. The data were analyzed using 2 way ANOVAs using genotype and treatment as the

independent variables. Statistical significance was set at $p \leq 0.05$ and levels not connected by the same letter are significantly different. The data represents average \pm SD, n=7-12 mice/group.

Table 2-3A: L5 trabecular parameters anabolic therapies

GROUP	L5 Tb.N	L5 Tb.Th	L5 Tb.Sp
VEH: WT/ <i>Nmp4</i> ^{-/-}	3.71±0.21/3.79±0.15	0.051±0.003/0.054±0.003	0.250±0.013/0.239±0.017
PTH: WT/ <i>Nmp4</i> ^{-/-}	5.82±0.64/6.26±0.49	0.047±0.002/0.054±0.002	0.191±0.020/0.182±0.021
PTH+ALN: WT/ <i>Nmp4</i> ^{-/-}	6.24±0.93/6.49±0.62	0.049±0.002/0.053±0.003	0.188±0.025/0.170±0.017
PTH+ZOL: WT/ <i>Nmp4</i> ^{-/-}	8.24±0.1.87/9.0±0.85	0.053±0.003/0.057±0.002	0.156±0.044/0.135±0.023
PTH+RAL: WT/ <i>Nmp4</i> ^{-/-}	7.79±0.65/8.05±0.81	0.052±0.002/0.061±0.002	0.172±0.003/0.159±0.027
Anabolic Therapy	G: p=0.0483 T: p<0.0001 PTH+ZOL A PTH+RAL A PTH+ALN B WT PTH B VEH C GxT: p=0.76	G: p<0.0001 T: p<0.0001 GxT: p=0.0010 <i>Nmp4</i> ^{-/-} PTH+RAL A <i>Nmp4</i> ^{-/-} PTH+ZOL B <i>Nmp4</i> ^{-/-} PTH BC <i>Nmp4</i> ^{-/-} VEH BCD WT PTH+ZOL CD <i>Nmp4</i> ^{-/-} PTH+ALN CD WT PTH+RAL CD WT VEH DE WT PTH+ALN EF WT PTH F	G: p=0.0091 T: p<0.0001 VEH A PTH B PTH+ALN B PTH+RAL BC PTH+ZOL C GxT: p=0.94

Table 2-3B: L5 trabecular parameters anti-catabolic therapies

GROUP	L5 Tb.N	L5 Tb.Th	L5 Tb.Sp
VEH: WT/ <i>Nmp4</i> ^{-/-}	3.71±0.21/3.79±0.15	0.051±0.003/0.054±0.003	0.250±0.013/0.239±0.017
ALN: WT/ <i>Nmp4</i> ^{-/-}	3.81±0.29/3.66±0.27	0.051±0.003/0.055±0.003	0.247±0.008/0.241±0.018
ZOL: WT/ <i>Nmp4</i> ^{-/-}	5.08±0.89/4.42±0.54	0.049±0.004/0.053±0.001	0.232±0.028/0.233±0.021
RAL: WT/ <i>Nmp4</i> ^{-/-}	4.01±0.40/4.44±0.34	0.049±0.003/0.054±0.002	0.245±0.026/0.230±0.019
Anti-Catabolic Therapy	G: p=0.4554 T: p<0.0001 ZOL A RAL B VEH C ALN C GxT: p=0.0067	G: p<0.0001 T: p=0.31 GxT: p=0.87	G: p=0.12 T: p=0.23 GxT: p=0.64

Table 2-3: The μ CT analyses of the L5 trabecular architecture in mice treated with [A] the anabolic therapies and [B] mice treated with the anti-catabolic therapies. The data were analyzed using 2 way ANOVAs comparing the anabolic therapies and the anti-catabolic mono-therapies. Statistical significance was set

at $p \leq 0.05$ and levels not connected by the same letter are significantly different.
The data represents average \pm SD, n=7-12 mice/group.

Table 2-4A: cortical geometry anabolic therapies

GROUP	Cortical Thickness	Marrow Area	Total Area	Endocortical Perimeter	Periosteal Perimeter
VEH: WT/KO	0.190±0.016/ 0.184±0.007	0.964±0.096/ 0.958±0.026	1.841±0.109/ 1.834±0.092	3.843±0.185/ 3.861±0.121	5.243±0.167/ 5.242±0.175
PTH: WT/KO	0.201±0.009/ 0.196±0.009	1.029±0.090/ 0.992±0.069	2.028±0.118/ 2.024±0.096	2.028±0.118/ 3.955±0.088	5.508±0.172/ 5.476±0.130
PTH+ALN: WT/KO	0.200±0.014/ 0.197±0.007	1.046±0.082/ 0.907±0.129	2.074±0.078/ 2.015±0.145	4.104±0.214/ 4.023±0.302	5.633±0.076/ 5.497±0.235
PTH+ZOL: WT/KO	0.207±0.009/ 0.198±0.011	1.012±0.084/ 0.957±0.092	2.074±0.159/ 2.061±0.126	4.038±0.151/ 4.301±0.477	5.595±0.246/ 5.543±0.220
PTH+RAL: WT/KO	0.206±0.015/ 0.203±0.020	0.891±0.136/ 0.822±0.149	2.061±0.116/ 2.005±0.111	3.958±0.404/ 3.860±0.262	5.550±0.225/ 5.546±0.327
Anabolic Therapy	G: p=0.0501 T: p=0.0003 PTH+RAL A PTH+ZOL A PTH A PTH+ALN A VEH B GxT: p=0.92	G: p=0.0028 T: p<0.0001 PTH A PTH+ZOL A PTH+ALN A VEH A PTH+RAL B GxT: p=0.92	G: p=0.23 T: p<0.0001 PTH+ZOL A PTH+ALN A PTH+RAL A PTH A VEH B GxT: p=0.89	G: p=0.9952 T: p=0.0029 PTH+ZOL A PTH+ALN AB PTH AB PTH+RAL B VEH B GxT: p=0.18	G: p=0.28 T: p<0.0001 PTH+ZOL A PTH+ALN A PTH+RAL A PTH A VEH B GxT: p=0.86

Table 2-4B: cortical geometry anti-catabolic therapies

GROUP	Cortical Thickness	Marrow Area	Total Area	Endocortical Perimeter	Periosteal Perimeter
VEH: WT/KO	0.190±0.016/ 0.184±0.007	0.964±0.096/ 0.958±0.026	1.841±0.109/ 1.834±0.092	3.843±0.185/ 3.861±0.121	5.243±0.167/ 5.242±0.175
ALN: WT/KO	0.187±0.013/ 0.181±0.012	0.968±0.050/ 0.963±0.085	1.865±0.099/ 1.836±0.112	3.870±0.143/ 3.874±0.161	5.251±0.105/ 5.204±0.162
ZOL: WT/KO	0.189±0.010/ 0.192±0.007	1.033±0.091/ 0.994±0.072	1.944±0.080/ 1.879±0.078	4.116±0.183/ 3.925±0.158	5.477±0.170/ 5.308±0.140
RAL: WT/KO	0.202±0.010/ 0.206±0.010	0.856±0.076/ 0.892±0.054	1.757±0.063/ 1.827±0.084	3.761±0.123/ 3.820±0.125	5.153±0.098/ 5.271±0.191
Anti-Catabolic Therapy	G: p=0.62 T: p<0.0001 RAL A ZOL B VEH B ALN B GxT: p=0.92	G: p=0.83 T: p<0.0001 ZOL A ALN A VEH A RAL B GxT: p=0.58	G: p=0.72 T: p=0.0094 ZOL A ALN AB VEH AB RAL B GxT: p=0.25	G: p=0.46 T: p=0.0010 ZOL A ALN B VEH B RAL B GxT: p=0.12	G: p=0.52 T: p=0.0073 ZOL A VEH B ALN B RAL B GxT: p=0.10

Table 2-4: The μ CT analyses of the femoral cortical geometry in mice treated with [A] the anabolic therapies and [B] mice treated with the anti-catabolic therapies.. The data were analyzed using 2 way ANOVAs comparing the anabolic therapies and the anti-catabolic mono-therapies. Statistical significance

was set at $p \leq 0.05$ and levels not connected by the same letter are significantly different. The data represents average \pm SD, n=7-12 mice/group.

Effects of Anti-Catabolic Treatments On Bone

RAL and ZOL promoted modest bone restoration; loss of Nmp4 further augmented RAL-induced increases in femoral trabecular bone

The *Nmp4* skeletal phenotype appears to be largely driven by the hyper-anabolic activity of osteogenic cells (Childress et al., 2015; He et al., 2013; Hino et al., 2007). Nevertheless, the response of the *Nmp4*^{-/-} mice to anti-resorptive therapy alone had not been reported therefore we analyzed the therapeutic efficacy of the SERM RAL, and the bisphosphonates ALN and ZOL on ovariectomized WT and *null* mice. The RAL and ZOL mono-therapies, significantly improved femoral and L5 BV/TV (Figures 2-2C&F), as well as WB BMD and cortical bone area (Figures 2-5C&F). However, RAL was particularly notable in that it was the only anti-catabolic that increased femoral Tb.Th in both genotypes (Table 2-2B), enhanced cortical area over the VEH cohorts (Figure 2-5F), and the only anti-resorptive that increased femoral cortical thickness and decreased femoral marrow area (Table 2-4B).

Unexpectedly, loss of *Nmp4* enhanced RAL-induced increases in femoral BV/TV compared to WT mice (genotype x treatment interaction p=0.03, Figure 2-2C). Moreover, under the RAL mono-therapy the *null* cohorts showed significantly higher femoral Tb.N and exhibited a lower femoral Tb.Sp compared to WT mice (Table 2-2B). Disabling *Nmp4* did not amplify the response to the bisphosphonates. This would suggest that *Nmp4* suppresses a SERM-mediated pathway(s) mediating femoral trabecular bone restoration in our preclinical model.

The Effects of Combination Treatments using Anabolic Agents on Osteoprogenitor Cells

The combination of PTH, RAL and loss of Nmp4 significantly expanded the bone marrow osteoprogenitor pool but had no similar impact on the number of marrow adipocytes or TRAP+ cells

To address the cellular basis underlying the improved femoral trabecular bone response of *Nmp4*^{-/-} mice over the WT animals we counted various cell

types in formalin-fixed, paraffin-embedded bone marrow sections using immunohistochemical analysis. We also employed flow cytometry to obtain bone marrow cellular profiles. Based on the μ CT imaging results we largely limited our focus to vehicle-control, the RAL, ZOL, and PTH mono-therapies, and the PTH+RAL and PTH+ZOL combination treatments.

We counted bone marrow cells that were positive for the early osteoblast-specific transcription factor Osterix (Nakashima et al., 2002) as one method to identify osteoprogenitors (Figures 2-9A-F). *Nmp4*^{-/-} mice under the PTH+RAL therapy harbored more osteoprogenitors than the WT cohorts treated with this regimen (genotype x treatment effect $p=0.0048$, Figures 2-8A&B). Additionally, the *null* mice harbored significantly more bone marrow osteoprogenitors under the PTH+RAL therapy than under the PTH+ZOL treatment but the WT cohorts did not exhibit this dichotomy (Figures 2-8A&B). As a complementary approach we performed flow cytometry analysis of WT and *Nmp4*^{-/-} bone marrow CD45⁻/CD105⁺/CD146⁺/nestin⁺ cells, which have been used as markers to identify MSPC/osteoprogenitors (Mizoguchi et al., 2014; Sacchetti et al., 2007) (Figure 2-8D&E). As observed with IHC staining the *Nmp4*^{-/-} mice under the PTH+RAL therapy exhibited a significantly expanded population of these cells compared to WT mice treated with this combination regimen (treatment x genotype $p=0.0004$, Figures 2-8D&E). Moreover, as determined with the IHC analysis, the flow cytometry analysis revealed that the *null* mice harbored significantly more bone marrow CD45⁻/CD105⁺/CD146⁺/nestin⁺ cells under the PTH+RAL therapy than under the PTH+ZOL treatment and that the WT cohorts did not exhibit this contrast (Figures 2-8D&E).

We next addressed whether the anabolic treatment regimens and/or loss of *Nmp4* altered bone marrow adiposity because in addition to osteoprogenitors, MSPCs can differentiate into bone marrow fat cells. Treatments that included PTH, i.e. PTH mono-therapy, PTH+ZOL and PTH+RAL significantly decreased the number of bone marrow adipocytes (Figures 2-10A&B). Bone marrow sections from the VEH cohorts exhibited a high number of adipocytes throughout the marrow and near the growth plate, but adipocyte numbers were strikingly

lower in marrow from cohorts that included PTH in the treatment regimen (Figures 2-11A&B). However unlike the case with the osteoprogenitors, loss of *Nmp4* did not alter the frequency of these cells in the bone marrow and therefore did not appear to have a direct or indirect effect on adipogenic lineage commitment in our model.

We assessed femoral TRAP+S/BS as an indicator of osteoclast activity and whether *Nmp4* regulated the number of these cells under the anabolic treatments (Figures 2-10D&E). In contrast to the osteoprogenitor profiles, loss of *Nmp4* did not impact the number of TRAP+ cells under the PTH+RAL regimen or any of the other anabolic treatments (genotype x treatment $p=0.08$, Figure 2-10B). The PTH+RAL WT/*Nmp4*^{-/-} cohorts had fewer TRAP+ cells than the PTH groups but both were equivalent to PTH+ZOL- and VEH-treated mice (treatment effect $p=0.02$, Figure 2-10E).

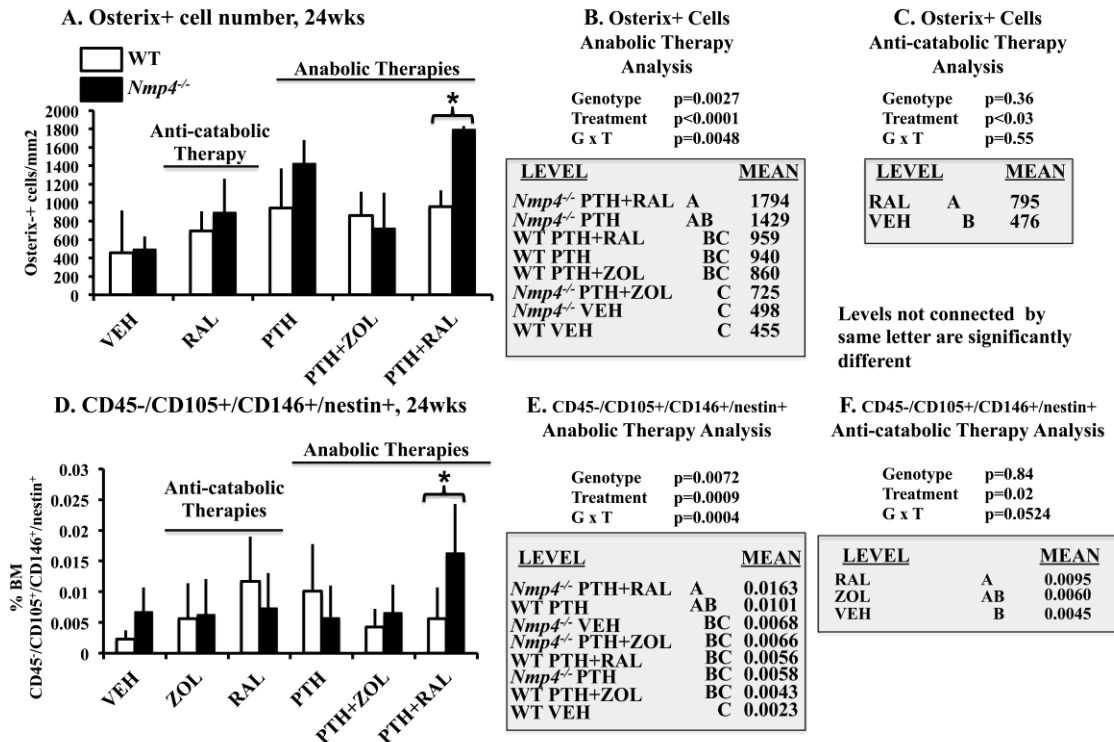


Figure 2-8: [A-C] Bone marrow osterix+ cells and [D-F] Flow cytometry analysis of the means of the frequency of femoral bone marrow CD45⁻/CD105⁺/CD146⁺/CD105⁺/nestin⁺ cells in ovx'ed WT and *Nmp4*^{-/-} mice (24wks of age). [B, E] We

compared the anabolic therapies PTH+RAL, PTH+ZOL, PTH, with each other and with VEH using either osterix+ expression or the expression profile of CD45⁻/CD105⁺/CD146⁺/CD105⁺/nestin⁺ as the endpoints. [C] We compared the number of osterix+ cells in the WT and *Nmp4*^{-/-} RAL mono-therapy cohorts [F] We compared the anti-catabolic treatments ZOL and RAL to each other and to VEH using the expression profile of CD45⁻/CD105⁺/CD146⁺/CD105⁺/nestin⁺ as the endpoint. Statistical analyses were performed using 2W ANOVAs setting genotype and treatment as the independent variables. Statistical significance was set at $p \leq 0.05$. The asterisk denotes genotype x treatment interaction. The data represents average \pm SD, n=4-6 osterix+ cells and n=7-12 mice/group for flow cytometry. See text for explanation of results.

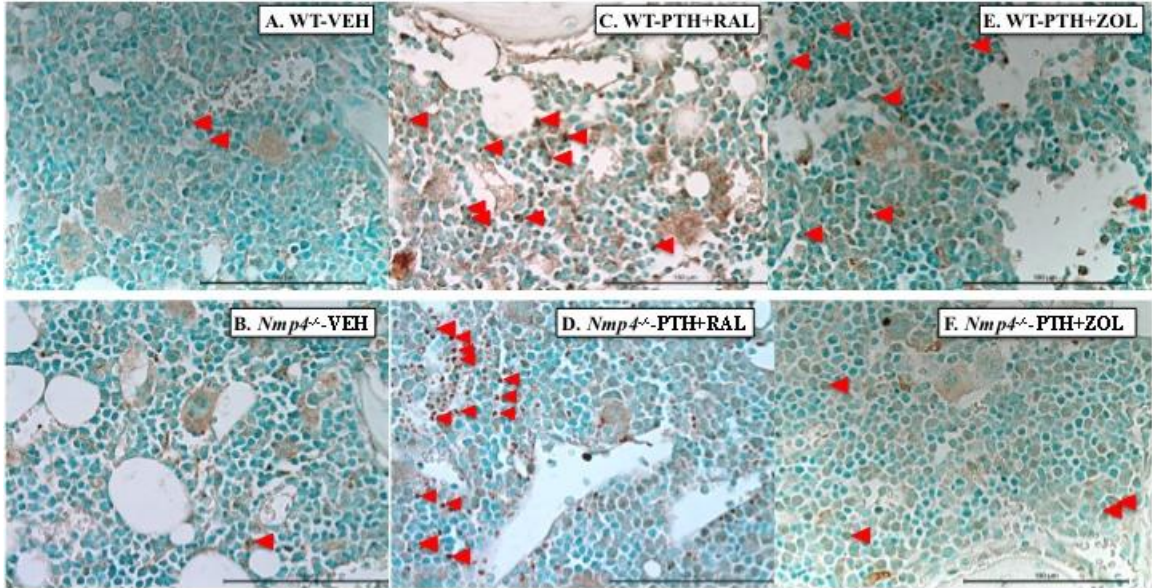


Figure 2-9: Immunohistochemical analysis of bone marrow osterix-positive cells. Osterix was detected as a brown coloration in the cell nucleus (arrowheads) on formalin-fixed, paraffin-embedded sections as described in the Materials and Methods. Representative sections are shown from [A, B] the WT and *Nmp4*^{-/-} VEH cohorts, [C, D] the WT and *Nmp4*^{-/-} PTH+RAL cohorts, and [E, F] the WT and *Nmp4*^{-/-} PTH+ZOL cohorts.

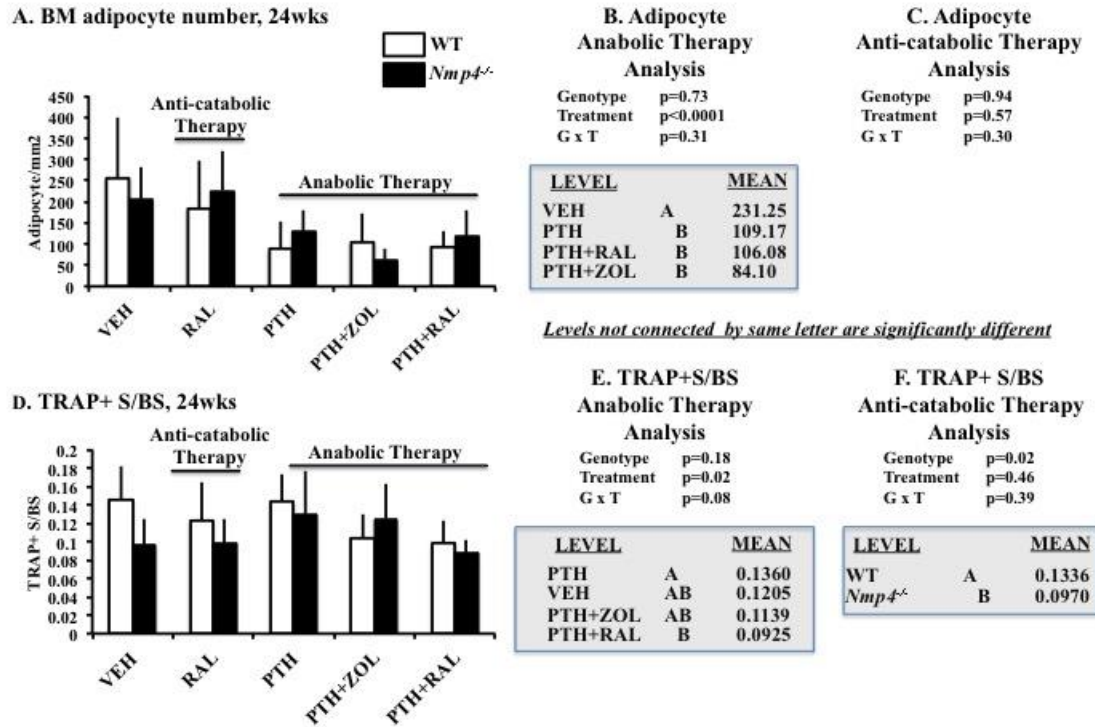


Figure 2-10: [A-C] Bone marrow adipocytes and [D-F] TRAP+ S/BS for WT and *Nmp4^{-/-}* mice (24wks of age). [B, E] We compared the anabolic therapies PTH+RAL, PTH+ZOL and PTH, with each other and with VEH using either adipocyte number or TRAP+S/BS as the endpoints [C, F] We compared the number of adipocytes or the TRAP+S/BS in the WT and *Nmp4^{-/-}* RAL mono-therapy cohorts. Statistical analyses were performed using 2W ANOVAs setting genotype and treatment as the independent variables. Statistical significance was set at $p \leq 0.05$. The data represents average \pm SD, $n=5$ fields from 6 mice/cohort for the adipocytes and $n=6$ mice/group (TRAP+ S/BS). See text for explanation of results.

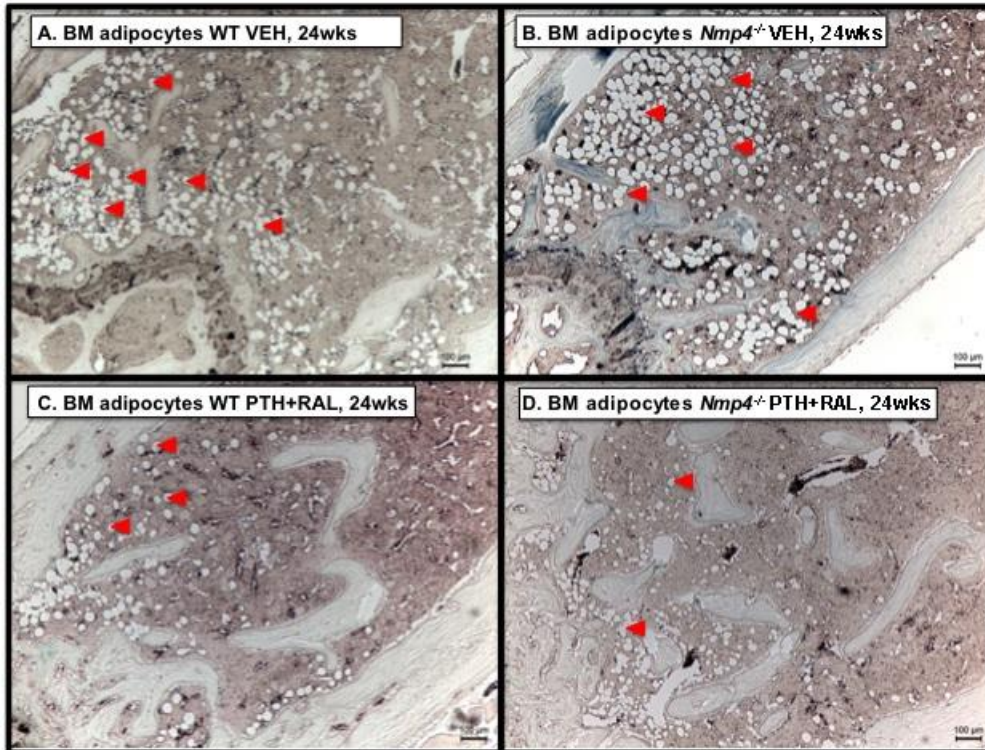


Figure 2-11: Immunohistochemical analysis of bone marrow adiposity. Adipocytes were detected with Sudan Black B (arrowheads) on formalin-fixed, paraffin-embedded sections as described in the Materials and Methods. Tissue sections stained with Sudan Black B showed the relatively small number of adipocytes in the WT and *Nmp4*^{-/-} PTH+RAL cohort compared to the vehicle-treated groups.

Effects of Anti-Catabolic Treatments on Osteoprogenitor Cells

We next addressed the impact of RAL, ZOL, and *Nmp4* on the bone marrow osteoprogenitor pool in the anti-catabolic arm of the study. The RAL mono-therapy significantly elevated the number of osteoprogenitors compared to VEH cohorts as determined by both IHC and flow cytometry analyses but loss of *Nmp4* did not impact the response of these cell populations to this anti-resorptive (Figures 2-8C&F). ZOL mono-therapy did not significantly alter the number of CD45⁻/CD105⁺/CD146⁺/nestin⁺ cells compared to the VEH cohorts (Figure 2-8F). RAL mono-therapy had no impact on adipocyte number ($p=0.57$, Figure 10C) or TRAP⁺ S/BS (treatment effect $p=0.46$, Figure 2-10F) in our preclinical model. The statistical comparison between the RAL mono-therapy and VEH cohorts indicated that the *null* mice harbored fewer TRAP⁺ cells than WT animals (genotype effect $p=0.02$, Figure 2-10F). This genotype difference was not observed when analyzing the anabolic cohorts (Figure 2-10E).

We conclude that the combination of PTH, RAL, and loss of *Nmp4* is strongly restorative or nurturing for bone marrow osteoprogenitors and that the substitution of ZOL for RAL abrogates this tonic effect in the *null* mice. Moreover, the loss of *Nmp4* does not influence the number of bone marrow adipocytes or TRAP⁺ cells under the strongly anabolic PTH+RAL therapy.

Effects of Treatments on Bone Turnover Markers

Nmp4 status did not influence serum profile response to any treatment

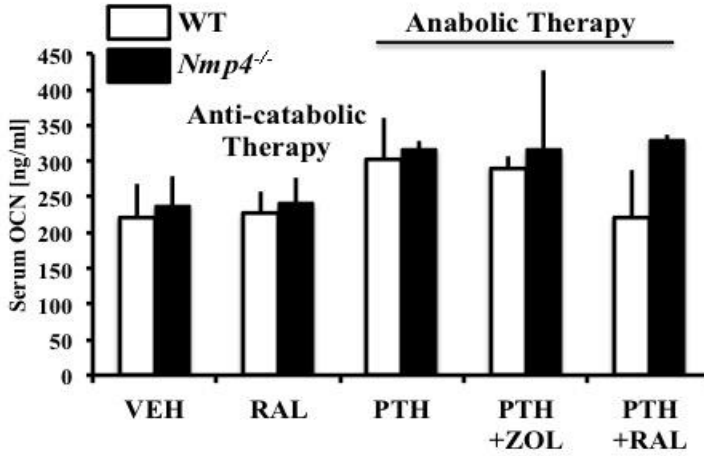
To address the impact of *Nmp4* on serum bone formation and resorption makers of select therapies we evaluated osteocalcin, CTX, and the RANKL/OPG ratio in mice under the PTH, RAL, PTH+RAL, PTH+ZOL and VEH therapies. Loss of *Nmp4* elevated levels of the serum bone formation marker osteocalcin in mice under the anabolic therapies however there was no genotype x treatment interaction (genotype effect, $p=0.01$, genotype x treatment, $p=0.12$, Figures 2-12A&B). The treatment groups PTH and PTH+ZOL exhibited significantly elevated serum osteocalcin compared to VEH controls whereas the PTH+RAL

cohorts were not significantly different from either VEH or the other two groups (treatment effect, $p=0.0022$, Figure 2-12B).

Disabling *Nmp4* had no impact on serum CTX and serum RANKL/OPG (no genotype effect or genotype x treatment interaction, Figures 2-12C~G). Analysis by treatment groups showed that mice from the PTH+RAL therapy exhibited significantly elevated serum CTX levels compared to mice from the PTH+ZOL and VEH treatments (Figure 2-12D). The PTH+ZOL cohorts exhibited a significantly larger RANKL/OPG ratio than PTH and PTH+RAL but none of these treatments were statistically different from the VEH controls (Figure 2-12F).

The RAL mono-therapy did not alter serum osteocalcin or CTX. This treatment did however elevate RANKL/OPG (Figure 2-12G). Therefore only serum osteocalcin, and not the resorption markers, could broadly discriminate between the genotypes (genotype effect $p=0.0107$, Figure 2-12B). However, *Nmp4* status did not influence how any of treatments altered serum marker profiles (no genotype x treatment interactions, Figure 2-12A~G). Finally, we noticed that the parameters of osteoclast size and bone resorption did not necessarily move in a parallel manner in our analysis. We have reported on this phenomenon before in healthy, non-ovariectomized *Nmp4*^{-/-} mice (Childress et al., 2011). This dissociation between CTX levels and osteoclast area may be due in part to the fact that CTX is a systemic measurement whereas osteoclast area is a local measurement. An example of a similar observation is described in the Prx1-Cre; RBPjk^{fl/fl} mouse (Tu et al., 2012). Finally, Weinstein and colleagues report that long-term alendronate treatment 412 is associated with an increase in the number of osteoclasts, and an increase in osteoclast size in healthy postmenopausal women (Weinstein et al., 2009).

A. Serum osteocalcin (OCN), 24wks

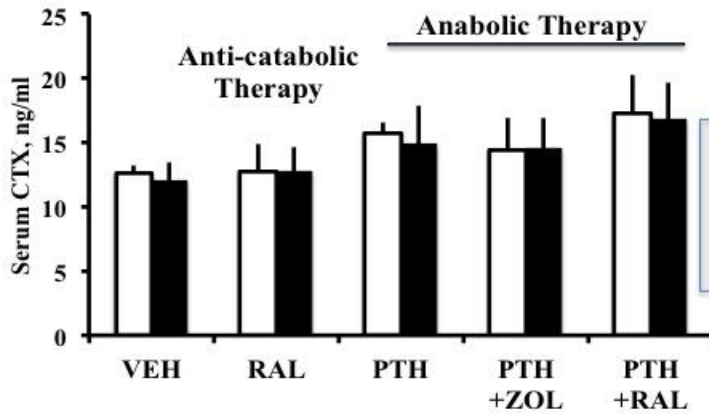


B. OCN Anabolic Therapy Analysis

Genotype p=0.0107
 Treatment p=0.0022
 G x T p=0.12

LEVEL	MEAN
PTH	A 310
PTH+ZOL	A 303
PTH+RAL	AB 275
VEH	B 229

C. Serum CTX, 24wks

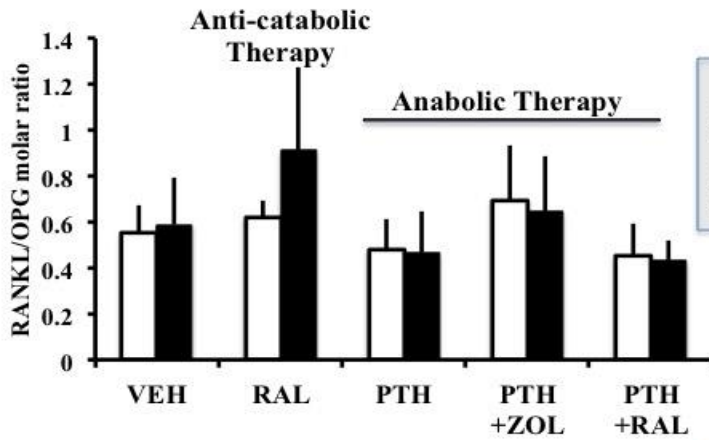


D. CTX Anabolic Therapy Analysis

Genotype p=0.49
 Treatment p<0.0001
 G x T p=0.95

LEVEL	MEAN
PTH+RAL	A 17.04
PTH	AB 15.26
PTH+ZOL	BC 14.45
VEH	C 12.31

E. Serum RANKL/OPG, 24wks



F. RANKL/OPG Anabolic Therapy Analysis

Genotype p=0.83
 Treatment p=0.0150
 GxT p=0.94

LEVEL	MEAN
PTH+ZOL	A 0.670
VEH	AB 0.570
PTH	B 0.474
PTH+RAL	B 0.441

G. RANKL/OPG Anti-catabolic Therapy Analysis

Genotype p=0.83
 Treatment p=0.0150
 GxT p=0.94

LEVEL	MEAN
RAL	A 0.766
VEH	B 0.570

Levels not connected by same letter are significantly different

FIGURE 2-12: [A, B] Serum osteocalcin (OCN) [C, D] serum CTX, and [E, F] serum RANKL/OPG for WT and *Nmp4^{-/-}* mice (24wks of age). [B, D, F] We compared the anabolic therapies PTH+RAL, PTH+ZOL and PTH, with each other and with VEH using the three serum parameters as endpoints [G] We compared VEH with RAL-monotherapy using RANKL/OPG as the endpoint. Statistical analyses were performed using 2W ANOVAs setting genotype and treatment as the independent variables. Statistical significance was set at $p \leq 0.05$. The data represents average \pm SD, $n=6-7$ (OCN, CTX, RANKL/OPG). See text for explanation of results.

DISCUSSION

The blunting of PTH bone-forming efficacy may be a principal limitation of osteoporosis combination therapies (Eriksen and Brown, 2016). We have previously demonstrated that deletion of *Nmp4* enhances PTH-induced trabecular bone formation in experimental mice and as such the goals of this study were to determine whether combining this sustained anabolic response with an anti-catabolic results in superior bone acquisition compared to either PTH mono-therapy. Additionally we inquired whether *Nmp4* interferes with anti-catabolic efficacy. In principle, PTH combination therapies have the potential to maximize skeletal mass while maintaining a tonic level of remodeling by boosting bias toward bone formation and minimizing loss from resorption. We evaluated 7 therapies against a control including three anti-catabolics singly and in concurrent combination with PTH in a preclinical osteoporosis model, comparing skeletal improvement in WT and *Nmp4*^{-/-} mice. The PTH+RAL and PTH+ZOL combination treatments outperformed the PTH mono-therapy throughout the skeleton and loss of *Nmp4* further leveraged the potency of these bone-restoring osteoanabolic regimens in some of the trabecular compartments. Unexpectedly, the *Nmp4*^{-/-} mice also exhibited an enhanced femoral BV/TV response to RAL mono-therapy. These improvements in the restoration of the trabecular bone compartment did not come at the expense of gains in cortical bone. Altogether, this is an exciting proof of principle in scenarios of heightened osteoanabolism combination treatment can be more effective than PTH alone.

The bone-forming efficacy of the concurrent PTH combination treatments in this study generally corresponded with PTH+RAL=PTH+ZOL>PTH+ALN=PTH>VEH, which parallels the results observed in several individual clinical studies thus supporting the medical relevance of our novel findings and the potential clinical impact of disabling *Nmp4*. Deal *et al.* compared the efficacy of PTH mono-therapy with concurrent PTH+RAL in 117 postmenopausal women over a 6-month period (Deal et al., 2005). BMD in the concurrent group was numerically higher than the PTH mono-therapy at the spine and hip, but this increase was only statistically significant at the hip (Deal et al., 2005). In the

PATH study (Black et al., 2003) treatments of naive women were randomized to 3 groups: i) PTH mono-therapy; ii) ALN mono-therapy and iii) concurrent PTH+ALN. Quantitative computed tomography (QCT) revealed severe blunting of BMD increases to PTH in the PTH+ALN group. Finally, patients on concurrent PTH+ZOL therapy were compared to patients on ZOL alone or PTH mono-therapy (Cosman et al., 2011). Contrary to the results obtained with ALN in the PATH study, greater increases in BMD were observed with concurrent PTH+ZOL treatment, than the mono-therapies (Black et al., 2003; Cosman et al., 2011; Deal et al., 2005; Eriksen and Brown, 2016). In the present study PTH and RAL showed a synergistic drug interaction throughout the analyzed skeletal sites including the whole body BMD, cortical bone area, femur and L5 trabecular bone volume. PTH+ZOL generally equaled the therapeutic performance of PTH+RAL with respect to bone gain but the synergistic interaction of PTH and ZOL was more limited with respect to skeletal sites. PTH+ALN was the least efficacious of the concurrent combination therapies and did not outperform the PTH mono-therapy.

The loss of *Nmp4* further improved the gains in femoral trabecular bone obtained with the concurrent PTH+RAL and PTH+ZOL combination treatments and with the RAL mono-therapy, resolving our primary queries as to whether the heightened osteoanabolism of the *Nmp4*^{-/-} skeleton would boost the restorative response to diverse osteoporosis treatments. We observed a strong genotype x treatment interaction under the anabolic therapies of PTH, PTH+RAL, and PTH+ZOL for femoral BV/TV and for multiple trabecular bone architectural parameters. The improved RAL mono-therapy-induced increases in femoral BV/TV and other trabecular architectural parameters were unanticipated since the *Nmp4*^{-/-} skeletal phenotype is distinguished by the exaggerated response to anabolic cues (Childress et al., 2015; He et al., 2013; Hino et al., 2007; Morinobu et al., 2005; Yang et al., 2010). And indeed in the present study the *Nmp4*^{-/-} mice showed no improved response with the bisphosphonates.

The hyper-anabolic phenotype of the *Nmp4*^{-/-} bone marrow osteoprogenitors and their progeny likely drive the improved responses to the

osteoporosis therapies observed in the present study. Moreover, loss of *Nmp4* had no effect on the cellular or serum parameters of the resorption arm in cohorts under the anabolic therapies. The elevated expressions of c-MYC and GADD34 in the *Nmp4*^{-/-} cells (Young et al., 2016) may underlie their precocious and enhanced mineralization in culture (Childress et al., 2015). c-MYC is a potent inducer of ribosome biogenesis (Van Riggelen et al., 2010) and the *Nmp4*^{-/-} MSPCs show significantly elevated global protein synthesis (Young et al., 2016), consistent with the increased bone matrix production. The subsequent increase in the load of ER client proteins typically triggers the UPR, which in turn diminishes global protein synthesis via the phosphorylation of eIF2 α (Chambers and Marciniak, 2014). Upon resolution of ER stress GADD34 serves as a feedback mechanism to dephosphorylate eIF2 α , facilitating resumption of protein synthesis. However in the *Nmp4*^{-/-} cells the high expression of GADD34 maintains elevated matrix synthesis throughout UPR activation without initiating apoptosis (Young et al., 2016).

In the present study, the PTH+RAL therapy significantly expanded the bone marrow pool of the *Nmp4*^{-/-} hyper-anabolic osteoprogenitors. Although the RAL mono-therapy increased the number of these cells in both genotypes the heightened osteoanabolism of the *Nmp4*^{-/-} osteoprogenitors and their progeny is consistent with the enhanced RAL-induced increase in femoral BV/TV compared to the WT mice. RAL has been shown to have tonic effects on osteogenic cells both *in vivo* and *in vitro*, depending on the model system, and the concentration and duration of exposure to this drug (Giner et al., 2011; Lin et al., 2004; Liu et al., 2000; Matsumori et al., 2009; Miki et al., 2009; Somjen et al., 2011; Taranta et al., 2002; Viereck et al., 2003). The ZOL mono-therapy had no impact on this bone marrow population in our study but the substitution of ZOL for RAL in the concurrent combination regimen abrogated the expansion of the *Nmp4*^{-/-} osteoprogenitor pool suggesting that the PTH+ZOL combination lacked the boost to this cell population provided by combining PTH with RAL. Bisphosphonates have both tonic as well as toxic effects on osteogenic cells depending on various factors (Corrado et al., 2010; Lezcano et al., 2014; Pan et al., 2004; Plotkin et al.,

1999; Pozzi et al., 2009). Therefore, *Nmp4* may play a role in osteogenic cell response to anti-catabolics without influencing the impact of these drugs on the resorption arm. This may explain why treatment with the amino-bisphosphonate ALN was less successful at enhancing bone mass than the amino-bisphosphonate ZOL when applied either alone or in combination with PTH. There are a number of factors that may explain the differences between ALN and ZOL efficacy in our study. ZOL is a significantly more potent bisphosphonate than ALN due in part to its stronger binding to both farnesyl pyrophosphate synthase enzyme and to bone (Russell et al., 2008). Interestingly, the frequency of dosing may also contribute to the differences obtained in our investigation and prior studies. Specifically, osteoblasts may take up bisphosphonates by pinocytosis leading to the inhibition of the mevalonate pathway and it has been speculated that the more frequent dosing with ALN compared to ZOL may increase exposure of osteoblasts to bisphosphonates from the interstitial fluid (Eriksen and Brown, 2016). However, in the present model the PTH+ZOL therapy was equally effective as the PTH+RAL treatment at increasing femoral BV/TV. This observation is consistent with a previous study showing that intermittent PTH significantly increased the luciferase activity of tagged bone marrow stromal cells (BMSCs) used to generate bony ossicles implanted in immuno-compromised mice, but combining ZOL with PTH treatment reduced this hormone-mediated increase in luciferase activity without attenuating the PTH-induced increase in total bone (Pettway et al., 2008). Therefore it is likely that osteoprogenitors alone do not drive the heightened pharmacologically-induced osteoanabolism of the *Nmp4*^{-/-} mouse and that bone lining cells, osteoblasts, and perhaps osteocytes also contribute to this phenotype. Studies using conditional deletion of this gene are required to fully interrogate the cellular hierarchy of the *Nmp4*^{-/-} skeletal phenotype.

The implication regarding osteoporosis treatment is that disabling *Nmp4* will boost whatever anabolic activity is associated with any particular therapy. Suppression of sclerostin, a bone formation inhibitor with the drug romosozumab represents a route to bone anabolism and is proof of principle that impeding

osteogenic inhibitors is a powerful approach to therapy (Jilka, 2009). *Nmp4* is another kind of inhibitor in that its inactivation boosts the response potency to osteoanabolics but unlike romozosumab does not impact baseline skeletal phenotype.

The expansion of the *Nmp4*^{-/-} osteogenic reserve did not appear to occur at the expense of marrow adipogenic potential. Bone marrow fat cells derive from heterogeneous populations of MSCs, not all of which have the capacity for committing to the adipogenic lineage (Chan et al., 2015; Yue et al., 2016). Our present data revealed no genotype effect for adipocyte number. However, these data showed a strong treatment effect in that PTH-based therapies reduced bone marrow adipogenesis in both the WT and *Nmp4*^{-/-} mice. This is consistent with the previous observations that osteoporosis patients as well as ovariectomized rats exhibit an enhanced fat in the marrow (Cordes et al., 2016; Kulkarni et al., 2007) and that PTH attenuates marrow adiposity in both rats (Kulkarni et al., 2007) and in postmenopausal osteopenic women (Yang et al., 2016).

The improved gains in the *Nmp4*^{-/-} L5 trabecular architecture were more moderate than those observed in the femur although loss of *Nmp4* increased L5 BV/TV across the anabolic treatment groups as a whole and improved anabolic therapeutic thickening of the trabeculae. The observed weaker response of the rodent spine to PTH-based therapies compared with that of the femur is consistent with previous observations in C57BL/6 mice and is perhaps related to weight bearing (Iida-Klein et al., 2002).

The exaggerated recovery of *Nmp4*^{-/-} trabecular bone did not come at the cost of therapeutic gains in the cortical compartment. We previously demonstrated that the *Nmp4*^{-/-} osteoprogenitors express elevated levels of the *PTH1R* receptor and that these *null* cells exhibited an exaggerated response to hormone challenge (Childress et al., 2015). Calvi *et al.*, reported that constitutively active PTH1R in osteoblasts resulted in mice with increased trabecular bone volume but decreased cortical thickness (Calvi et al., 2001). Additionally, the elevation in PTH-induced remodeling typically leads to increased cortical porosity (Burr et al., 2001; Dempster et al., 1993; Fox et al., 2007;

Hansen et al., 2013) with potentially detrimental effects on bone strength (Eriksen and Brown, 2016). However, our present data showed that the exaggerated response to PTH and the concurrent combination therapies in the *Nmp4*^{-/-} mice did not compromise improvements in cortical area and cortical thickness nor WB BMD, which is typically 80% cortical.

“The quest will continue for the ‘holy grail’ of anabolic osteoporosis therapies, which will optimize the impact on bone formation relative to resorption” (Black and Schafer, 2013). This medical objective requires the use of clinical, preclinical, and basic science research. Jilka has incisively described the advantages and limitations of mouse models for investigating the pathophysiology of osteoporosis and its treatment (Jilka, 2013) and the present model is no exception. However, the principal extraordinary feature of the *Nmp4*^{-/-} phenotype is the exaggerated skeletal responses to diverse osteoanabolic therapies while bone development, growth and baseline phenotype are all largely unexceptional in the absence of provocation (Childress et al., 2011; Childress et al., 2015; Morinobu et al., 2005; Robling et al., 2009). This demonstrates a clear and unique advantage of developing *Nmp4* or one of its upstream/downstream components as a target to significantly improve efficacy of existing therapies. Moreover, since the loss of *Nmp4* appears to enhance the response potency to other anabolic signals (Morinobu et al., 2005), we propose that abaloparatide or other PTH peptides may produce a similar heightened anabolism in these mice. Finally, this unique preclinical tool provides an opportunity for investigating the intrinsic critical barriers to pharmacologically-induced bone formation.

CONTRIBUTIONS

In the project described above, I took part in the mice treatment, DXA scanning and tissue collection (i.e. serum and bone); I also conducted the immunohistochemistry, part of the serum analysis (i.e. OCN) and part of the statistical analysis.

CHAPTER 3

MAPPING THE *Nmp4* ANTI-ANABOLIC BONE TRANSCRIPTOME

INTRODUCTION

Several questions remain to be addressed to clarify the cellular and molecular mechanisms driving the *Nmp4*^{-/-} hyper-anabolism phenotype. What pathways and biological functions are altered in naïve and early-differentiating MSCs? What key regulators are involved in these pathways and biological functions altered by NMP4? How do these alterations contribute to the *Nmp4*^{-/-} anabolic phenotype? To answer these questions, we undertook transcriptome analysis of non-differentiated and early osteogenic-differentiating MSCs. Pathway analysis and results from manually annotating this RNA-seq data provided a more comprehensive overview of the *Nmp4*^{-/-} osteogenic cell phenotype. For example loss of *Nmp4* alters the expression profile of multiple matrix proteins that regulate the mechanical properties of bone. Additionally, the alterations in the *null* cell transcriptome indicated that NMP4 regulates cellular metabolism. This analysis provided thorough descriptions of the changes induced by disabling *Nmp4* in pathways controlling the secretory machinery of the cell. Of interest disabling NMP4 also perturbs pathways that regulate the immunomodulatory phenotype of mesenchymal stem cells. Guided by this pathway analysis we evaluated some aspects of (i) bone material properties, (ii) cell metabolism, and (iii) the unfolded protein response.

MATERIALS AND METHODS

Cell culture

Expanded mesenchymal stem/progenitor cell (MSC) cultures were established as previously described (Childress et al., 2015; Wu et al., 2006). Briefly, the BM mononuclear cells (BMMNCs) were flushed from the femurs and tibias of 6~8-week old WT or *Nmp4*^{-/-} mice, isolated by Ficoll gradient, plated in Mesencult™ Media+Mesencult™ Stimulatory Supplement (StemCell™ Technologies, Vancouver BC, Canada) and maintained in culture for 3-4 weeks

without passaging. Every 5-7 days 50% of the culture media was replaced. The cells were then passaged at 1:3 dilutions for 5 passages at 80% confluence. The cells were only used for experiments between passage 5 and 10.

To induce osteogenic differentiation of MSCs, WT and *Nmp4^{-/-}* MSCs between passage 5 and 10 were seeded into 12-well plates at 25,000 cells/well in α MEM medium. After 48 hours, the medium was replaced by osteogenic medium, which was comprised of α MEM medium supplemented with 50 μ g/ml ascorbic acid (Sigma-Aldrich), 10mM glycerol 2-phosphate disodium salt hydrate (BGP, Sigma-Aldrich) and 10nM dexamethasone (Sigma-Aldrich). The osteogenic medium was replenished on a regular basis until clear sign of mineralization could be observed under the microscope and the cells were stained with Alizarin red. To study the effect of GADD34 inhibition on mineralization, the aforementioned protocol was used and 5 μ M of salubrinal or same amount of dimethyl sulfoxide (DMSO as vehicle) was added to the medium 48 hours after the initial seeding.

To prepare naïve and early-differentiating MSCs for RNA-Seq analysis, WT and *Nmp4^{-/-}* MSCs between passage 5 and 10 were seeded into 12-well plates at either 10,000 cells/well or 25,000 cells/well. The plates with 10,000 cells/well were cultured in Mesencult Medium supplemented with Mesencult Stimulatory Supplement for 3 days before harvest. The plates with 25,000 cells/well were induced for osteogenic differentiation as described above and the cells were harvested on Day 7 post-seeding. RNeasy Mini Kit (QIAGEN) was used to harvest mRNA. Each sample had 4 replicates.

Alizarin red staining for mineralization

The mineralized cells were washed in 1X Hank's balanced salt solution (HBSS), fixed in 10% formalin for 30 minutes, and then washed in water. Subsequently, the cells were stained with Alizarin red S (pH=4.2) for 7 minutes and washed in water 3 times before scanning for images.

RNA-Seq

Total RNA was harvested; the concentration and quality of each RNA

sample were measured and evaluated. Only samples with the ratio of 260/280 >2 and RNA integrity number (RIN) >8 were used for subsequent RNA-Seq assay. Samples were submitted to Beijing Genomics Institute (BGI) for transcriptome sequencing. In brief, magnetic beads with Oligo (dT) were used to isolate mRNA and synthesize cDNA. The cDNA was fragmented and then constructed into HiSeq 2000 strand-specific libraries. The 2 × 100-nt paired-end reads were generated by Illumina HiSeq™ 2000. Clean reads filtered from raw sequence reads were returned from BGI. The following rules were used by BGI to filter raw reads into clean reads: 1) Remove reads in which the percentage of bases with quality <10 was >50%. 2) Remove reads in which unknown bases were more than 10%. 3) Remove reads with adapters. The clean reads were mapped to *Mus musculus* reference mm10 using STAR (version 2.4.2a) (Dobin et al., 2013). Gene-based expression levels were quantified with featureCounts (Liao et al., 2014). Differential expression of genes across different treatments was determined with edgeR (Robinson et al., 2010). Expression of all genes was normalized based on the expression of *Gusb*.

Bioinformatics profiling

The RNA-Seq data on day 3 was filtered by the following criteria: 1) Fold change between *Nmp4*^{-/-} and WT counts per million (cpm) must be greater than 2 or less than -2; 2) FDR<0.05. In this scenario, only genes that are differentially expressed in WT and *Nmp4*^{-/-} MSPCs would be selected and submitted to IPA. The RNA-Seq data on day 7 was analyzed in the same way. The genes passing these filters were defined as “candidate NMP4 targets”. IPA produced two parameters for each pathway: p-value and activation z-score. While the p-value described whether the impact of NMP4 on a specific pathway was statistically significant; the activation z-score described whether the pathway was activated (z-score>2) or inhibited (z-score<-2) in *Nmp4*^{-/-} cells. Pathways of interests were then selected. Other than direct IPA output, We also manually annotated the RNA-seq data set by compiling gene lists of pathways or proteins of special interest in osteoblast biology. All of these genes for each pathway or function of interests were presented in heat maps made by “ggplot2” package in R (R Core

Team). We also determined whether these genes of interest have NMP4 binding sites in the promoter and intron regions based on our previous ChIP-Seq study (Childress et al., 2015). The genes were defined as “direct candidate NMP4 targets” if they have binding sites for NMP4 in the promoter and intron regions; otherwise, the genes were defined as “indirect candidate NMP4 targets”.

Seahorse Assay for mitochondria stress test

To determine the profiles of mitochondrial respiration between WT and *Nmp4*^{-/-} MSPC cells, Seahorse Assay was performed using XF Cell Mito Stress Test Kit (Agilent Technologies). Cells were seeded (70,000 cells/well) into XF Cell Culture Microplate 24 hours prior to the experiment. Meanwhile, cartridges were hydrated by placing 1 mL of calibrant into each of the wells in the utility plate and place in a non-CO₂ 37°C incubator overnight. On the next day, assay medium (pH=7.4) that contained XF Base Medium (Agilent Technologies) supplemented with 10 mM glucose, 1 mM pyruvate and 2 mM L-glutamine was added to XF Cell Culture Microplate and incubated for 1 hour in the non-CO₂ 37°C incubator. Four compounds including 1 μM oligomycin, 1 μM carbonyl cyanide-p-trifluoromethoxyphenylhydrazone (FCCP) and 1 μM Rotenone/Antimycin A were then added sequentially to the ports adjacent to each well. The addition of oligomycin leads to suppression of ATP synthase activity, allowing the calculation of oxygen consumption coupled to ATP production; FCCP disrupts the proton gradient across the mitochondrial membrane and uncouples oxygen consumption from ATP production, stimulating the oxygen consumption to the maximum; rotenone and antimycin A are inhibitors of electron transfer complex (ETC) I and III respectively, the addition of which shut down the whole mitochondrial respiration and allow the calculation of non-mitochondrial respiration driven by the process other than mitochondria. The plate was then loaded into and read by XF^e24 Analyzer (Agilent Technologies). During this process, the oxygen consumption rate (OCR) was first measured without the addition of any compounds. The compounds mentioned above were then injected into the wells serially 30 minutes in between and OCRs were measured in each phase. The raw data were then normalized with cell count in each well

and analyzed via Wave (Agilent Technologies).

Several respiration parameters were derived or calculated based on the raw Seahorse Assay data. The OCR before the addition of any compounds represents the basal level respiration (OCR_{basal}). ATP production is represented by oligomycin-induced OCR decrease ($OCR_{\text{oligomycin}} - OCR_{\text{basal}}$). Proton leak is the remaining basal respiration not coupled to ATP production ($OCR_{\text{oligomycin}}$). The maximal respiration (OCR_{FCCP}) is induced by FCCP to stimulate the full capacity of the respiratory chain. The spare respiratory capacity is measured by the OCR increase induced by FCCP ($OCR_{\text{FCCP}} - OCR_{\text{basal}}$) and is an indicator of cell fitness and flexibility when an energetic demand is needed. Finally, the non-mitochondrial respiration ($OCR_{\text{rotenone \& antimycin A}}$) is derived upon the addition of rotenone and antimycin A to the wells.

Mice

As described before, global *Nmp4*^{-/-} mice together with their wild type (WT) littermates were generated by backcrossing with C57BL/6J mice for 7 generations (Robling et al., 2009). The mice were maintained in our colony at Indiana University Bioresearch Facility, Indiana University School of Dentistry. All the husbandry practices and experimental procedures mentioned in this study have been approved by our local Institute Animal Care and Use Committee.

Therapies

At 10wks of age WT and *Nmp4*^{-/-} female mice, intact (estrogen replete) were sorted by weight into eight treatment groups into 8 groups: 1) vehicle-treated WT; 2) vehicle-treated *Nmp4*^{-/-}; 3) PTH-treated WT; 4) PTH-treated *Nmp4*^{-/-}; 5) RAL-treated WT; 6) RAL-treated *Nmp4*^{-/-}; 7) PTH+RAL-treated WT; 8) PTH+RAL-treated *Nmp4*^{-/-}. For vehicle control, the mice received daily subcutaneous injection of PTH diluent (0.2% BSA/1.0 μ N HCl in saline, Abbott Laboratory, North Chicago, IL) and RAL diluent (20% hydroxypropyl- β -cyclodextrin). Mice receiving PTH mono treatment were injected daily subcutaneously with one dose of synthetic human PTH (hPTH) 1–34 acetate salt (Bachem Bioscience, Inc) at 30 μ g/kg and one dose of RAL diluent. Mice receiving RAL mono treatment were injected daily subcutaneously with one dose

of RAL at 1 mg/kg and one dose of PTH diluent. Mice getting PTH+RAL treatment received both PTH and RAL injections subcutaneously every day. All the treatments lasted for 7 weeks (Figure 3-1).

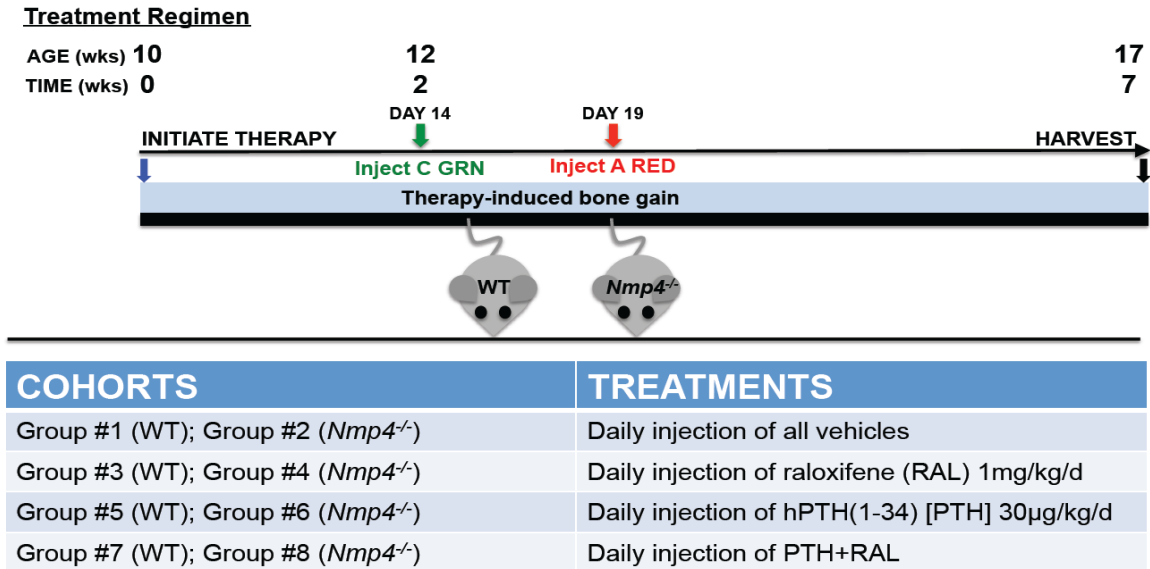


Figure 3-1: At 10wks of age, WT and *Nmp4^{-/-}* mice were sorted into 8 treatment groups by weight and genotype. Each mouse received two sequential 100µl injections/day containing the drugs or vehicle(s) as shown for 7wks. Mice were euthanized and the bones processed for analysis at 17wks of age.

WT and *Nmp4^{-/-}* mice were administered the following treatments:

- Vehicle-control: inject subcutaneously (sc) 100 µl 0.2% Bovine serum albumin/0.1% 1.0 µN HCl in 0.9% NaCl (abbreviation BHN diluent for PTH) + 100 µl 20% Hydroxypropyl-β-Cyclodextrin (abbreviation HBC diluent for raloxifene (RAL) diluent)
- Daily raloxifene (RAL): inject sc 100 µl RAL at 1 mg/kg/d +100 µl BHN
- Daily parathyroid hormone (PTH): inject sc 100 µl synthetic human PTH 1–34 acetate salt, Bachem Bioscience Inc, PA, at 30 µg/kg/d + 100 µl HBC
- Daily PTH+RAL: inject sc 100 µl RAL +100 µl PTH.

Bone Storage

After 7-week treatment, femurs, tibias and L5 vertebrae were collected from 17-week-old WT and *Nmp4^{-/-}* mice. Femurs and tibias were soaked in 0.9%

saline, wrapped with gauze and preserved in -20°C for mechanical testing. L5 vertebra were placed in 10% buffered formalin, 4°C for 48 hours before transferred to 70% ethanol at 4°C until analyzed.

Microcomputed tomography (μCT)

For μCT analysis of the femur, a section of 2.6 mm at the excised distal femoral metaphysis was scanned using a Skyscan 1172. All scans were conducted at a 6 μm scan resolution. For the vertebra the whole bone was scanned by standard methods (Skyscan 1172). The reconstruction and analysis of the bone were then performed using the manufacturer's software. The trabecular and cortical bones were analyzed separately. From the three-dimensional reconstruction, several parameters were acquired using the Skyscan software analysis: trabecular bone volume per total volume (BV/TV, %), trabecular number (Tb.N, mm^{-1}), trabecular thickness (Tb.Th, mm), trabecular spacing (Tb.Sp, mm) and cortical bone area (mm^2). The Skyscan software also afforded the following data for femoral cortical bone: periosteal perimeter (mm), endocortical perimeter (mm), total area (mm^2), marrow area (mm^2), bone area (mm^2), cortical thickness (mm), cortical porosity (%), maximum moment of inertia (I_{max} , mm^4), minimum moment of inertia (I_{min} , mm^4), and polar moment of inertia (I_{p} , mm^4).

Three-point bending

Left femurs from each animal were slowly thawed to room temperature and monotonically tested to failure in three-point bending at a displacement rate of 0.025 mm/sec using a support span of 9 mm. The bones were placed in the anterior-posterior direction with the anterior side in tension. The moment of inertia about the medial-lateral axis and the extreme fiber in the anterior direction were obtained from the μCT images using a seven slice region centered on the failure site, and were utilized to map load-displacement to stress-strain, employing standard beam bending equations. Structural-level and tissue-level mechanical properties were then obtained from the load-displacement and stress-strain curves.

Typical mechanical parameters obtained through this study included yield force and ultimate force. The yield force is the maximal force reached in the elastic phase, when the displacement of the bone can be fully recovered if the external force is removed. The ultimate force is the maximal force reached before the bone fracture occurs. Typical material parameters obtained included yield stress and ultimate stress, both of which were generated from yield force and ultimate force respectively normalized with the bone geometry.

Some other mechanical parameters that interest us include post-yield displacement, total displacement and work to yield; post-yield displacement is measurement of displacement in the plastic phase and is a measure of ductility; total displacement is the displacement from beginning to fracture; work to yield is the total energy absorbed during the elastic phase. Some other material parameters that interest us include total strain, modulus and resilience; total strain is the total deformation withstood by the specimen; modulus is a measure of material stiffness; resilience is the energy absorbed per unit volume during the elastic phase.

Influenza infection

WT and *Nmp4*^{-/-} mice were anesthetized with intraperitoneal injection of Ketamine/Xylazine. After the anesthetization, the animals were held at an upright position and inoculated with influenza A/PR8 (H1N1), ~150 plaque-forming units (pfu) (diluted in serum-free medium) drop wise into the nares. The survival rate of was then observed over 15 days.

Statistical analysis (for bone mechanical study and Seahorse Assay)

To determine the treatment response of WT and *Nmp4*^{-/-} mice to combination therapies and phenotypic difference between WT and *Nmp4*^{-/-} MSCs (e.g. oxygen consumption rate), the statistical package JMP version 7.0.1 was employed (SAS Institute, Cary, NC). Some analyses were performed using SAS version 9.4 (SAS Institute, Cary, NC). Data were first screened for outliers using the IQR method to evaluate the distribution dispersion and all the outliers identified were removed from further analysis. Analyses comparing only two groups were run via student's t test; analyses comparing more than two

groups and involving two independent variables (e.g. genotype and treatment) were run via 2-way ANOVA followed by Tukey-Kramer post hoc test for multiple comparison purposes. The statistic significance was set at $p \leq 0.05$.

RESULTS

Differentiating $Nmp4^{-/-}$ MSPCs mineralize earlier than WT MSPCs

One noteworthy phenotype in $Nmp4^{-/-}$ MSPCs is the cells mineralize faster than the WT counterpart when cultured in osteogenic medium (Childress et al., 2015). We further expanded this study to evaluate the mineralization capacity in other MSPC cell lines, each of which was derived from a single mouse. Of the six MSPC cell lines recruited, two were male WTs, two male $Nmp4^{-/-}$, one female WT and one female $Nmp4^{-/-}$. More specifically, one WT line and one $Nmp4^{-/-}$ line were derived from biological brothers. The mineralization assay showed the $Nmp4^{-/-}$ cells mineralized within 7-9 days after initial seeding, whereas WT cells took 15-24 days to show first sign of mineralization (Figure 3-2). Furthermore, all the $Nmp4^{-/-}$ MSPC lines were heavily mineralized 3 days after mineralization first started while two WT MSPC lines remained lightly mineralized after 3 days (Figure 3-2). The accelerated mineralization in $Nmp4^{-/-}$ MSPCs was consistently observed among different cell lines. Our experimental observations that (i) $Nmp4^{-/-}$ mice exhibit an enhanced PTH-induced increase in bone formation (Childress et al., 2015; Robling et al., 2009; Yu Shao, 2017), (ii) that these mice harbor more bone marrow osteoprogenitors (Childress et al., 2015; He et al., 2013), and (iii) that isolated $Nmp4^{-/-}$ MPSCs exhibit a precocious and enhanced mineralization raised a number of questions about the phenotype of these cells. Do these cells elaborate a unique bone matrix that leads to improved bone material properties? Does loss of $Nmp4$ lead to alterations in the differentiation process? How are the pathways that regulate osteoblast secretion altered? What other changes in the transcriptome support the hyper-anabolic phenotype of these cells?

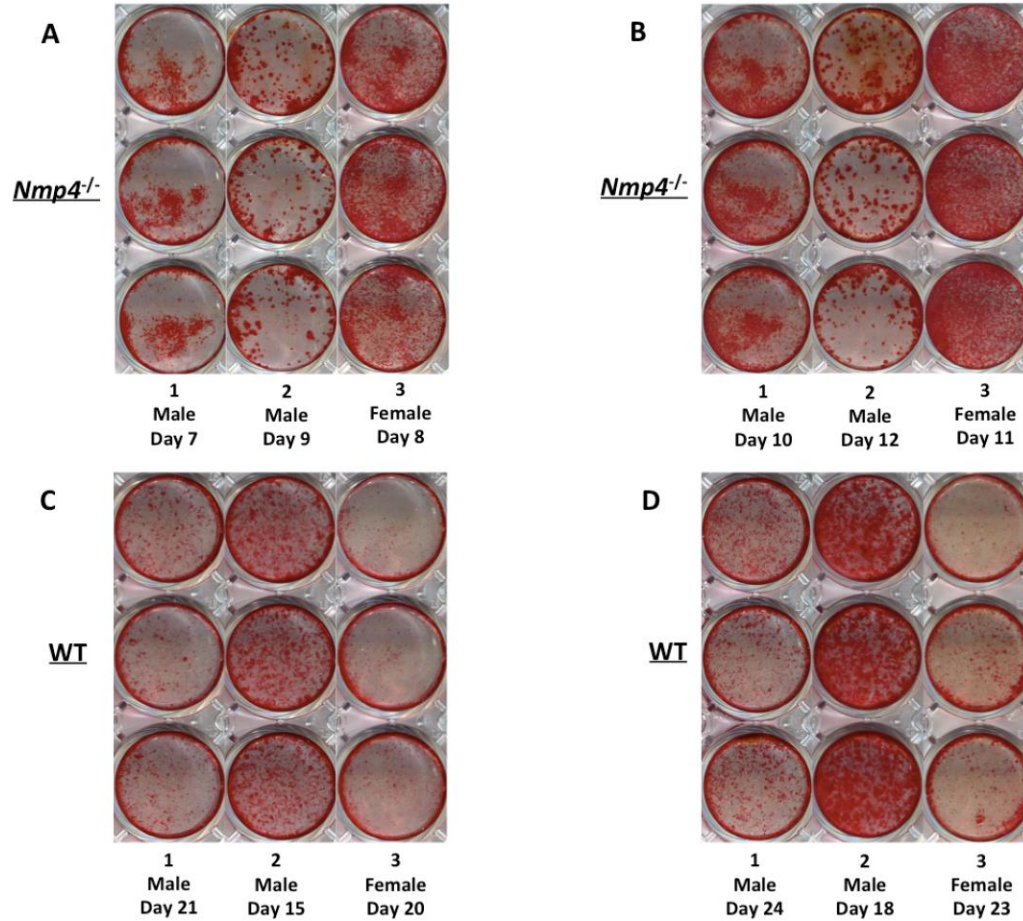


Figure 3-2: Alizarin red staining of the differentiating WT and *Nmp4^{-/-}* MSCs [A] Two male and one female *Nmp4^{-/-}* MSC lines were stained on the first day when mineralization emerged. [B] The same three *Nmp4^{-/-}* MSC lines were stained again 3 days after their first staining. [C] Two male and one female WT MSC lines were stained on the first day when mineralization emerged. [D] The same three WT MSC lines were stained again 3 days after their first staining.

Loss of Nmp4 significantly alters extracellular matrix/mineralization transcriptome

NMP4 is expressed in almost all cell types (Nakamoto et al., 2000; Thunyakitpibal et al., 2001; Young et al., 2016). Our previous ChIP-Seq study showed 2114 core genes were candidate direct targets of NMP4 in 4 different cell lines and NMP4 exerts significant impacts on different cellular and biological functions (Childress et al., 2015). Moreover NMP4 is context-dependent architectural transcription factor that can either upregulate or downregulate a certain gene (Torrunguang et al., 2002). To further understand this anti-anabolic axis regulated by NMP4, it was helpful for us to acquire the gene expression profiles of MSCs upon osteogenic differentiation. As a follow-up study of our previous ChIP-Seq analysis, the RNA-Seq experiment was conducted to compare expression profiles between WT and *Nmp4*^{-/-} MSCs when undifferentiated (Day 3) and during early osteogenic differentiation (Day 7).

As the first step of our transcriptome analysis in *Nmp4*^{-/-} MSCs, we measured the expression of extracellular matrix (ECM) genes and genes regulating mineralization. We manually annotated 77 genes (Chiellini et al., 2008; Kim et al., 2013; Morgan et al., 2015; Robey and Boskey, 2009; Romanello et al., 2014) from our RNA-Seq database into the multiple protein classes that comprise the osteoblast secretome and generated a heatmap from this gene list (Figure 3-3). The ratio of *Nmp4*^{-/-}: WT mRNA expression at Day 3 in culture (uncommitted MSCs) and Day 7 (early osteogenesis) was calculated in the form of log fold change (logFC) and was color coded. Based on our previous findings from our ChIP-Seq analysis, NMP4 might directly regulates multiple ECM genes, particularly the collagenous proteins, proteoglycans, and most importantly those affecting bone mechanical properties; Most of these genes were upregulated upon loss of *Nmp4* (Figure 3-3). For instance, osteocalcin (*Bglap2*) was upregulated 24-fold in differentiating *Nmp4*^{-/-} MSCs compared to the WT cells on Day 7, which is consistent with our previous published finding that PTH-treated *Nmp4*^{-/-} mice exhibited elevated level of serum osteocalcin (Childress et al., 2011; He et al., 2013). Furthermore, several genes that were known to promote mineralization were also upregulated in *Nmp4*^{-/-} MSCs (Figure 3-3). For

instance, PHOSPHO1 is a direct target of NMP4 and was upregulated in *Nmp4*^{-/-} MSCs by 12-fold on Day 3 and Day 7; previous studies showed PHOSPHO1 is responsible for generating inorganic phosphate for matrix mineralization while ablation of this gene resulted in loss of skeletal mineralization in mice (Stewart et al., 2006; Yadav et al., 2011). These findings may explain at least in part the accelerated and enhanced mineralization we observed in differentiating *Nmp4*^{-/-} MSCs.

Of interest, the expression of multiple genes involved in mediating bone strength was impacted by loss of *Nmp4*. For example, mRNA expression of osteocalcin (*Bglap2*) and osteopontin (*Spp1*) were significantly elevated on Day 7. Osteocalcin and osteopontin have been implicated in playing roles in bone quality, formation of collagen fibrils and their organization, hydroxyapatite crystallinity, and bone material properties (Morgan et al., 2015). For example, Vashishth and colleagues found that osteocalcin, osteopontin and other non-collagenous proteins (NCPs) acted as “glue” at the collagen-mineral interface to resist the separation of the mineralized fibrils and consequently enhanced bone toughness (Morgan et al., 2015; Nikel et al., 2013; Poundarik et al., 2012). Therefore anabolic therapies that induce the formation of osteocalcin/osteopontin-enriched bone may further reduce fracture risk.

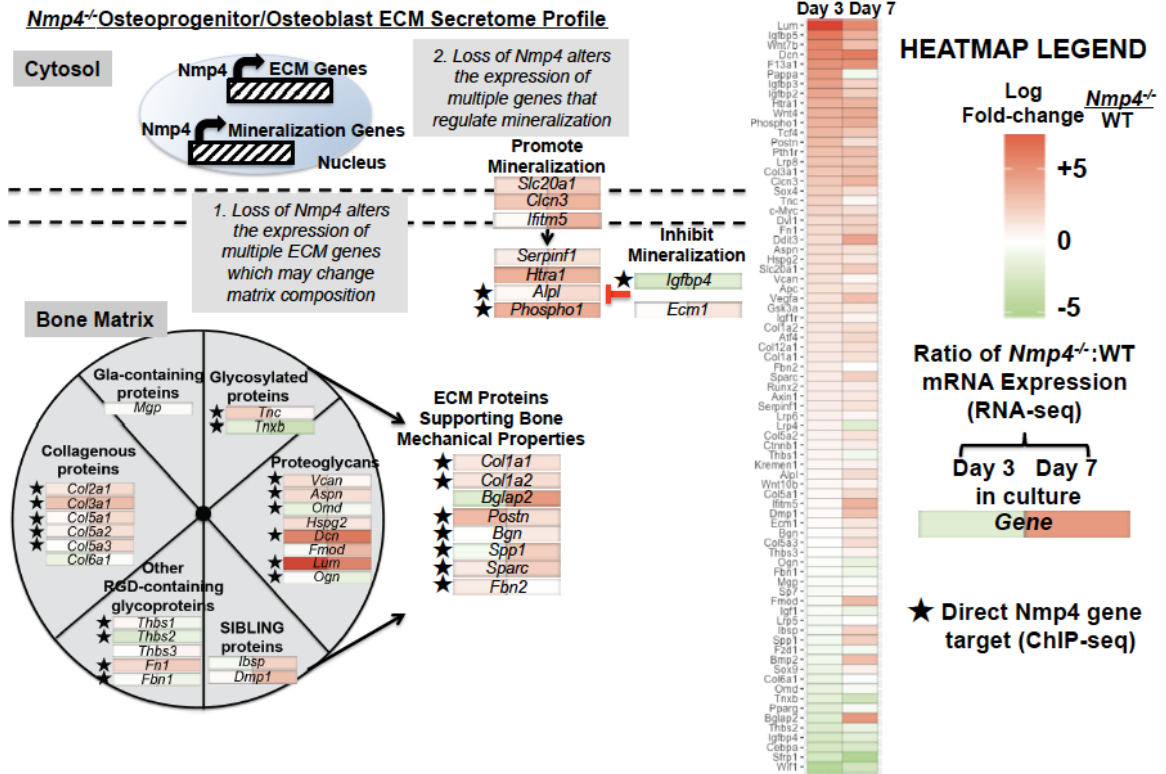


Figure 3-3: Loss of *Nmp4* alters the ECM secretome of MSPCs and osteoblasts. On the left: The *Nmp4*^{-/-} osteoprogenitor/osteoblast ECM secretome profile; loss of *Nmp4* alters 1) the expression of multiple ECM genes which may change the matrix composition and thus bone material property; 2) the expression of multiple genes that regulate mineralization. On the right: The heatmap of ECM secretome; red-upregulation in the null cells; green-downregulation in the null cells; left-Day 3 expression; right-Day 7 expression; star-direct candidate NMP4 target (ChIP-Seq).

Loss of Nmp4 improved trabecular bone gain in healthy mice treated with PTH and PTH+RAL therapies

To generate bone samples for our biomechanical analyses, we treated healthy, estrogen-replete WT and *Nmp4*^{-/-} mice with PTH, RAL, PTH+RAL and vehicle control for 7 weeks (see Materials and Methods). These results recapitulated what we have previously observed (Childress et al., 2015; Robling et al., 2009; Yu Shao, 2017), i.e. PTH+RAL was the most efficacious therapy for adding trabecular bone to the skeleton and loss of NMP4 enhanced this response. We summarize the bone geometry parameters obtained with these mice in Figures 3-4, 3-5 and Table 3-1.

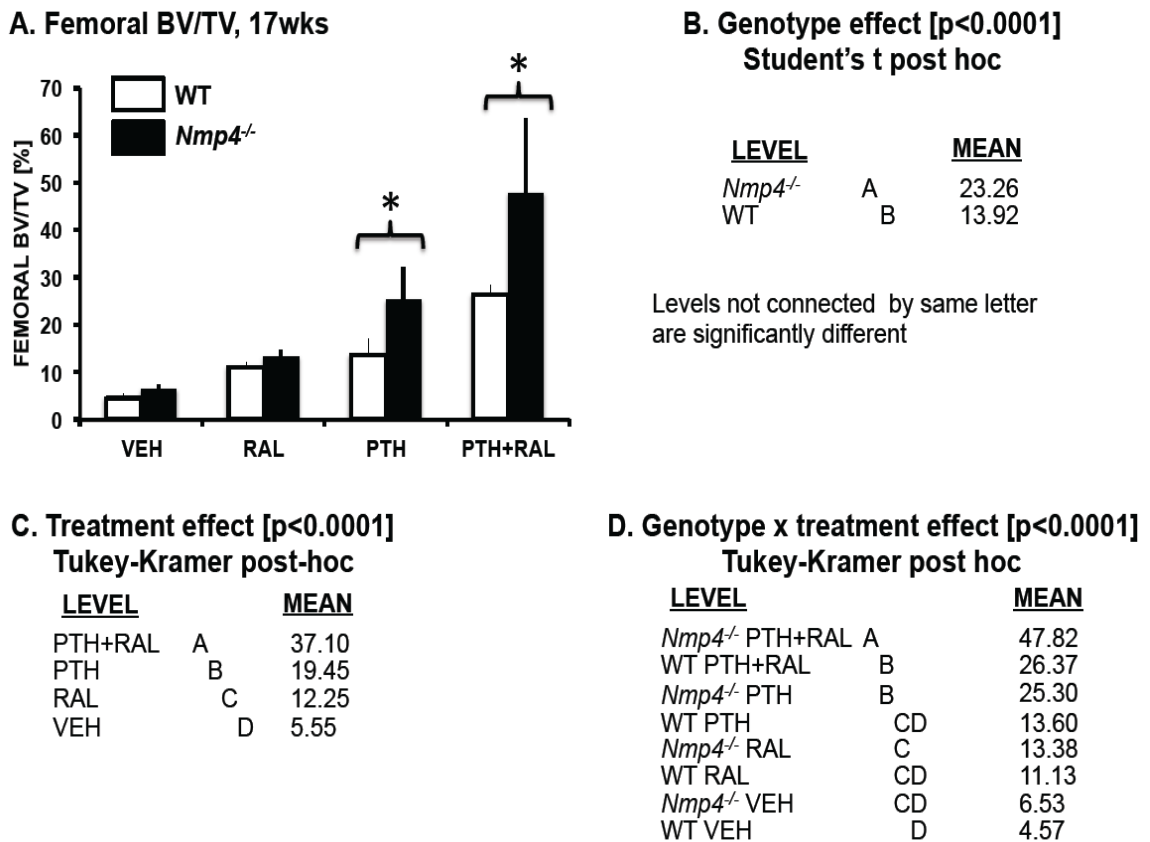
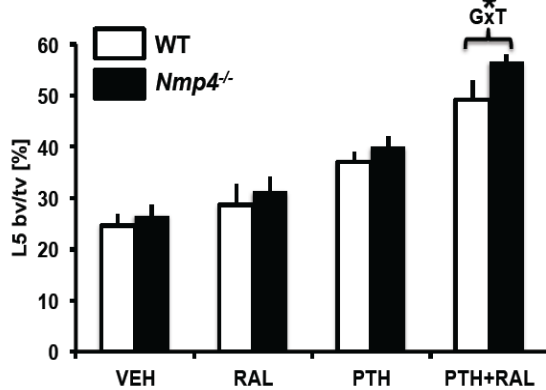


Figure 3-4: Femoral BV/TV (17wks of age) for WT and *Nmp4*^{-/-} mice under all treatment groups [A] The bar graph represents the means of femoral BV/TVs for all the experimental cohorts. The data were analyzed using a 2W ANOVA using genotype and treatment as the independent variables. [B] There was a significant genotype effect (p<0.0001). A Student's t post hoc test showed that the *Nmp4*^{-/-}

mice as a group exhibited a higher femoral BV/TV than the WT mice. [C] There was a significant treatment effect ($p < 0.0001$). A Tukey-Kramer HSD post hoc test revealed the differences between all the means of the treatment cohorts combining WT and *Nmp4*^{-/-} mice. The mice under the PTH+RAL therapy had the highest femoral BV/TV. PTH treatment produced the second highest and this was followed by RAL therapy. All the 3 therapies gave rise to higher BV/TV than the VEH control [D] There was a strong genotype x treatment (G x T) interaction. A Tukey-Kramer HSD post hoc test revealed that loss of *Nmp4* improved the PTH+RAL- and PTH-induced gain in femoral BV/TV. The data represents average \pm SD, n=7-14 mice/group.

A. L5 BV/TV, 17wks



**B. Genotype effect [p<0.0001]
Student's t post hoc**

LEVEL	MEAN
<i>Nmp4</i> ^{-/-} A	38.52
WT B	34.87

Levels not connected by same letter are significantly different

**C. Treatment effect [p<0.0001]
Tukey-Kramer post-hoc**

LEVEL	MEAN
PTH+RAL A	52.85
PTH B	38.46
RAL C	29.91
VEH D	25.61

**D. Genotype x treatment effect [p=0.0067]
Tukey-Kramer post hoc**

LEVEL	MEAN
<i>Nmp4</i> ^{-/-} PTH+RAL A	56.51
WT PTH+RAL B	49.20
<i>Nmp4</i> ^{-/-} PTH C	39.90
WT PTH C	37.02
<i>Nmp4</i> ^{-/-} RAL D	31.20
WT RAL DE	28.62
<i>Nmp4</i> ^{-/-} VEH EF	26.56
WT VEH F	24.66

Figure 3-5: L5 (17wks of age) for WT and *Nmp4*^{-/-} mice under all treatment groups. The data were analyzed using a 2W ANOVA using genotype and treatment as the independent variables followed by a Student's t or Tukey-Kramer HSD post-hoc test. [A] The bar graph represents the means of L5 BV/TVs for all the experimental cohorts. [B] There was a significant genotype effect (p<0.0001). A Student's t post hoc test showed that the *Nmp4*^{-/-} mice as a group exhibited a higher L5 BV/TV than the WT mice. [C] There was a significant treatment effect (p<0.0001). A Tukey-Kramer HSD post hoc test revealed the differences between all the means of the treatment cohorts combining WT and *Nmp4*^{-/-} mice using the connecting letter format. [D] There was a strong genotype x treatment (G x T) interaction (p=0.0067). A Tukey-Kramer HSD post hoc test revealed that loss of *Nmp4* improved the PTH+RAL-induced gain in L5 BV/TV. The data represents average ± SD, n=7-14 mice/group

Table 3-1

GROUP	Total CSA (mm ²)	Marrow Area (mm ²)	Cortical Thickness (mm)	Periosteal BS (mm)	Endocortical BS (mm)	AP Width (mm)	ML Width (mm)
WT VEH	1.77±0.10	0.940±0.049	0.204±0.008	5.393±0.139	4.140±0.114	1.33±0.03	1.74±0.06
<i>Nmp4</i> ^{-/-} VEH	1.75±0.06	0.913±0.049	0.209±0.009	5.353±0.090	4.078±0.106	1.32±0.03	1.73±0.06
WT RAL	1.76±0.09	0.895±0.064	0.216±0.006	5.344±0.090	4.019±0.095	1.31±0.02	1.74±0.04
<i>Nmp4</i> ^{-/-} RAL	1.73±0.08	0.879±0.039	0.218±0.010	5.332±0.111	4.004±0.103	1.32±0.04	1.72±0.04
WT PTH	1.94±0.13	0.969±0.048	0.221±0.010	5.617±0.196	4.213±0.108	1.39±0.04	1.82±0.09
<i>Nmp4</i> ^{-/-} PTH	1.89±0.04	0.931±0.064	0.230±0.012	5.564±0.087	4.142±0.116	1.38±0.03	1.78±0.07
WT PTH+RAL	1.89±0.10	0.892±0.043	0.239±0.007	5.552±0.152	4.084±0.106	1.37±0.03	1.82±0.08
<i>Nmp4</i> ^{-/-} PTH+RAL	1.85±0.09	0.852±0.029	0.249±0.013	5.472±0.124	3.970±0.047	1.38±0.03	1.75±0.05
2W ANOVA	G: p=0.83 T: p<0.0001 PTH: A PTH+RAL: A VEH: B RAL: B GXT: p=0.95	G: p=0.0035 T: p<0.0001 PTH: A VEH: A RAL: B PTH+RAL: B GXT: p=0.81	G: p=0.0023 T: p<0.0001 PTH+RAL: A PTH: B RAL: C VEH: D GXT: p=0.46	G: p=0.0407 T: p<0.0001 PTH: A PTH+RAL: A VEH: B RAL: B GXT: p=0.95	G: p=0.0025 T: p<0.0001 PTH: A VEH: A PTH+RAL: B RAL: B GXT: p=0.42	G: p=0.57 T: p<0.0001 PTH: A PTH+RAL: A VEH: B RAL: B GXT: p=0.60	G: p=0.0102 T: p=0.0002 PTH: A PTH+RAL: A VEH: B RAL: B GXT: p=0.41

Table 3-1: The femoral cortical data of various groups show significant treatment effect. PTH+RAL and PTH-only therapies resulted in largest cortical area (CSA) and PTH+RAL resulted in thickest cortical bone. There was no difference in femoral cortical area between the WT and *Nmp4*^{-/-} mice. However, *Nmp4*^{-/-} mice exhibited a modest but significantly greater cortical thickness. Additionally, the *Nmp4*^{-/-} animals exhibited a moderate but significant decrease in femoral marrow area, periosteal bone surface, endocortical bone surface and ML width compared to the WT mice.

Loss of Nmp4 improves bone structural and estimated material properties

To evaluate the bone mechanical and material properties of our treated mice, 3-point bending test was performed on the left femurs. For both yield force and ultimate force, significant genotype effects were observed ($p=0.0058$ and 0.0362 respectively, Figures 3-6A-D), which implies that femurs from *Nmp4*^{-/-} mice could sustain a higher external force prior to failure compared to WT mice. Meanwhile, mice (both WT and *Nmp4*^{-/-}) receiving PTH+RAL therapy acquired the highest ultimate force among all the treatment groups; PTH+RAL therapy also improved the yield force compared to mice receiving VEH control (Figures 3-6A-D). The bone material properties, which account for difference in bone geometry, also showed significant genotype effect with yield stress and ultimate stress ($p=0.0092$ and 0.0016 respectively, Figures 3-7A-D), suggesting that deletion of *Nmp4* imparts mechanical benefit by enhancing the tissue properties. No G x T interaction was found, indicating the improvement of bone strength under PTH+RAL treatment was not further enhanced by disabling *Nmp4* (Figures 3-7A&C). For the treatment effect on bone material property, PTH+RAL gave rise to the highest ultimate stress; surprisingly, PTH treatment led to lower yield stress than RAL and VEH treatment (Figures 3-7A&C).

Interestingly, even though some other mechanical and material parameters showed limited or no statistical difference (i.e. p close to or greater than 0.05), it was still noticeable that a trend of difference between WT and *Nmp4*^{-/-} bones existed when we analyzed post-yield displacement, total displacement, work to yield, total strain, modulus and resilience (Tables 3-2, 3-3 and Figure 3-8), suggesting that *Nmp4*^{-/-} bones in general exhibited increased bone strength, stiffness and energy absorbed before fracture. Treatment-wise, PTH and PTH+RAL therapies improved bone mechanical properties (Table 3-2). We summarized the mechanical and material properties obtained in these mice in Tables 3-2 and 3-3. These results suggest that loss of *Nmp4* improves bone material and mechanical properties, irrespective of the treatment status; our transcriptome data provides an accurate guide to understanding at the cellular and molecular level of the *Nmp4*^{-/-} phenotype.

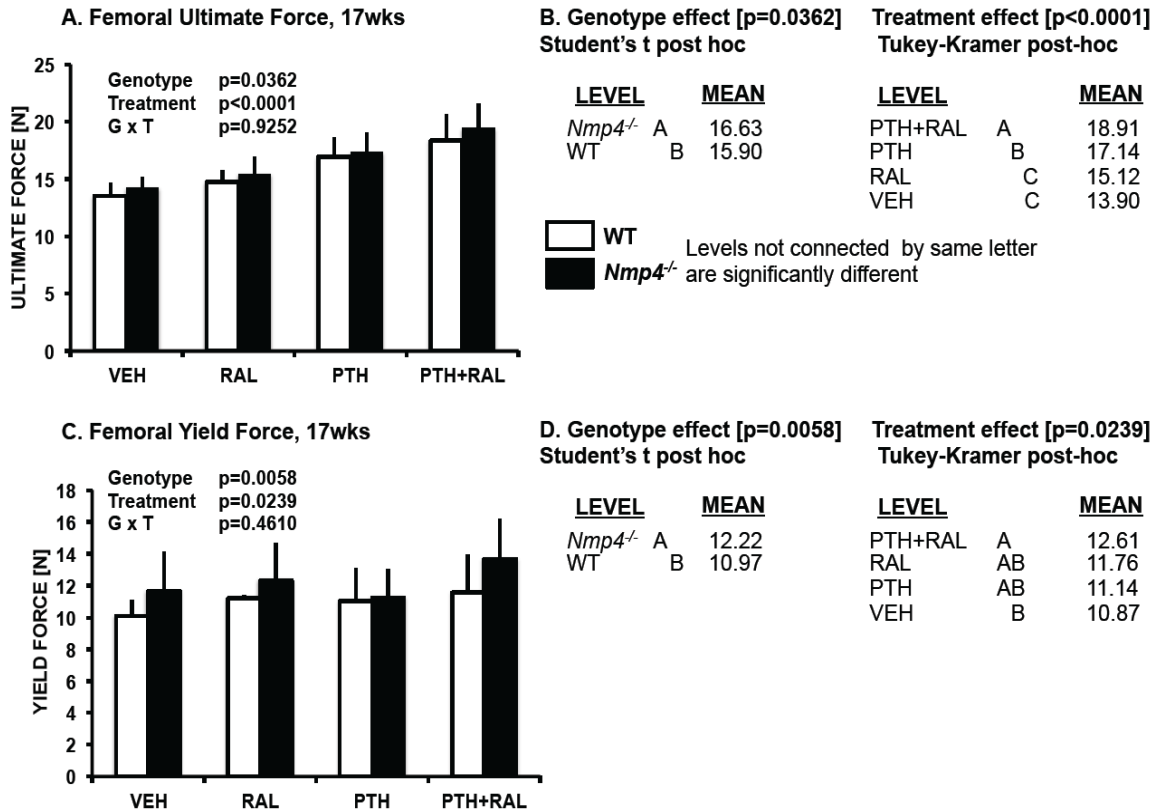


Figure 3-6: 3-point binding results and statistical analysis of the femur from the four treatment groups (17wks of age) for WT and *Nmp4*^{-/-} mice [A] The bar graph represents the means of femoral ultimate force. The data were analyzed using a 2W ANOVA using genotype and treatment as the independent variables. [B] There was a significant genotype effect (p=0.0362). A Student's t-test reveals that loss of *Nmp4* modestly but significantly enhances ultimate force. A Tukey-Kramer post hoc test showed that PTH+RAL>PTH>RAL=VEH (treatment effect p<0.0001). [C] The bar graph represents the means of femoral yield force. [D] There was a significant genotype effect (p=0.0058). A Student's t-test reveals that loss of *Nmp4* modestly but significantly enhances yield force. A Tukey-Kramer post hoc test showed that PTH+RAL>VEH. PTH and RAL did not significantly increase yield force over VEH. However, PTH and RAL were not significantly different from PTH+RAL. The data represents average \pm SD, n=7-14 mice/group.

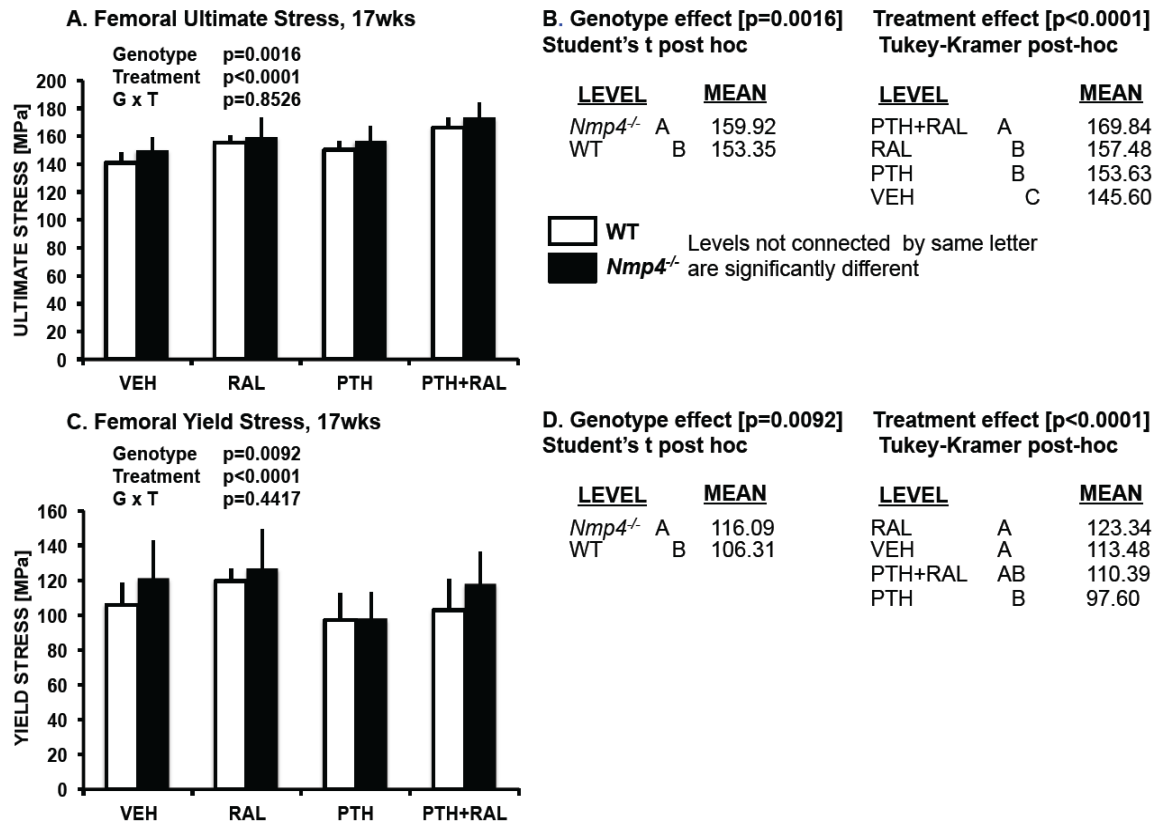


Figure 3-7: 3-point binding results and statistical analysis of the femur from the four treatment groups (17wks of age) for WT and *Nmp4*^{-/-} mice [A] The bar graph represents the means of femoral ultimate stress. The data were analyzed using a 2W ANOVA using genotype and treatment as the independent variables. [B] There was a significant genotype effect (p=0.0016). A Student's t-test reveals that loss of *Nmp4* modestly but significantly enhances ultimate stress. A Tukey-Kramer post hoc test showed that PTH+RAL>RAL=PTH>VEH (treatment effect p<0.0001). [C] The bar graph represents the means of femoral yield stress. [D] There was a significant genotype effect (p=0.0092). A Student's t-test reveals that loss of *Nmp4* modestly but significantly enhances yield stress. A Tukey-Kramer post hoc test showed considerable overall between the treatments but RAL and VEH> PTH. The data represents average \pm SD, n=7-14 mice/group.

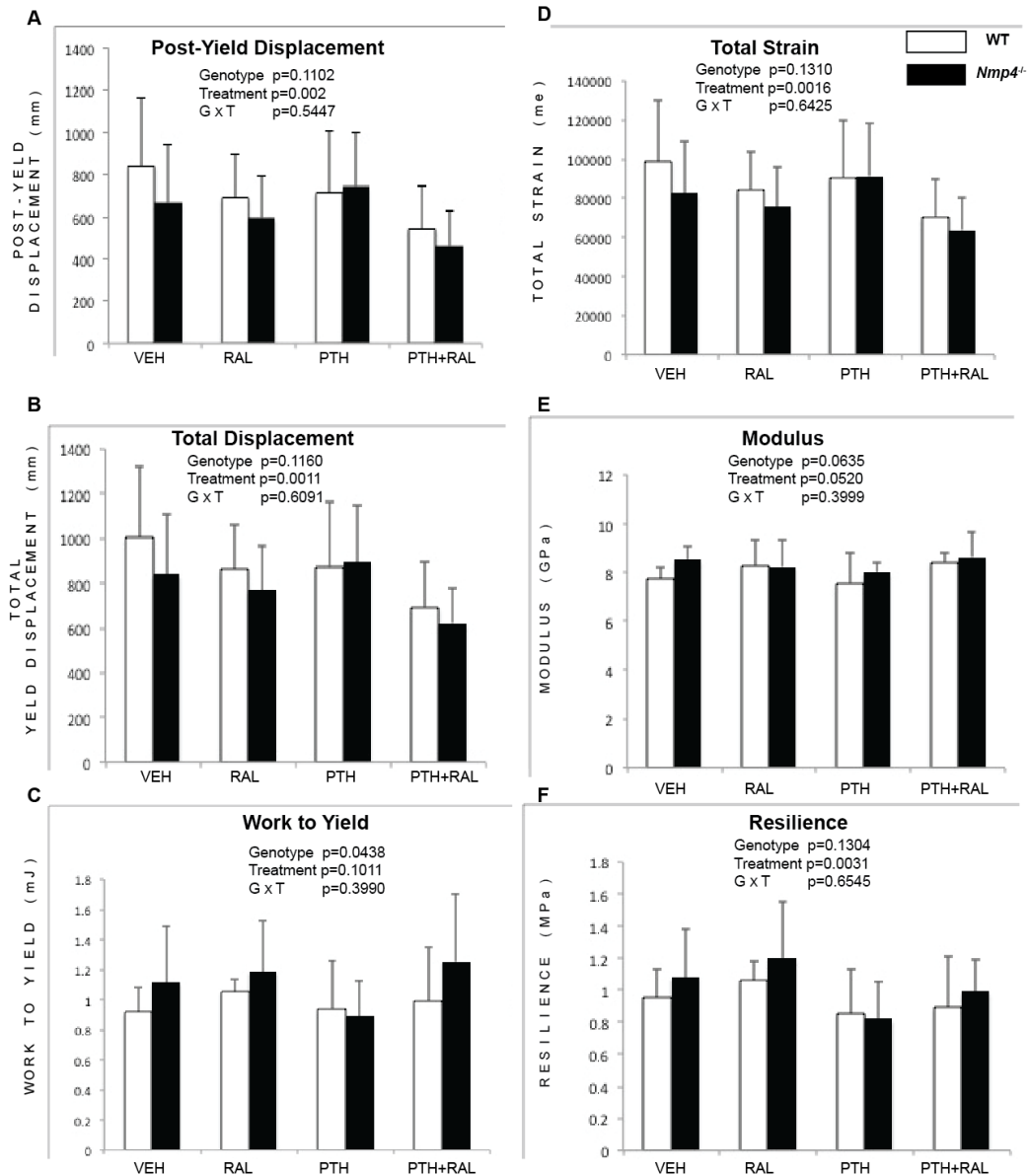


Figure 3-8: Select femoral mechanical and material parameters. The data were analyzed using a 2W ANOVA using genotype and treatment as the independent variables followed by a Student's t or Tukey-Kramer HSD post-hoc test. [A-C] the mechanical parameters post-yield displacement, total displacement and work to yield were shown. Refer to [Table 3-2](#) for more details. [D-F] the material parameters total strain, modulus and resilience were shown. Refer to [Table 3-3](#) for more details. The data represents average \pm SD, n=7-14 mice/group.

Table 3-2

PARAMETER	GENOTYPE	TREATMENT	GXT	COMMENTS
Yield Force (N)	p=0.0058 <i>Nmp4</i> ^{-/-} =12.22 A WT =10.97 B	p=0.0239 PTH+RAL=12.61 A RAL =11.76 AB PTH =11.13 AB VEH =10.87 B	p=0.9252	Loss of Nmp4 significantly enhances YIELD FORCE. PTH+RAL therapy significantly elevated yield force compared to VEH
Ultimate Force (N)	p=0.0362 <i>Nmp4</i> ^{-/-} =16.63 A WT =15.90 B	p<0.0001 PTH+RAL=18.91 A PTH =17.14 B RAL =15.12 C VEH =13.90 C	p=0.9252	Loss of Nmp4 significantly enhances ULTIMATE FORCE. PTH+RAL therapy elevates ultimate stress over all other treatments
Displacement to Yield (mm)	p=0.9103	p=0.0149 RAL =172.81 A VEH =167.57 AB PTH =155.0 AB PTH+RAL =153.51 B	p=0.2527	RAL has the highest DISPLACEMENT TO YIELD and is significantly higher than PTH+RAL but there is considerable overlap between the treatments
Post Yield Displacement (mm)	p=0.1102	p=0.0020 VEH =754.34 A PTH =726.78 A RAL =642.02 AB PTH+RAL =499.63 B	p=0.5447	PTH+RAL has the lowest POST YIELD DISPLACEMENT and is significantly lower than the VEH and PTH treatments
Total Displacement (mm)	p=0.1160	p=0.0011 VEH =921.92 A PTH =884.59 A RAL =815.41 AB PTH+RAL =654.05 B	p=0.6091	PTH+RAL has the lowest TOTAL DISPLACEMENT and is significantly lower than the VEH and PTH treatments
Stiffness (N/mm)	p=0.3316	p<0.0001 PTH+RAL=131.66 A PTH =120.97 A RAL =105.74 B VEH =100.06 B	p=0.7575	PTH+RAL and PTH enhance femoral STIFFNESS compared to RAL and VEH
Work to Yield (mJ)	p=0.0438 <i>Nmp4</i> ^{-/-} =1.11 A WT =0.975 B	p=0.1011	p=0.3990	Loss of Nmp4 enhances WORK TO YIELD
Post Yield Work (mJ)	p=0.8291	p=0.0103 PTH =9.84 A RAL =7.87 B PTH+RAL =7.83 B VEH =7.77 B	p=0.7762	PTH has the highest POST YIELD WORK and there is no difference between the other treatments
Total Work	p=0.8989	p=0.0159 PTH =10.78 A RAL =9.03 AB PTH+RAL =8.95 B VEH =8.78 B	p=0.8461	PTH has the highest TOTAL WORK and is significantly higher than PTH+RAL and VEH

Table 3-2: The femoral mechanical properties of WT and *Nmp4*^{-/-} mice. Loss of Nmp4 improved the yield force, ultimate force and work to yield. PTH and PTH+RAL treatments increase bone strength, stiffness and energy absorbed during the experiment. See comments for details of each parameter.

Table 3-3

PARAMETER	GENOTYPE	TREATMENT	GXT	COMMENTS
Yield Stress (MPa)	p=0.0092 <i>Nmp4</i> ^{-/-} =116.09 A WT =106.31 B	p<0.0001 RAL =123.34 A VEH =113.48 AB PTH+RAL=110.39 AB PTH =97.60 B	p=0.4417	Loss of Nmp4 significantly enhances YIELD STRESS. RAL is significantly higher than PTH but there is considerable overlap between the treatments
Ultimate Stress (MPa)	p=0.0016 <i>Nmp4</i> ^{-/-} =159.92 A WT =153.35 B	p<0.0001 PTH+RAL=169.84 A RAL =157.48 B PTH =153.63 B VEH =145.60 C	p=0.8526	Loss of Nmp4 significantly enhances ULTIMATE STRESS. PTH+RAL therapy elevates ultimate stress over all other treatments
Strain to Yield (me)	p=0.8617	p=0.5483	p=0.1791	STRAIN TO YIELD was not influenced by genotype or treatment
Total Strain (me)	p=0.1310	p=0.0016 PTH =90864.45 A VEH =90703.78 A RAL =79736.66 AB PTH+RAL =66816.31 B	p=0.6425	PTH+RAL and RAL has the lowest TOTAL STRAIN and the former is significantly lower than the VEH and PTH treatments
Modulus (GPa)	p=0.0635	p=0.0520	p=0.3999	There is a nearly significant increase in the bone MODULUS with loss of Nmp4
Resilience (MPa)	p=0.1304	p=0.0031 RAL =1.13 A VEH =1.01 AB PTH+RAL=0.94 AB PTH =0.84 B	p=0.6545	RAL is significantly higher than PTH but there is considerable overlap between the treatments
Toughness (MPa)	p=0.8913	p=0.0553	p=0.7901	TOUGHNESS was not influenced by genotype or treatment

Table 3-3: The femoral material properties of WT and *Nmp4*^{-/-} mice. Loss of Nmp4 improved the yield stress and ultimate stress. See comments for details of each parameter.

Loss of Nmp4 biased MSPCs towards osteogenesis

Does loss of *Nmp4* lead to alterations in the differentiation process? Our previous study indicated that although loss of *Nmp4* leads to precocious mineralization in MSPCs, the alkaline phosphatase activity as an indicator of osteoblast activity remains the same between the WT and *Nmp4*^{-/-} MSPCs during osteogenic differentiation (Childress et al., 2015). As the next step of our analysis, we then examined the expression profiles of some select MSPC markers as well as differentiation markers. We observed that many well-accepted MSPC markers, including *Vcam1* (CD106), *Atxn1* (SCA1) and *Nes* (Nestin), were each expressed (absolute read count mean > 10) in both WT and *Nmp4*^{-/-} MSPCs on Day 3 and Day 7 (Table 3-4). On Day 3, expression of *Atxn1* and *Nes* were elevated in the *Nmp4*^{-/-} MSPCs, whereas *Vcam1* was downregulated. On Day 7, *Vcam1* and *Nes* were downregulated in the *null* cells. Furthermore, *Atxn1* was maintained at the similar level with the WT (Table 3-4). Two key transcription factors *Runx2* and *Sp7* that promote osteogenesis exhibited no significant expression difference on both days with $|\log_2(\text{cpm fold change})| < 1$ (Figure 3-9, Table 3-4). By comparison, the key transcription factors that drive adipogenesis and chondrogenesis were largely downregulated in the *null* cells (e.g. *Ppary*, *Sox5* and *Sox9*, Figure 3-9). The transcription factors *Atf4* and *Ddit3* were over-expressed in the *Nmp4*^{-/-} MSPCs (Figure 3-9). These proteins drive osteoblast differentiation (Pereira et al., 2004; Saito et al., 2011). They also act cooperatively to induce multiple genes involved in amino acid synthesis, transport and protein delivery (e.g. ribosome biogenesis, tRNA charging, and the UPR) (Dey et al., 2012; Fusakio et al., 2016). Therefore, *Atf4* and *Ddit3* over-expression may contribute to the precocious and enhanced mineralization observed in *Nmp4*^{-/-} cell cultures. We conclude that loss of *Nmp4* enhances part of the osteogenic differentiation process in MSPCs, possibly by promoting their secretory capacity; the *Nmp4*^{-/-} MSPCs are more biased towards osteogenesis but we lack clear evidence to claim the WT and *Nmp4*^{-/-} MSPCs are completely two different cell types by Day 7 of differentiation.

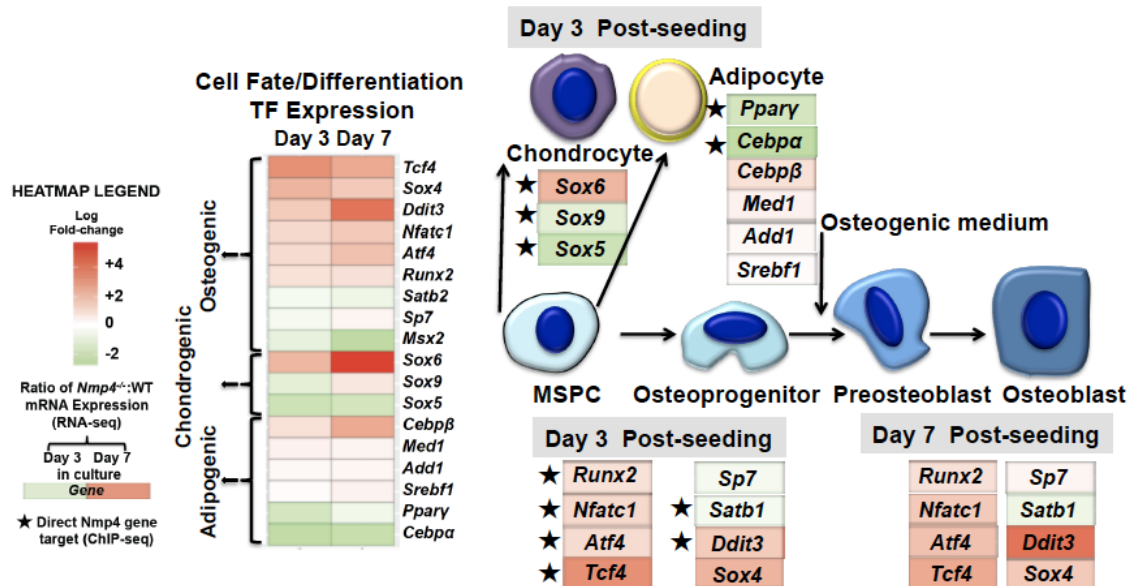


Figure 3-9: Loss of *Nmp4* biases MSCs towards osteogenic lineage. On the left: heatmap for the cell fate/differentiation transcription factor (TF) expression; red-upregulation in the *null* cells; green-downregulation in the *null* cells; left-Day 3 expression; right-Day 7 expression; star-direct candidate NMP4 target (ChIP-Seq); the genes were clustered into 3 categories: TFs promote osteogenic/chondrogenic/adipogenic lineages. On the right: on Day 3 several key TFs (e.g. *Sox5*, *Sox9*, *Pparγ* and *Cebpa*) that promote chondrogenesis and adipogenesis were downregulated in the *Nmp4*^{-/-} MSCs; while on both days several key TFs (e.g. *Atf4*, *Tcf4* and *Ddit3*) driving osteogenesis were upregulated in the *Nmp4*^{-/-} MSCs; Notice *Runx2* and *Sp7* exhibit no significant expression difference.

Table 3-4

MSPC Markers						
	Day 3			Day 7		
Gene	WT-CPM mean	<i>Nmp4</i> ^{-/-} -CPM mean	Fold change	WT-CPM mean	<i>Nmp4</i> ^{-/-} -CPM mean	Fold change
<i>Vcam1</i>	246.864	93.325	0.378	187.210	72.227	0.386
<i>Atxn1</i>	31.907	65.300	2.047	24.570	29.194	1.188
<i>Nes</i>	19.965	66.607	3.336	16.271	5.059	0.311
Osteogenic Differentiation Markers						
	Day 3			Day 7		
Gene	WT-CPM mean	<i>Nmp4</i> ^{-/-} -CPM mean	Fold change	WT-CPM mean	<i>Nmp4</i> ^{-/-} -CPM mean	Fold change
<i>Sp7</i>	66.479	49.529	0.745	139.111	173.428	1.247
<i>Runx2</i>	91.622	166.514	1.817	114.618	213.123	1.860

Table 3-4: The expression profiles of select MSPC markers and osteogenic differentiation markers in WT and *Nmp4*^{-/-} MSPCs on Day 3 and Day 7. On Day 3, *Atxn1* and *Nes* were elevated in the *Nmp4*^{-/-} MSPCs; while *Vcam1* was downregulated; On Day 7, *Vcam1* and *Nes* were downregulated in the *null* cells; while *Atxn1* was maintained at the similar level with the WT. Two key transcription factors *Runx2* and *Sp7* that promote osteogenesis exhibited no significant expression difference on both days with cpm fold change<2.

Loss of Nmp4 promotes pathways that directly regulate osteoblast function and bone formation

To further explore the impact of NMP4 on the development of the osteoblast phenotype, we expanded our analysis of RNA-Seq data. Data from Day 3 and Day 7 were separated into two datasets; any genes with $\log_2(\text{cpm fold change})$ or $\log\text{FC} > 1$ or < -1 and $\text{FDR} < 0.05$ were selected and uploaded to IPA; the predicted pathways were further filtered by $p\text{-value} < 0.05$. More than 200 pathways were identified, suggesting once again that NMP4 impacts the activities of many molecular pathways.

Multiple pathways that directly affect osteoblast function and bone formation were perturbed by the loss of *Nmp4*. The transforming growth factor beta (TGF β) signaling pathway was significantly activated ($p < 0.0001$, z score=3.29 on Day 3; $p = 0.0003$, z score=2.5 on Day 7; see Materials and Methods for explanation; Table 3-5); several genes involved in this pathway were upregulated in *Nmp4*^{-/-} MSPCs, such as *Smad2*, *Smad4* and *Tgfb2* (Figure 3-10A). This pathway is particularly relevant to the *Nmp4* phenotype. TGF β signaling favors bone formation by promoting osteoprogenitor enrichment, pre-osteoblast commitment and early differentiation (Crane et al., 2016; Matsunobu et al., 2009; Tang et al., 2009). This finding was consistent with what we observed *in vivo* and *in vitro* (Childress et al., 2015; He et al., 2013). The IGF-1 pathway is highly upregulated on Day 3 (z score=4.13); on Day 7, this pathway does not pass our filter ($p\text{-value} = 0.0562$) but it is still highly activated (z score=2.59) (Table 3-5). Our ChIP-Seq data indicated multiple genes in this pathway are candidate direct targets of NMP4 (Childress et al., 2015) and here we show 49 genes affected by NMP4 in MSPCs are involved in this pathway (Figure 3-10B). For instance, the secreted IGF binding proteins (IGFBPs: *Igfbp2*, *Igfbp3*, *Igfbp4*, *Igfbp5* and *Igfbp6*) are all affected by NMP4 and are known to affect osteogenesis via direct binding to IGF-1 in the blood circulation; *Igf1r* and several of its downstream pathway factors (e.g. MAP kinases, *Grb10*, *Akt2*, *Akt3* and *Ptpn11*) are upregulated in the *null* cells (Figure 3-10B). Previous studies have shown IGF-1 signaling is required for the anabolic action of PTH (Bikle et

al., 2002; Esen et al., 2015). IGF-1 signaling has also been shown to be important for osteoblast differentiation and mineralization (Fujita et al., 2004; Zhang et al., 2002). All of these again matched the anabolic phenotype we observed in *Nmp4^{-/-}* animal and cells (Childress et al., 2015; He et al., 2013).

Other pathways that play a role in osteoblast development & functions such as BMP signaling (z score=3.4 on Day 3 and 2.84 on Day 7) and Wnt pathway (z score= 1.73 on Day 3 and 1.04 on Day 7) are also under impact from NMP4 (Figures 3-10C&D, Table 3-5). We paid particular interest to these two pathways since just like IGF-1 pathway, Wnt is known to mediate the anabolic action of PTH; both Wnt and BMP pathways can promote osteoblast mineralization (Guo et al., 2010; Rawadi et al., 2003). All of these 4 pathways mentioned above may mediate the *Nmp4^{-/-}* phenotype and shed light on the molecular mechanism of NMP4.

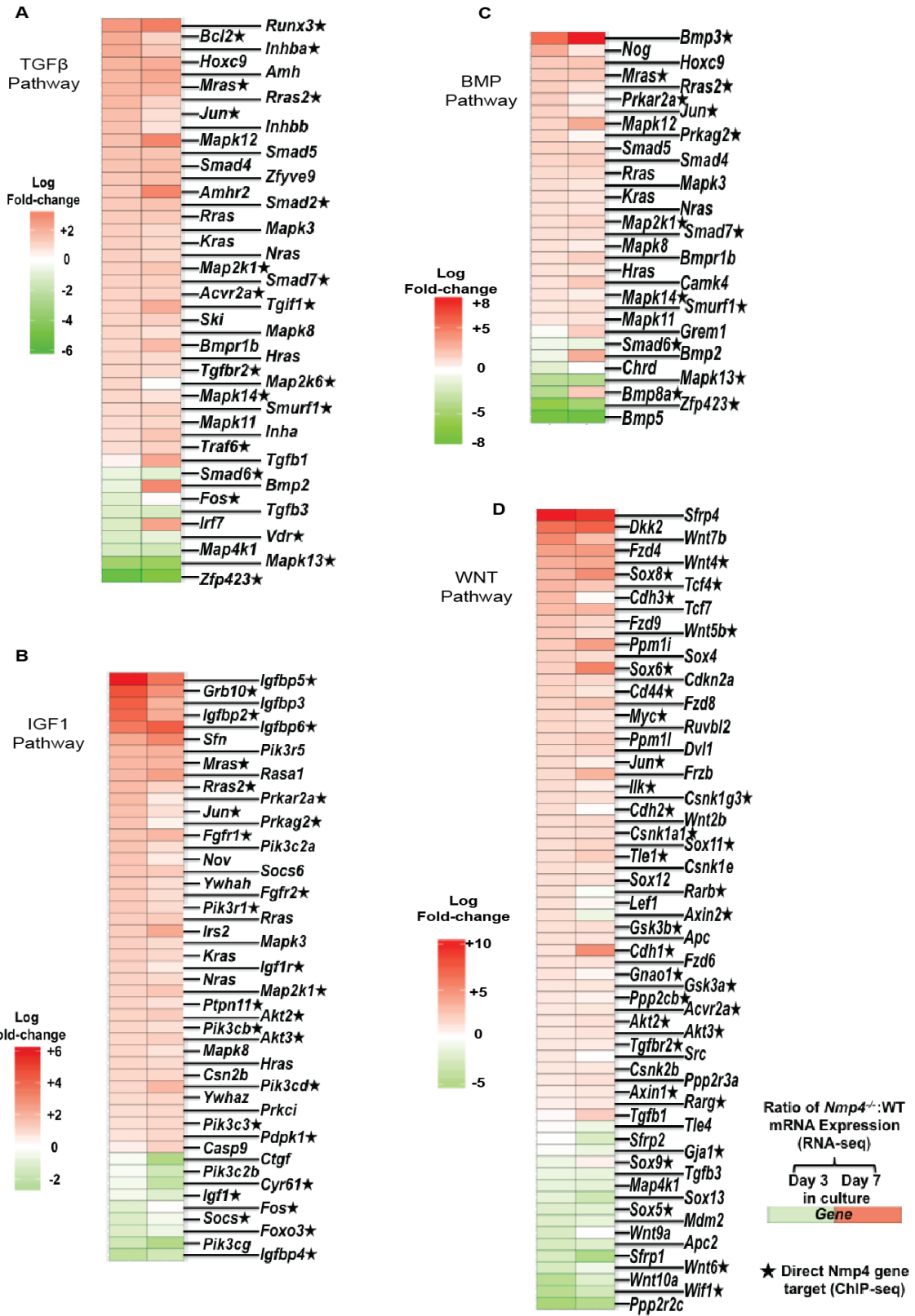


Figure 3-10: Loss of *Nmp4* activates multiple pathways that promote osteoprogenitor expansion, osteoblast differentiation and bone formation. The heatmaps presented include genes with 1) FDR<0.05 and 2) fold change of *Nmp4*: WT>2 or <-2 for [A] IGF pathway, [B] BMP pathway, [C] TGF β pathway and [D] Wnt pathway. *Red*-upregulation in the *null* cells; *green*-downregulation in the *null* cells; *left*-Day 3 expression; *right*-Day 7 expression; *star*-direct candidate NMP4 gene target (ChIP-Seq).

Bone-Related Pathways	p-value	Z-SCORE	# OF GENES
DAY 3 IGF-1 Signaling	2.69153E-05	4.131	40
DAY 7 IGF-1 Signaling	0.056234133	2.558	31
DAY 3 Ephrin Receptor Signaling	8.70964E-06	3.479	60
DAY 7 Ephrin Receptor Signaling	3.80189E-05	3.569	62
DAY 3 Glucocorticoid Receptor Signaling	1.34896E-07		96
DAY 7 Glucocorticoid Receptor Signaling	0.003162278		84
DAY 3 Wnt/ β -catenin Signaling	8.70964E-07	1.732	61
DAY 7 Wnt/ β -catenin Signaling	0.000724436	1.043	56
DAY 3 STAT3 Pathway	6.91831E-09	3.781	37
DAY 7 STAT3 Pathway	0.012589254	3	25
DAY 3 Estrogen Receptor Signaling	1.91E-04		43
DAY 7 Estrogen Receptor Signaling	0.00676083		41
DAY 3 VEGF Signaling	2.0893E-06	4	43
DAY 7 VEGF Signaling	0.000512861	3.43	38
DAY 3 TGF- β Signaling	1.25893E-06	3.286	37
DAY 7 TGF- β Signaling	0.000295121	2.502	34
DAY 3 BMP signaling pathway	0.001380384	3.4	27
DAY 7 BMP signaling pathway	0.064565423	2.837	23

Table 3-5: Manually annotated bone-related pathways affected by NMP4. The p-value of each pathway, predicted activation z-score and number of genes being affected by NMP4 were also listed.

Loss of Nmp4 affects unfolded protein response (UPR) and ribosomal biogenesis

Our transcriptome analysis also revealed that several pathways affected by NMP4 are important in regulating protein synthesis and associated functions (Table 3-6). Among these pathways, the UPR pathway together with the c-MYC-mediated ribosomal biogenesis has been studied by us before (Young et al., 2016). Based on the IPA output, 34 out of 63 UPR genes were found significantly altered in the *null* cells on either Day 3 or Day 7; majority of these genes' expression was further intensified (upregulated or downregulated) on Day 7 (Figure 3-11). Some genes that play major roles in regulating the UPR pathway such as *Atf4*, *Atf6*, *Xbp1*, *Gadd34* (*Ppp1r15a*) and *Chop* (*Ddit3*) were highly upregulated, suggesting a major alteration of the UPR pathway in the *null* cells (Figure 3-11), although the activation z-score could not be determined by IPA. Since MSPCs and osteoblasts are professional secretory cells that rely heavily on functioning ER for protein processing, it is likely that UPR pathway plays a critical role in bone formation. For instance, *Perk*^{-/-} mice were found to develop osteopenia and studies also indicated CHOP can induce osteoblast differentiation (Pereira et al., 2004; Wei et al., 2008).

Of these altered UPR genes, ATF4 is highly expressed in osteoblast and modestly upregulated in *Nmp4*^{-/-} MSPCs (2-fold on Day 3 and 4-fold on Day 7, Figure 3-11). Not only does it induce expression of key UPR genes *Gadd34* and *Chop*, it also plays a central role in osteoblast differentiation and bone formation via crosstalk with other pathways important for osteoblast functions. For instance, ATF4 is known to be able to promote osteogenesis from MSPCs via β -catenin and RUNX2 (Lin et al., 2010; Yu et al., 2013). Another study confirmed ATF4 enhanced osteoblast function via interaction with BMP2 pathway (Saito et al., 2011).

According to our previous finding, GADD34 and c-MYC are important mediators of the *Nmp4 null* phenotype, making the *null* cells super-secretory (Young et al., 2016). Our transcriptome analysis further confirmed this finding. GADD34 was upregulated by 6-fold on Day 3 and 16-fold on Day 7 in the *null* cells; while c-MYC was modestly upregulated by 3-fold on both days in the *null*

cells (Figure 3-11). A previous study showed c-MYC is capable of enhancing BMP2-induced osteogenesis (Piek et al., 2010).

To evaluate the impact of GADD34 on precocious mineralization of *Nmp4*^{-/-} MSCs, we performed preliminary study by challenging WT and *Nmp4*^{-/-} MSCs with salubrinal, a selective inhibitor of GADD34 during osteogenic differentiation. The mineralization in one *null* MSC line under salubrinal treatment was largely attenuated on Day 7 when the *null* cells first started to mineralize (Figure 3-12). The extent of mineralization for the *null* MSC line was similar to that of the WT MSC line on Day 12, when the WT cells first started to mineralize (Figure 3-12). We observed inhibition of salubrinal-induced mineralization in another set of WT and *Nmp4*^{-/-} lines. Notice that the inhibition of GADD34 also affected the mineralization of the WT line (Figure 3-12). This raises the question whether the null cells are more sensitive to the inhibition of GADD34 and further quantitative studies are required to address this question.

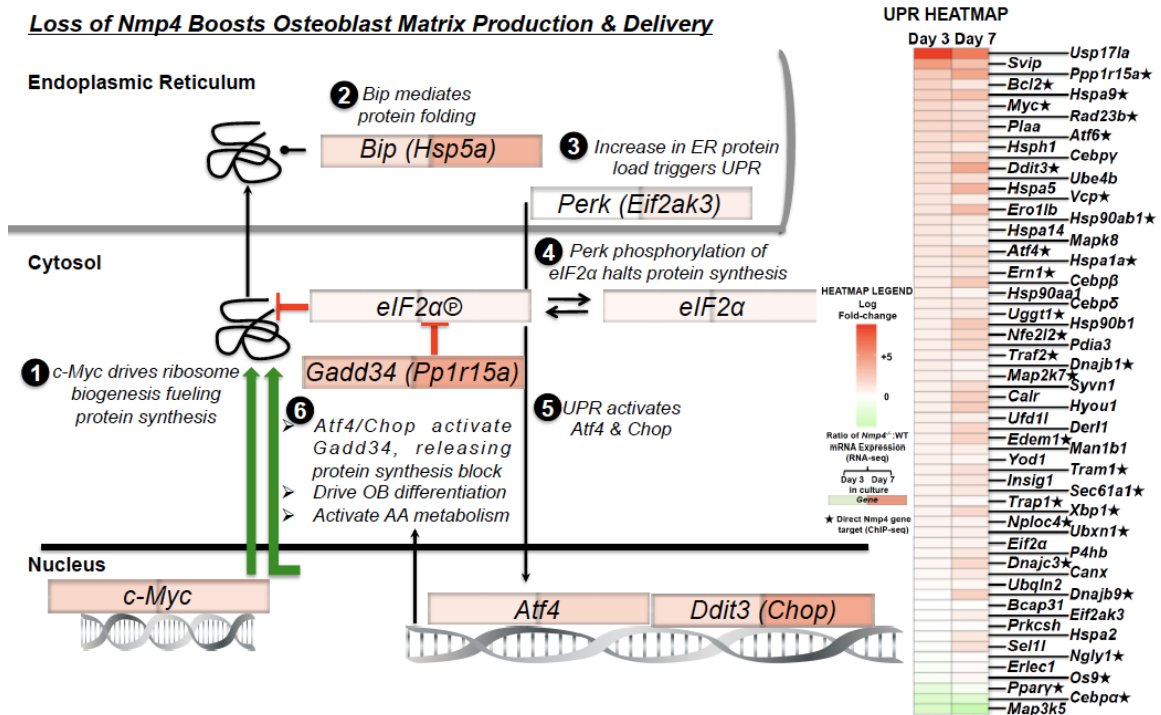


Figure 3-11: Loss of *Nmp4* alters UPR pathways and enhances ribosomal biogenesis. On the left: Loss of *Nmp4* boosts osteoblast matrix production &

delivery via enhanced ribosome biogenesis and altered UPR pathways; 1) c-MYC drives ribosome biogenesis fueling protein synthesis; 2) BiP modulates protein folding; 3) increase in ER protein load triggers UPR; 4) PERK phosphorylation of eIF2 α halts protein synthesis; 5) UPR activates *Atf4* and *Chop*; 6) ATF4/CHOP activate *Gadd34*, releasing protein synthesis block, which further drive osteoblast differentiation and activate amino acid metabolism. On the right: heatmap for the UPR pathways and ribosome biogenesis; *red*-upregulation in the *null* cells; *green*-downregulation in the *null* cells; *left*-Day 3 expression; *right*-Day 7 expression; *star*-direct candidate NMP4 target (ChIP-Seq).

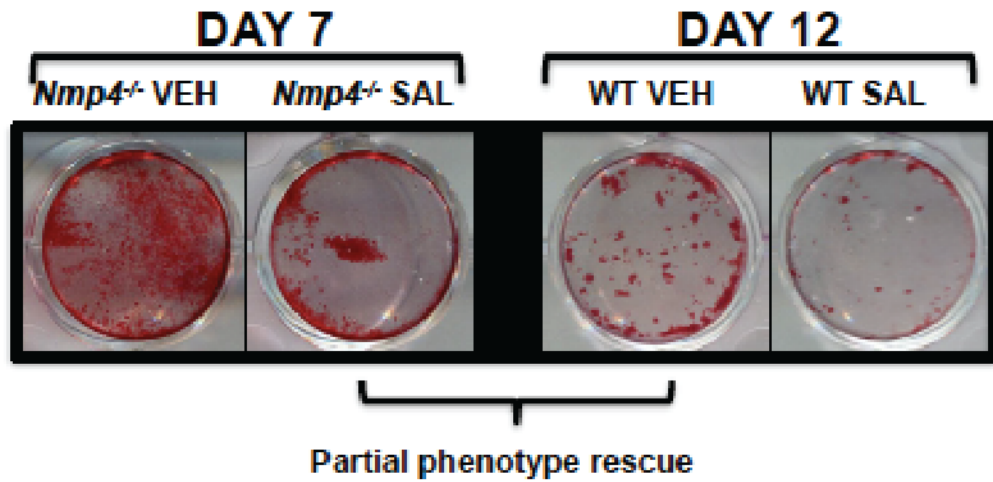


Figure 3-12: Inhibition of GADD34 partially rescues the enhanced mineralization phenotype of the *Nmp4*^{-/-} MSCs. On the left: the alizarin red staining of one *Nmp4*^{-/-} MSC line under vehicle and 10 μ M salubrinal treatments on Day 7. On the right: the alizarin red staining of one WT MSC line under vehicle and 10 μ M salubrinal treatments on Day 12.

Protein Synthesis and Associated Pathways	p-value	Z-SCORE	# OF GENES
DAY 3 Regulation of eIF4 and p70S6K Signaling	7.14E-06	3.16	56
DAY 7 Regulation of eIF4 and p70S6K Signaling	0.001122018	2.558	52
DAY 3 tRNA Charging	1.26E-01		21
DAY 7 tRNA Charging	1.47911E-07		24
DAY 3 Unfolded protein response	2.99E-02		17
DAY 7 Unfolded protein response	1.86209E-06		28
DAY 3 mTOR Signaling	4.90E-04	2.949	61
DAY 7 mTOR Signaling	0.000776247	2.714	64
DAY 3 AMPK Signaling	9.33254E-05	1.98	64
DAY 7 AMPK Signaling	0.002630268	1.64	59
DAY 3 NRF2-mediated Oxidative Stress Response	1.02329E-06	4.333	67
DAY 7 NRF2-mediated Oxidative Stress Response	2.51189E-05	4.226	68
DAY 3 Assembly of RNA Polymerase II Complex	0.000870964		20
DAY 7 Assembly of RNA Polymerase II Complex	0.001380384		21
DAY 3 Glycolysis I	0.023442288		14
DAY 7 Glycolysis I	0.00025704		14

Table 3-6: Manually annotated protein synthesis and associated pathways affected by NMP4. The p-value of each pathway, predicted activation z-score and number of genes being affected by NMP4 were also listed.

Loss of Nmp4 alters glycolysis and enhances mitochondrial respiration capacity

To fulfill the increased anabolic activity in *Nmp4 null* MSPCs, the cells need a generally higher level of catabolism for glucose and other energy sources (Funes et al., 2007; Mylotte et al., 2008). As revealed by our IPA output, glycolysis was significantly impacted by loss of *Nmp4* (Table 3-6). Combined with manual annotation (Damman et al., 2015; Soltysova et al., 2015) and Kyoto Encyclopedia of Genes and Genomes (KEGG) database, the data suggested multiple genes involved in glycolysis were significantly altered; these included but not limited to the glucose transporter genes *Slc2a1*, *Slc2a3* and *Slc2a4*, genes encoding for key enzymes in glycolysis: *Aldoa*, *Pgk1*, *Eno3* and *Pkm*, regulatory genes such as *Pdk1*, which inhibits pyruvate from going into the tricarboxylic acid (TCA) cycle as well as lactate transporter genes such as *Slc16a3* (Figure 3-13). Interestingly, several genes encoding for enzymes in the TCA cycle: *Pdha1*, *Pdhb* and *Pdhx* were also mildly upregulated (Figure 3-13).

The Seahorse Mito Stress Assay was performed to evaluate the impact of NMP4 on oxidative phosphorylation in MSPCs. One WT MSPC line and one *Nmp4^{-/-}* MSPC line were used to measure their OCRs under challenges from different drugs. The *null* cells exhibited higher OCRs within each phase of the assay, indicating a higher respiratory rate at basal and maximal level of these cells (Figures 3-14A-C). The ATP production is higher in the *Nmp4^{-/-}* MSPCs (Figures 3-14E), suggesting a higher energy production and consumption level in these cells. The *null* cells also presented higher spare respiratory capacity (Figures 3-14D). This indicated these cells might have larger potential to cope with the increasing energetic demand to meet their metabolic challenge by quickly oxidizing the substrates (e.g. sugar, fat and protein). This finding fits well into our RNA-Seq result that loss of *Nmp4* enhances cellular metabolism.

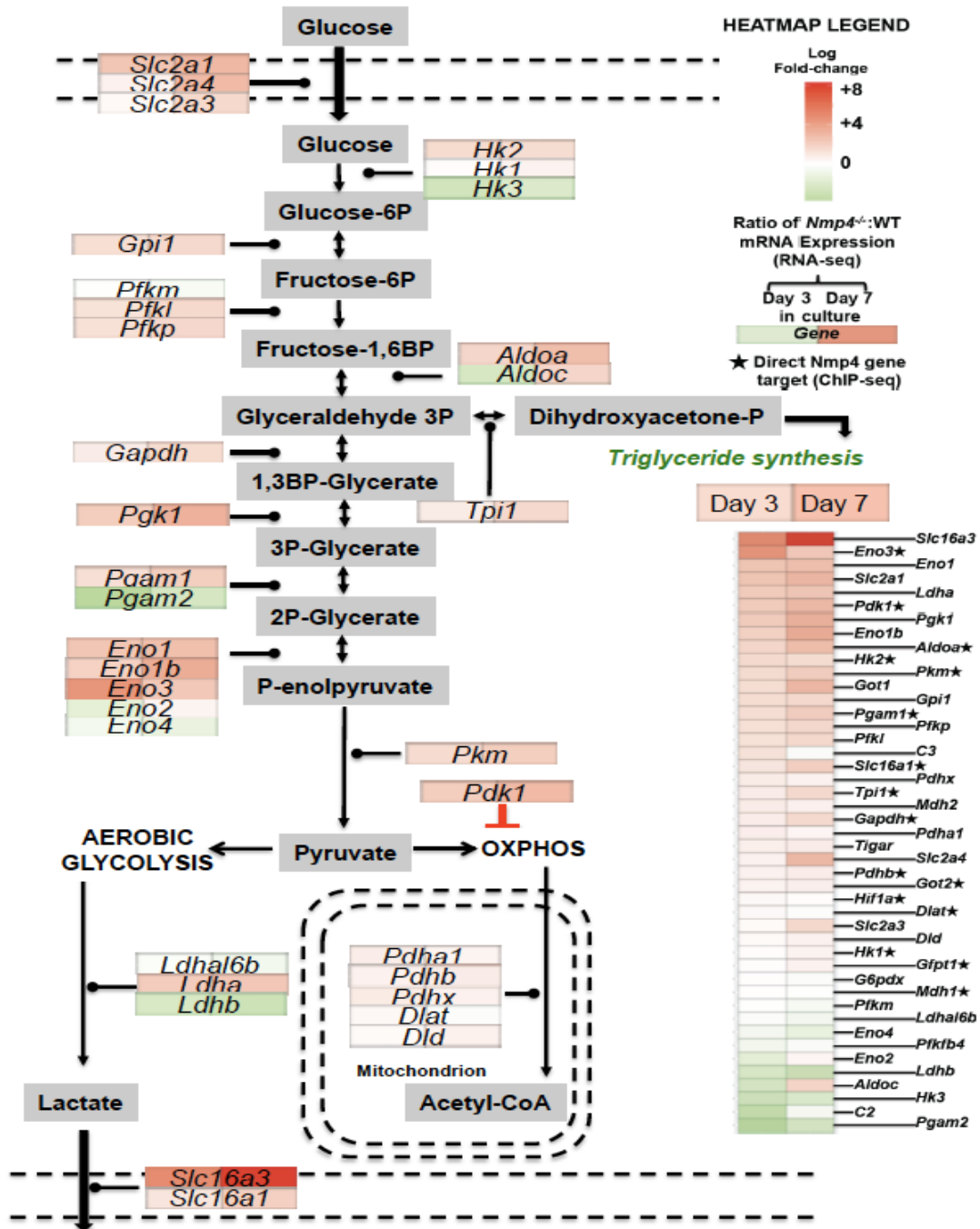


Figure 3-13: Loss of *Nmp4* impacts aerobic glycolysis and oxidative phosphorylation. Genes important for glycolysis and oxidative phosphorylation were generated from IPA and also manually annotated. In the heatmap: *red*-upregulation in the *null* cells; *green*-downregulation in the *null* cells; *left*-Day 3 expression; *right*-Day 7 expression; *star*-direct candidate NMP4 target (ChIP-Seq).

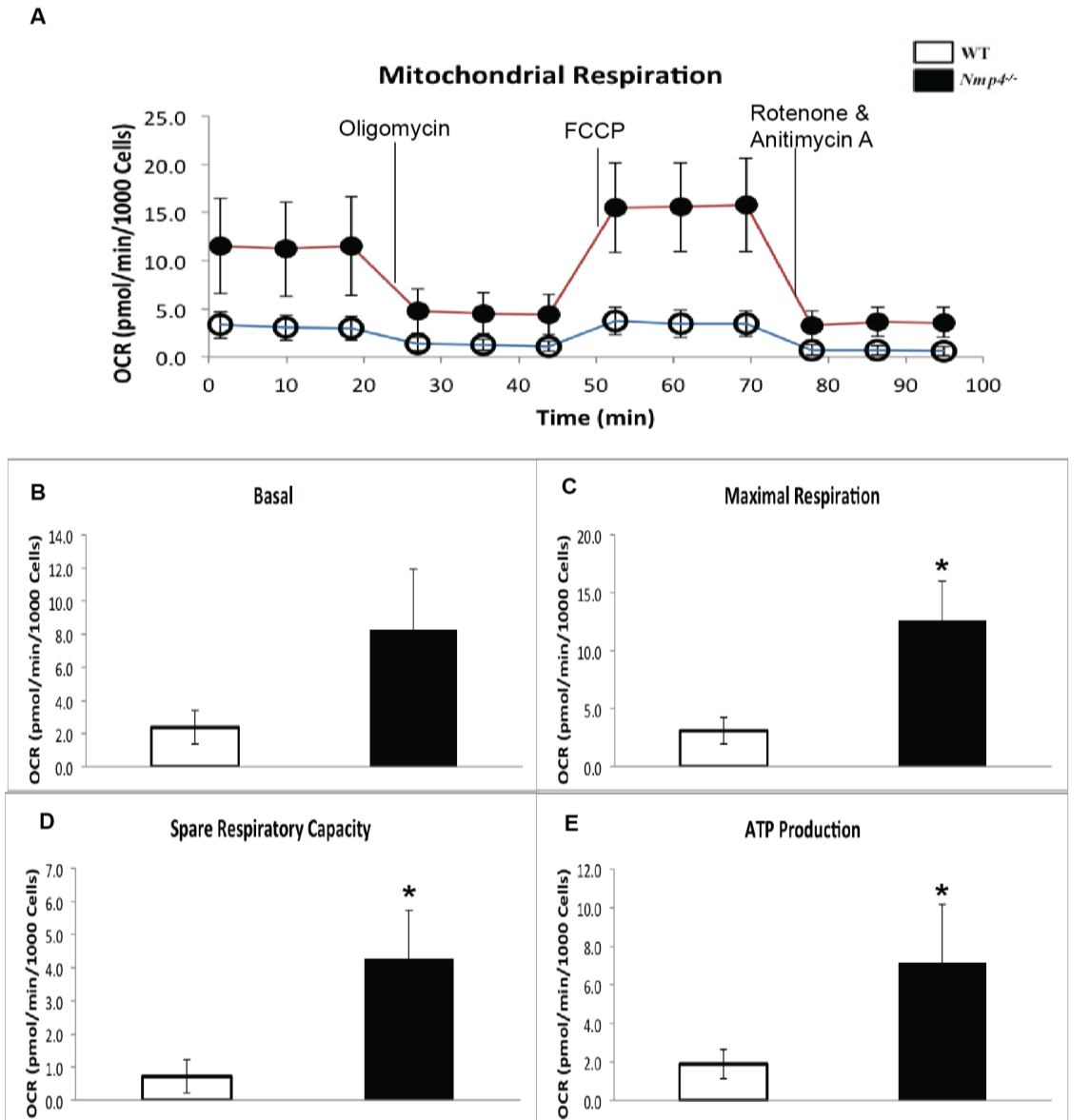


Figure 3-14: The oxidative phosphorylation activity of WT and *Nmp4^{-/-}* MSCs. [A] the oxygen consumption rates of WT and *Nmp4^{-/-}* MSCs upon different drug challenges; the drugs (i.e. oligomycin, FCCP and rotenone & antimycin A) were sequentially added to the culture; OCRs were normalized with cell number [B-E] to compare the aerobic respiration levels between WT and *Nmp4^{-/-}* MSCs, student's t test was used after basal respiration ($p=0.053$), maximal respiration ($p=0.014$), spare respiratory capacity ($p=0.019$) and ATP production ($p=0.044$) were measured or calculated. The data represents average \pm SD.

Loss of Nmp4 impacts immunomodulation

MSPC is an important and active player in immunomodulation; more specifically MSPCs quench down immune response by inhibiting proliferation, differentiation and activation of multiple immune cell types (Abomaray et al., 2015; Cassatella et al., 2011; Gerdoni et al., 2007; Jiang et al., 2016; Selmani et al., 2008). The toll-like receptors (TLRs) were altered in *Nmp4*^{-/-} cells on Day 3 (z-score=-0.5, Table 3-7). *Tlr1-Tlr3* and *Tlr5-Tlr8* were significantly attenuated in mRNA expression in the *Nmp4*^{-/-} cells (Figure 3-15A). Furthermore, multiple immunomodulation pathways in interleukin system were upregulated (Table 3-7). Totally 93 genes directly or indirectly involved in IL-6 signaling are affected by NMP4 (z-score=2.897 on Day 3 and 2.596 on Day 7) (Figure 3-15B, Table 3-7). These include but not limit to major MAP kinase (MAPK) pathway components, AKT family, PI3K complex as well as several downstream targets such as *Vegf* and *Socs3*. All of these suggested an enhanced anti-inflammatory effect of *Nmp4*^{-/-} MSPCs.

To further evaluate the immunomodulatory effect of MSPCs upon loss of *Nmp4*, we performed preliminary study by infecting both WT and *Nmp4*^{-/-} mice with influenza. Our data showed *Nmp4*^{-/-} mice exhibited improved survival to auto-immune response induced by influenza infection, as 15 days after influenza infection, there was no fatality incurring to the *null* mice, while 60% of WT mice were dead (Figure 3-15C). This suggested NMP4 plays a major role in immunomodulation.

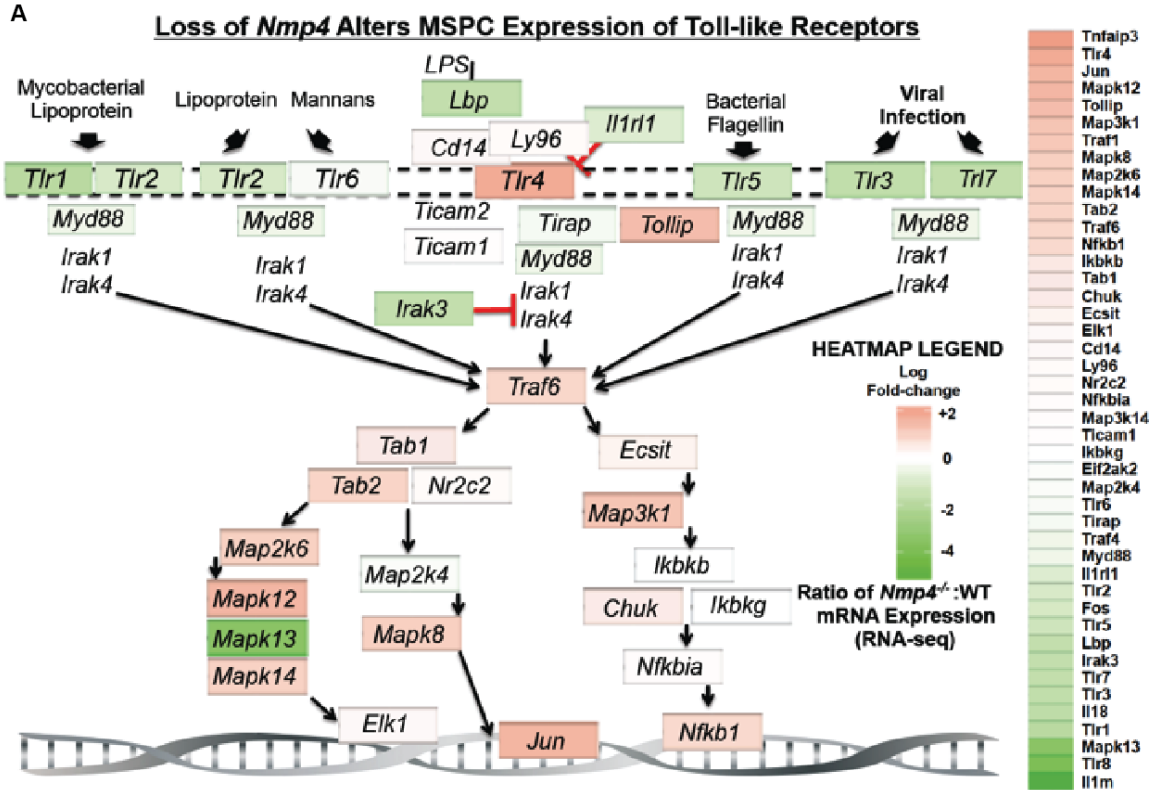
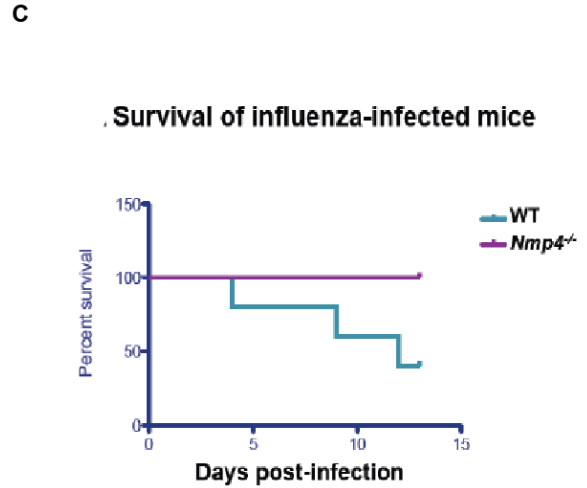
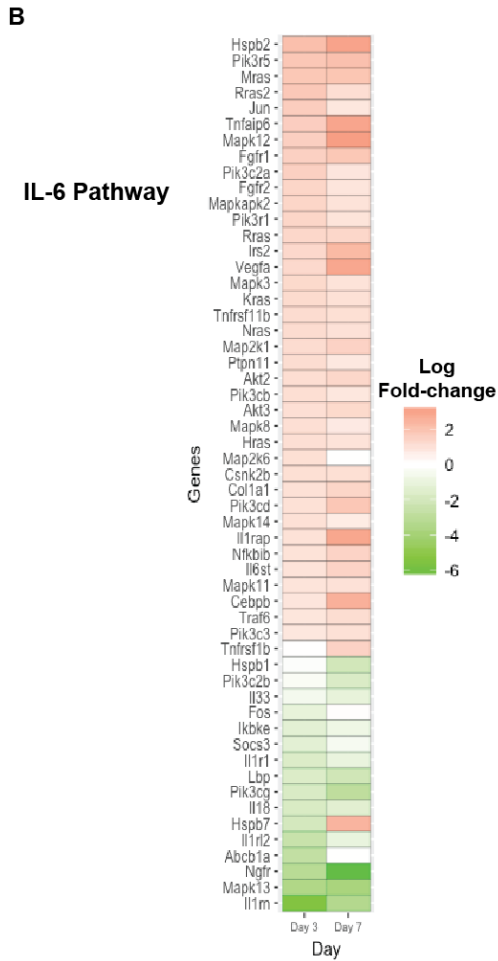


Figure 3-15A: Loss of *Nmp4* impacts immunomodulation, typically through TLR and interleukin pathways. [A] On the left: the schematic of the toll-like receptor signaling pathway; The TLR pathway was significantly enriched for genes showing at least a 2-fold increase or decrease in expression (IPA $p \leq 0.05$, z score = -0.5). *Tlr1-Tlr3* and *Tlr5-Tlr8* were significantly attenuated in mRNA expression in the *Nmp4*^{-/-} cells. On the right: The heatmap of TLR pathway on Day 3 only; *red*-upregulation in the *null* cells; *green*-downregulation in the *null* cells.



Figures 3-15B&C: [B] heatmap for the IL-6 pathway; *red*-upregulation in the *null* cells; *green*-downregulation in the *null* cells; *left*-Day 3 expression; *right*-Day 7 expression. [C] Percentage survival curve of influenza-infected WT and *Nmp4^{-/-}* mice. N=5 mice per group.

Immunomodulation	p-value	Z-SCORE	# OF GENES
DAY 3 IL-1	0.000933254	0.816	32
DAY 7 IL-1	0.037153523	1.964	28
Day 3 IL-2	7.94328E-06	2.353	29
Day 7 IL-2	0.033884416	1.789	21
DAY 3 IL-3	2.5704E-05	1	33
DAY 7 IL-3	0.095499259	1.342	24
Day 3 IL-4	0.000489779		32
Day 7 IL-4	0.047863009		27
Day 3 IL-6	7.24436E-05	2.897	44
Day 7 IL-6	0.016595869	2.596	39
Day 3 IL-8	1.20226E-09	3.064	77
Day 7 IL-8	0.000331131	2.994	65

Table 3-7: Manually annotated immunomodulation pathways affected by NMP4. The p-value of each pathway, predicted activation z-score and number of genes being affected by NMP4 were also listed.

DISCUSSION

The analysis on MSPC secretome showed Loss of *Nmp4* significantly altered extracellular matrix/mineralization transcriptome, which might exert direct impact on bone mechanical and material properties in *Nmp4*^{-/-} animal. Our bone mechanical study involving PTH and PTH+RAL combo therapies first recapitulated what we found in the past that both of these therapies can result in more trabecular bone in the distal femur and L5; meanwhile loss of *Nmp4* further enhances the efficacy of these two therapies in both healthy and OVX mice. On the other hand, however, increased bone turnover and enhanced bone formation often lead to compromised bone quality; for instance, sodium fluoride (NaF) enhances bone formation but the newly formed trabecular bone under NaF treatment is weak with abnormality in the mineral deposit and less trabecular connectivity (Carter and Beaupré, 1990; Everett, 2011; Riggs et al., 1990; Sogaard et al., 1994). Mechanical load can promote bone anabolism but high mechanical load often triggers the formation of woven bone with disorganized bone material and inferior mechanical property (Hernandez et al., 2004; McBride and Silva, 2012). Our study showed loss of *Nmp4* enhanced bone formation under PTH or PTH+RAL treatments, but this was not at the cost of losing bone mechanical properties. This study addresses important question we have with our NMP4 knowledge and is crucial for any further evaluation of this pre-clinical model.

The *Nmp4 null* MSPCs exhibited accelerated mineralization capacity in osteogenic medium and this conclusion was further consolidated in this study by using MSPC cell lines derived from different mice of different genders. One pair of MSPC cell lines derived from WT and *Nmp4*^{-/-} brothers were used in this study, making the evidence more compelling. Our transcriptome analysis revealed multiple genes promoting adipogenesis and chondrogenesis were dampened and several pathways that promote osteoblast differentiation/proliferation were upregulated. Notice that osteogenic differentiation is a delicate, complex and fine-tuned process; it requires multiple transcription factors and signaling pathways to exert their regulatory effects coherently. Loss of *Nmp4* clearly alters

part of this phenotype. For instance, *Nmp4*^{-/-} MSCs over-expressed *Atf4* and *Ddit3*, both of which promote osteogenesis (Pereira et al., 2004; Saito et al., 2011), but these two transcription factors also play a second role in UPR pathway, protein synthesis and secretion (Dey et al., 2012; Fusakio et al., 2016; Willy et al., 2015), which implies the upregulation of these two genes might not necessarily correspond to enhancement of early osteogenesis. Furthermore, although BMP and TGF β signaling pathways were highly activated in the *null* cells, several genes in these pathways (e.g. *Bmp3* and *Runx3*) were known to either inhibit osteogenesis or favor the differentiation towards other lineages (Kokabu et al., 2012; Soung et al., 2007; Yoshida et al., 2004). Most importantly, the master osteogenic transcription factors RUNX2 and OSTERIX exhibited no significant expression difference between WT and *Nmp4*^{-/-} cells. Collectively, all of these suggest that the *Nmp4*^{-/-} MSCs are more biased towards osteogenesis as part of the differentiation phenotype is activated, which coincides with our previous findings of precocious mineralization in *Nmp4*^{-/-} MSCs and elevated osteoprogenitor number in the *null* animal (Childress et al., 2015; He et al., 2013).

Our previous ChIP-Seq analysis and TLDA assay showed that NMP4 exerts its impact on a great variety of pathways and biological/cellular functions (Childress et al., 2015). Our RNA-Seq data supported this finding. The expressions of hundreds of genes were altered with the loss of *Nmp4*. Loss of *Nmp4* impacts IGF1, Wnt, BMP, and TGF- β signaling pathways, all of which were known to promote osteoblast differentiation, proliferation, mineralization and bone formation (Day et al., 2005; De Boer et al., 2004; Hughes-Fulford and Li, 2011; Jia and Heersche, 2000; Mbalaviele et al., 2005; Raucci et al., 2008; Suzuki et al., 2014; Tonna et al., 2014; Xing et al., 2010). Most importantly, crosstalk between these pathways is required for osteoblast development. For example, in one study Wnt/ β -catenin can activate BMP2 expression in osteoblast (Zhang et al., 2013). On the contrary, BMP2 signaling can activate *Dkk1* and *Sost*, the inhibitors of Wnt signaling (Kamiya et al., 2010). TGF- β upregulates IGF1 expression in osteoblast, while prolonged exposure to TGF- β suppresses

osteoblast differentiation via inhibition of IGF1 expression (Ochiai et al., 2012; Okazaki et al., 1995).

A large number of pathways targeted by NMP4 regulate the protein synthesis and associated functions, particularly in cell metabolism, homeostasis and stress response. Loss of *Nmp4* results in upregulation of secretome delivery (expanded ER capacity and UPR pathway), protein synthesis (ribosome biogenesis, tRNA charging, amino acid biosynthesis), redox maintenance and bioenergetics & biosynthesis (Figure 3-16). Two important mediators: mTOR and c-MYC are involved in the upregulation of protein synthesis (Figure 3-16). Loss of *Nmp4* also impacts the TCA cycle via upregulating aerobic glycolysis, the same mechanism exploited by cancer cells to fulfill their high metabolic demands (Cairns et al., 2011; Daye and Wellen, 2012; Hsu and Sabatini, 2008; Wise and Thompson, 2010) (Figure 3-16). All of these altered protein synthesis and associated pathways correlated with increased cell proliferation & differentiation and decreased apoptosis. Meanwhile, we also noticed an increased expression of *Pthr* and *gp130*, suggesting a hyper-responsiveness to PTH (Figure 3-16). These changes may explain the anabolic phenotype we observed in *Nmp4*^{-/-} mice, though further confirmatory studies are required.

Glycolysis, especially lactate-producing aerobic glycolysis plays an essential role in regulating osteoblast function. One study showed both aerobic glycolysis and oxidative phosphorylation were utilized during osteoblast differentiation (Guntur et al., 2014). Wnt signaling as a crucial pathway stimulating osteoblast differentiation was found to induce aerobic glycolysis during this process (Esen et al., 2013). Moreover, a recent study showed intermittent PTH induced IGF1 signaling, which in turn promoted bone anabolism via aerobic glycolysis (Esen et al., 2015). All of these findings make glycolysis as well as oxidative phosphorylation promising targets in the anti-anabolic axis of NMP4 for further study. Additionally, as shown by the IPA output, tRNA charging was also a major target of NMP4. Previous studies implied this pathway might also be able to contribute to osteogenesis via promoting osteoblast survival and function (Park et al., 2009; Yamaguchi and Sugimoto, 2000). Together with

enhanced c-MYC mediated ribosomal biogenesis and the UPR pathway, the *Nmp4 null* MSCs become super-secretory and hyper-anabolic.

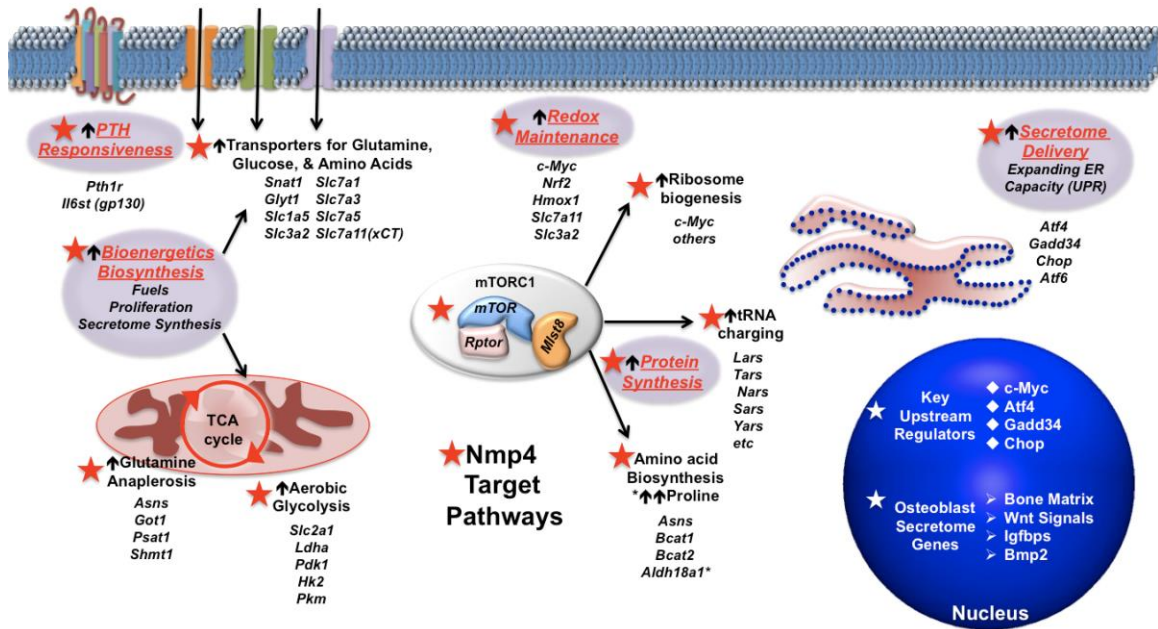


Figure 3-16: The Nmp4 Anti-Anabolic Bone Axis. Nmp4 is an apex regulator of several pathways that are important for protein synthesis and associated functions, driving PTH-induced osteoprogenitor proliferation and osteoblast bone matrix synthesis and delivery. Not shown, the loss of Nmp4 biases MSC lineage commitment toward osteogenesis. Only a few of the Nmp4 target genes (direct and indirect based on genomic and transcriptomic data) are shown.

Finally, our study showed that NMP4 impacts pathways involving immunomodulation. MSCs are known to suppress immune response by inhibiting proliferation, differentiation and activation of multiple immune cell types (Abomaray et al., 2015; Cassatella et al., 2011; Gerdoni et al., 2007; Jiang et al., 2016; Selmani et al., 2008). Multiple reports have associated the immunomodulation function of MSCs with interleukin families and TLR pathways. For instance, MSCs exhibit anti-inflammatory effect via secreting IL-1, IL-6 and expressing *Tlr3/Tlr4* (Liotta et al., 2008; Melief et al., 2013; Ortiz et al., 2007). More interestingly, our preliminary data showed that the *Nmp4^{-/-}* mice were more resistant to the host immune response induced by influenza virus (Figure 3-15C). In fact, we propose that the improved survival of infected *Nmp4^{-/-}* mice was caused by 1) super-secretory activity of lung alveolar type 2 (AT2) cells due to the global alteration of UPR pathways in *Nmp4^{-/-}* mice and enhanced clearance of apoptotic neutrophils (PMNs) and 2) Altered TLR pathways in *Nmp4^{-/-}* MSCs that enhanced their anti-inflammatory effect on PMNs. To clarify the role of NMP4 in immunomodulation, more studies are needed.

Although *Nmp4* is expressed in almost all tissues in the body, our previous ChIP-Seq data revealed that its candidate gene targets are not exactly the same between different cell types (Childress et al., 2015). This is possibly due to the fact that different cells adopt different chromatin structures, making the targets of NMP4 more or less likely to get access to (Li, 2002). Moreover, NMP4 is a context-dependent transcription factor that may exert different impacts on the same gene in different cell types (Torrunguang et al., 2002). Collectively, these clues may imply different transcriptome profiles are present in tissues other than bone and explain why loss of *Nmp4* does not cause a global phenotype of enhanced anabolism.

NEW QUESTIONS AND FUTURE DIRECTIONS

Although we have collected a lot of evidence to delineate the molecular mechanism of *Nmp4*'s phenotype in bone, we still lack solid confirmatory data to consolidate our findings through the transcriptome profiling. The expression

profiles of several representative genes such as *c-Myc*, *Atf4* and *Gadd34* need to be determined in other MSPC lines. Our Seahorse Assay showed NMP4 restricts the level of oxidative phosphorylation in MSPCs but more experiments are needed to evaluate the glycolytic levels between WT and *null* cells. Our salubrinal-induced phenotype rescue experiment requires quantitation and further optimization. To conclude, this study is not yet complete, but we are confident to claim thousands of genes and multiple signaling pathways are candidate NMP4 targets, each of which to some degree may contribute to the bone phenotype of *Nmp4*; at the tissue level, loss of *Nmp4* may affect bone development, function as well as ECM secretome via altered UPR pathway and elevated ribosomal biogenesis, and thus improves the mechanical and material properties of the bone.

CONTRIBUTIONS

In the project described above, I grow and expanded MSPCs, filtered and sorted the RNA-Seq data, ran IPA analysis and generated heatmaps for pathways and biological functions; I took part in the mice treatment, bone collection/storage and was involved in the three-point bending experiment. I conducted the MSPC mineralization assay and the phenotype rescue experiment with salubrinal as well. I also worked with my colleague Kylie Jacob in the Seahorse Mitochondria Stress Test.

CHAPTER 4

SUMMARY

We demonstrated that the heightened osteoanabolism of the *Nmp4*^{-/-} skeleton enhances the effectiveness of diverse osteoporosis treatments, in part by increasing hyper-anabolic osteoprogenitors. In general, the efficacies of anabolic therapies corresponded with PTH+RAL=PTH+ZOL>PTH+ALN=PTH>VEH. The enhanced trabecular bone gain in *Nmp4*^{-/-} mice did not impair the gain in cortical bone under PTH+RAL or PTH+ZOL. The response of WT and *Nmp4*^{-/-} mice to single anti-catabolic drugs was also examined and the result revealed both RAL and ZOL treatments resulted in modest but significant restoration of bone. Unexpectedly, loss of *Nmp4* improved RAL treatment response at the site of femoral trabeculae. Immunohistochemistry and flow cytometry revealed elevated number of BM osteoprogenitors in *Nmp4*^{-/-} mice under PTH+RAL but not PTH+ZOL treatment compared to the WT counterpart; while the WT cohorts did not show this dichotomy. Our data suggest that the enhanced response to anabolic therapies observed in *Nmp4*^{-/-} mice could be partially but not completely attributed to the expanded osteoprogenitor pool. Loss of *Nmp4* did not affect adipogenesis or osteoclastogenesis in the BM. *Nmp4* status did not influence bone serum marker responses to treatments but *Nmp4*^{-/-} mice as a group showed elevated levels of the bone formation marker osteocalcin. The implication regarding osteoporosis treatment is that disabling *Nmp4* will boost the anabolic activity associated with any particular therapy. Suppression of the bone formation inhibitor sclerostin with the drug romosozumab represents a route to bone anabolism and is proof of principle that impeding osteogenic inhibitors is a powerful approach to therapy (Cosman et al., 2016a). NMP4 is another kind of inhibitor in that its inactivation boosts the response potency to osteoanabolics, but unlike romosozumab it does not impact baseline skeletal phenotype.

Consistent with previous *in vivo* studies (Childress et al., 2015; Robling et al., 2009) we found evidence that the *Nmp4*^{-/-} MSPCs exhibited enhanced and accelerated mineralization capacity over the WT counterpart upon osteogenic differentiation. The MSPCs in general tended to mineralize 7-14 days earlier than the WT cells. Furthermore, the mineral deposit in *Nmp4*^{-/-} MSPCs tended to accumulate faster than the WT, as they became heavily mineralized within 3 days after the first sign of mineralization.

The transcriptome analysis demonstrated the *Nmp4*^{-/-} MSPCs exhibited altered secretome profile including multiple ECM proteins and genes promoting mineralization and bone integrity, which suggested strengthened bone material and mechanical properties in the *null* animal. Our 3-point bending studies provide convincing preliminary data that this is indeed the case. The *Nmp4*^{-/-} bones showed a significant increase in ultimate stress, which is the force necessary to fracture a bone under specified conditions, normalized for the bone geometry. Yield stress, the force applied to the bone after which there is permanent damage, normalized for geometry, was also significantly higher in the *Nmp4*^{-/-} femurs. The study suggested no compromise was made to the bone quality for more rapid and increased bone formation in *Nmp4*^{-/-} mice.

Differential transcriptome analysis showed NMP4 directly or indirectly impacted several hundred pathways that could be classified into 3 categories: protein synthesis and associated pathways, bone-related pathways and immunomodulation pathways. For protein synthesis and associated pathways, pathways involving in protein synthesis and secretion (e.g. tRNA charging, ribosomal biogenesis, RNA polymerase II assembly and mTOR pathway) and metabolism (e.g. glycolysis) were upregulated or altered in *Nmp4*^{-/-} MSPCs. Bone-related pathways included but not limited to IGF-1, Ephrin, Glucocorticoid, Wnt/ β catenin, STAT3, estrogen receptor, VEGF, TGF- β and BMP signaling pathways; most of these pathways were upregulated in *Nmp4*^{-/-} MSPCs. NMP4 affected different aspects of immunomodulation and one particular group of pathways affecting MSPC function fell into the interleukin system.

Specifically, loss of *Nmp4* activates IGF1, Wnt, BMP and TGF- β signaling pathways, all of which play important roles in osteoprogenitor proliferation, osteoblast differentiation, mineralization and bone formation (Day et al., 2005; De Boer et al., 2004; Hughes-Fulford and Li, 2011; Jia and Heersche, 2000; Mbalaviele et al., 2005; Raucci et al., 2008; Suzuki et al., 2014; Tonna et al., 2014; Xing et al., 2010); moreover, the crosstalk between these pathways promotes osteogenesis (Kamiya et al., 2010; Ochiai et al., 2012; Zhang et al., 2013). Loss of *Nmp4* also alters expression of several key genes in the UPR pathway and ribosomal biogenesis (Figure 4-1); many of these genes (e.g. *Perk*, *Atf4*, *Ddit3* and *Myc*) have been found to be important for osteoblast differentiation and bone formation. Inhibition of GADD34 via salubrinal resulted in attenuated mineralization in *Nmp4*^{-/-} MSCs, suggesting the UPR pathway mediates part of *Nmp4*^{-/-} phenotype potentially by making the *null* cells super-secretory. Furthermore, loss of *Nmp4* also alters aerobic glycolysis, which was found to be intimately associated with osteogenesis (Esen et al., 2015; Guntur et al., 2014). Our Seahorse Assay showed elevated basal and spared capacities for oxidative phosphorylation in *Nmp4*^{-/-} MSCs. The elevated oxidative phosphorylation in *Nmp4*^{-/-} MSCs also resulted in much more ATP production compared to their WT counterparts. Finally, our preliminary data showed *Nmp4*^{-/-} mice exhibited stronger resistance to host immune response induced by influenza virus, providing direct evidence of the impact of disabling *Nmp4* on immunomodulation. We concluded that NMP4 is an apex regulator impacting directly or indirectly multiple protein synthesis and associated pathways, bone-related pathways and immunomodulation pathways; these pathways in turn affect protein synthesis and secretion, glucose metabolism, osteoprogenitor proliferation, osteoblast differentiation/ mineralization and immune response.

To complete the transcriptome analysis of NMP4, a few more follow-up studies shall be performed in the near future. The expression profiles of several key genes such as *c-Myc*, *Atf4* and *Gadd34* need to be determined in multiple other MSC lines. The glycolytic levels of several WT and *Nmp4*^{-/-} MSC lines

also need to be evaluated. Our salubrinal-induced phenotype rescue experiment requires quantitation and further optimization.

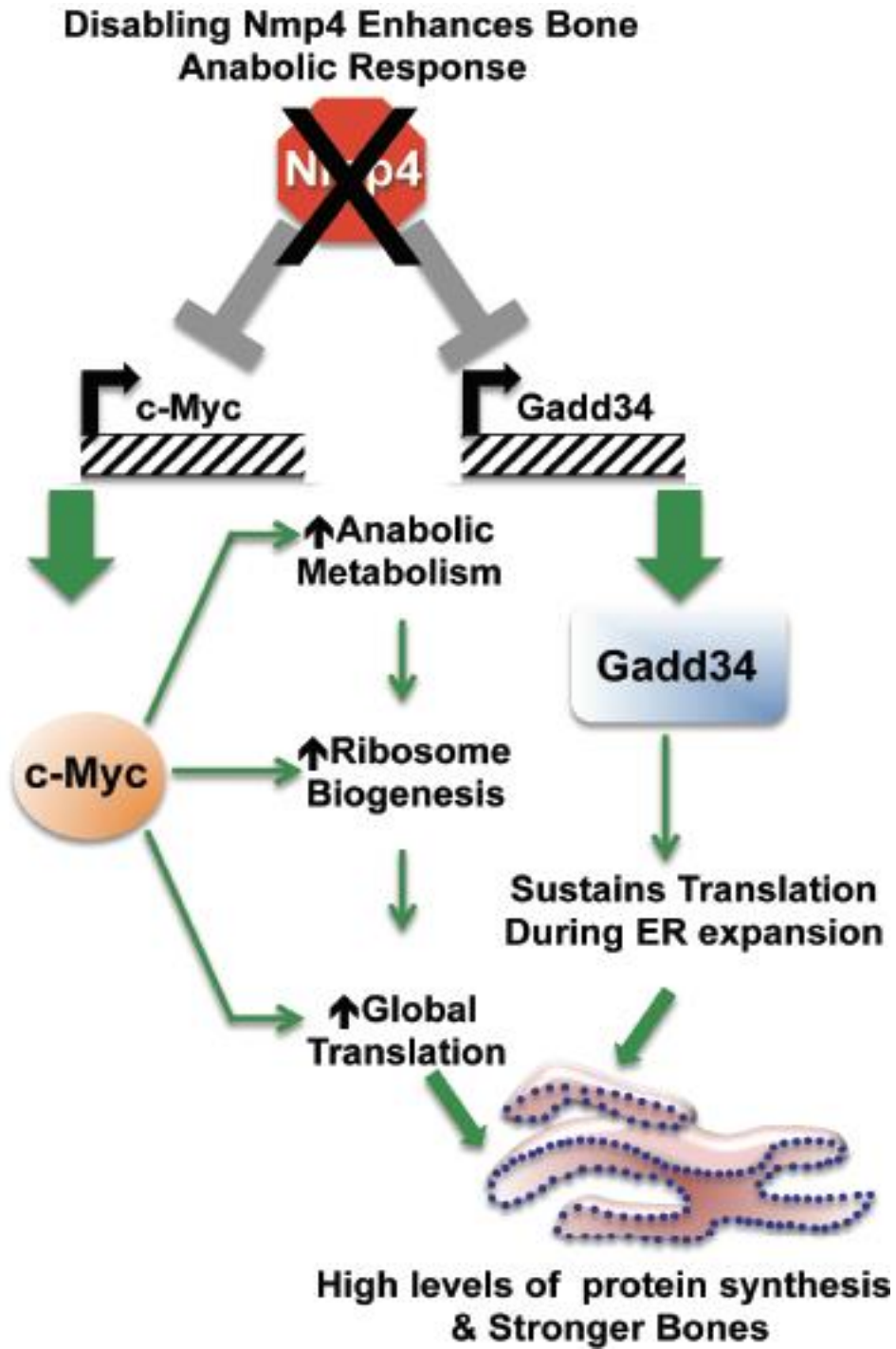


Figure 4-1: c-MYC and GADD34 are the key regulators that drive the *Nmp4*^{-/-} hyper-anabolism phenotype. Loss of *Nmp4* upregulates the expression of c-MYC

and GADD34. c-MYC promotes aerobic glycolysis (Shim et al., 1997), maintaining an elevated level of anabolic metabolism; c-MYC also enhances ribosomal biogenesis (Boon et al., 2001), leading to increased level of global protein synthesis. On the other hand, upregulated GADD34 suppresses eIF2 α upon activation the UPR pathway. This leads to sustained level of protein translation during ER expansion. Collectively, these changes in *Nmp4*^{-/-} MSCs result in hyper-anabolic and super-secretory cells, making the bone improve both in quantity and quality.

REFERENCES

Abomaray, F., Al Jumah, M., Kalionis, B., AlAskar, A., Al Harthy, S., Jawdat, D., Al Khaldi, A., Alkushi, A., Knawy, B., and Abumaree, M. (2015). Human chorionic villous mesenchymal stem cells modify the functions of human dendritic cells, and induce an anti-inflammatory phenotype in CD1+ dendritic cells. *Stem Cell Reviews and Reports* 11, 423-441.

Adachi, J.D., Saag, K.G., Delmas, P.D., Liberman, U.A., Emkey, R.D., Seeman, E., Lane, N.E., Kaufman, J.M., Poubelle, P.E., Hawkins, F., *et al.* (2001). Two-year effects of alendronate on bone mineral density and vertebral fracture in patients receiving glucocorticoids: a randomized, double-blind, placebo-controlled extension trial. *Arthritis and rheumatism* 44, 202-211.

Alvarez, M., Thunyakitpisal, P., Morrison, P., Onyia, J., Hock, J., and Bidwell, J.P. (1998). PTH-responsive osteoblast nuclear matrix architectural transcription factor binds to the rat type I collagen promoter. *Journal of Biological Chemistry* 69, 336-352.

Amugongo, S.K., Yao, W., Jia, J., Dai, W., Lay, Y.A., Jiang, L., Harvey, D., Zimmermann, E.A., Schaible, E., Dave, N., *et al.* (2014). Effect of sequential treatments with alendronate, parathyroid hormone (1-34) and raloxifene on cortical bone mass and strength in ovariectomized rats. *Bone* 67, 257-268.

Arai, F., Hirao, A., Ohmura, M., Sato, H., Matsuoka, S., Takubo, K., Ito, K., Koh, G.Y., and Suda, T. (2004). Tie2/angiopoietin-1 signaling regulates hematopoietic stem cell quiescence in the bone marrow niche. *Cell* 118, 149-161.

Banfi, A., Bianchi, G., Notaro, R., Luzzatto, L., Cancedda, R., and Quarto, R. (2002). Replicative aging and gene expression in long-term cultures of human bone marrow stromal cells. *Tissue engineering* 8, 901-910.

Bara, J.J., Richards, R.G., Alini, M., and Stoddart, M.J. (2014). Concise review: Bone marrow-derived mesenchymal stem cells change phenotype following in vitro culture: implications for basic research and the clinic. *Stem cells (Dayton, Ohio)* 32, 1713-1723.

Bath, P.M., and Gray, L.J. (2005). Association between hormone replacement therapy and subsequent stroke: a meta-analysis. *BMJ (Clinical research ed)* 330, 342.

Bedi, B., Li, J.-Y., Tawfeek, H., Baek, K.-H., Adams, J., Vangara, S.S., Chang, M.-K., Kneissel, M., Weitzmann, M.N., and Pacifici, R. (2012). Silencing of parathyroid hormone (PTH) receptor 1 in T cells blunts the bone anabolic activity of PTH. *Proceedings of the National Academy of Sciences* 109, E725-E733.

Bellido, T., Ali, A.A., Plotkin, L.I., Fu, Q., Gubrij, I., Roberson, P.K., Weinstein, R.S., O'Brien, C.A., Manolagas, S.C., and Jilka, R.L. (2003). Proteasomal degradation of Runx2 shortens parathyroid hormone-induced anti-apoptotic signaling in osteoblasts. A putative explanation for why intermittent administration is needed for bone anabolism. *The Journal of biological chemistry* 278, 50259-50272.

Bertolotti, A., Zhang, Y., Hendershot, L.M., Harding, H.P., and Ron, D. (2000). Dynamic interaction of BiP and ER stress transducers in the unfolded-protein response. *Nature cell biology* 2, 326-332.

Bikle, D.D., Sakata, T., Leary, C., Elalieh, H., Ginzinger, D., Rosen, C.J., Beamer, W., Majumdar, S., and Halloran, B.P. (2002). Insulin-like growth factor I is required for the anabolic actions of parathyroid hormone on mouse bone. *Journal of Bone and Mineral Research* 17, 1570-1578.

Bilezikian, J.P. (2008). Combination anabolic and antiresorptive therapy for osteoporosis: opening the anabolic window. *Current osteoporosis reports* 6, 24-30.

Black, D.M., Greenspan, S.L., Ensrud, K.E., Palermo, L., McGowan, J.A., Lang, T.F., Garnero, P., Bouxsein, M.L., Bilezikian, J.P., and Rosen, C.J. (2003). The effects of parathyroid hormone and alendronate alone or in combination in postmenopausal osteoporosis. *New England Journal of Medicine* 349, 1207-1215.

Black, D.M., and Schafer, A.L. (2013). The search for the optimal anabolic osteoporosis therapy. *Journal of Bone and Mineral Research* 28, 2263-2265.

Blocki, A., Wang, Y., Koch, M., Peh, P., Beyer, S., Law, P., Hui, J., and Raghunath, M. (2013). Not all MSCs can act as pericytes: functional in vitro assays to distinguish pericytes from other mesenchymal stem cells in angiogenesis. *Stem cells and development* 22, 2347-2355.

Bolland, M.J., Grey, A.B., Horne, A.M., Briggs, S.E., Thomas, M.G., Ellis-Pegler, R.B., Callon, K.E., Gamble, G.D., and Reid, I.R. (2008). Effects of intravenous zoledronate on bone turnover and BMD persist for at least 24 months. *Journal of bone and mineral research : the official journal of the American Society for Bone and Mineral Research* 23, 1304-1308.

Bonab, M.M., Alimoghaddam, K., Talebian, F., Ghaffari, S.H., Ghavamzadeh, A., and Nikbin, B. (2006). Aging of mesenchymal stem cell in vitro. *BMC cell biology* 7, 14.

Boon, K., Caron, H.N., van Asperen, R., Valentijn, L., Hermus, M.C., van Sluis, P., Roobeek, I., Weis, I., Voute, P., and Schwab, M. (2001). N-myc enhances the

expression of a large set of genes functioning in ribosome biogenesis and protein synthesis. *The EMBO journal* 20, 1383-1393.

Boonen, S., Marin, F., Obermayer-Pietsch, B., Simoes, M.E., Barker, C., Glass, E.V., Hadji, P., Lyritis, G., Oertel, H., Nickelsen, T., *et al.* (2008). Effects of previous antiresorptive therapy on the bone mineral density response to two years of teriparatide treatment in postmenopausal women with osteoporosis. *The Journal of clinical endocrinology and metabolism* 93, 852-860.

Boregowda, S., Krishnappa, V., Chambers, J., LoGrasso, P.V., Lai, W.T., Ortiz, L.A., and Phinney, D.G. (2012). Atmospheric Oxygen Inhibits Growth and Differentiation of Marrow-Derived Mouse Mesenchymal Stem Cells via a p53 Dependent Mechanism: Implications for Long-Term Culture Expansion. *Stem cells (Dayton, Ohio)* 30, 975-987.

Borrelli, J. (2012). Taking Control: The Osteoporosis Epidemic. *Injury* 43, 1235-1236.

Bruder, S.P., Jaiswal, N., and Haynesworth, S.E. (1997). Growth kinetics, self-renewal, and the osteogenic potential of purified human mesenchymal stem cells during extensive subcultivation and following cryopreservation. *Journal of cellular biochemistry* 64, 278-294.

Brush, M.H., Weiser, D.C., and Shenolikar, S. (2003). Growth arrest and DNA damage-inducible protein GADD34 targets protein phosphatase 1 α to the endoplasmic reticulum and promotes dephosphorylation of the α subunit of eukaryotic translation initiation factor 2. *Molecular and cellular biology* 23, 1292-1303.

Burr, D.B., Hirano, T., Turner, C.H., Hotchkiss, C., Brommage, R., and Hock, J.M. (2001). Intermittently administered human parathyroid hormone(1-34) treatment increases intracortical bone turnover and porosity without reducing bone strength in the humerus of ovariectomized cynomolgus monkeys. *Journal of Bone and Mineral Research* 16, 157-165.

Burr, D.B., Liu, Z., and Allen, M.R. (2015). Duration-dependent effects of clinically relevant oral alendronate doses on cortical bone toughness in beagle dogs. *Bone* 71, 58-62.

Cairns, R.A., Harris, I.S., and Mak, T.W. (2011). Regulation of cancer cell metabolism. *Nature Reviews Cancer* 11, 85-95.

Calleja, V., Laguerre, M., de las Heras-Martinez, G., Parker, P.J., Requejo-Isidro, J., and Larijani, B. (2014). Acute regulation of PDK1 by a complex interplay of molecular switches (Biochemical Society Transactions: Portland Press Limited).

Calvi, L.M., Adams, G.B., Weibrecht, K.W., Weber, J.M., Olson, D.P., Knight, M.C., Martin, R.P., Schipani, E., Divieti, P., Bringhurst, F.R., *et al.* (2003). Osteoblastic cells regulate the haematopoietic stem cell niche. *Nature* 425, 841-846.

Calvi, L.M., Sims, N.A., Hunzelman, J.L., Knight, M.C., Giovannetti, A., Saxton, J.M., Kronenberg, H.M., Baron, R., and Schipani, E. (2001). Activated parathyroid hormone/parathyroid hormone-related protein receptor in osteoblastic cells differentially affects cortical and trabecular bone. *The Journal of clinical investigation* 107, 277-286.

Cano, A., Dapia, S., Noguera, I., Pineda, B., Hermenegildo, C., del Val, R., Caeiro, J.R., and Garcia-Perez, M.A. (2008). Comparative effects of 17beta-estradiol, raloxifene and genistein on bone 3D microarchitecture and volumetric

bone mineral density in the ovariectomized mice. *Osteoporosis international* 19, 793-800.

Caplan, A.I. (2007). Adult mesenchymal stem cells for tissue engineering versus regenerative medicine. *Journal of cellular physiology* 213, 341-347.

Carter, D.R., and Beaupré, G.S. (1990). Effects of fluoride treatment on bone strength. *Journal of Bone and Mineral Research* 5, S177-S184.

Cary, L.A., Han, D.C., Polte, T.R., Hanks, S.K., and Guan, J.L. (1998). Identification of p130Cas as a mediator of focal adhesion kinase-promoted cell migration. *The Journal of cell biology* 140, 211-221.

Cassatella, M.A., Mosna, F., Micheletti, A., Lisi, V., Tamassia, N., Cont, C., Calzetti, F., Pelletier, M., Pizzolo, G., and Krampera, M. (2011). Toll-like receptor-3-activated human mesenchymal stromal cells significantly prolong the survival and function of neutrophils. *Stem Cells* 29, 1001-1011.

Cauley, J.A., Norton, L., Lippman, M.E., Eckert, S., Krueger, K.A., Purdie, D.W., Farrerons, J., Karasik, A., Mellstrom, D., Ng, K.W., *et al.* (2001). Continued breast cancer risk reduction in postmenopausal women treated with raloxifene: 4-year results from the MORE trial. Multiple outcomes of raloxifene evaluation. *Breast cancer research and treatment* 65, 125-134.

Chambers, J.E., and Marciniak, S.J. (2014). Cellular mechanisms of endoplasmic reticulum stress signaling in health and disease. 2. Protein misfolding and ER stress. *American Journal of Physiology-Cell Physiology* 307, C657-C670.

Chan, C.K., Chen, C.C., Luppen, C.A., Kim, J.B., DeBoer, A.T., Wei, K., Helms, J.A., Kuo, C.J., Kraft, D.L., and Weissman, I.L. (2009). Endochondral ossification is required for haematopoietic stem-cell niche formation. *Nature* 457, 490-494.

Chan, C.K., Seo, E.Y., Chen, J.Y., Lo, D., McArdle, A., Sinha, R., Tevlin, R., Seita, J., Vincent-Tompkins, J., Wearda, T., *et al.* (2015). Identification and specification of the mouse skeletal stem cell. *Cell* 160, 285-298.

Chiellini, C., Cochet, O., Negroni, L., Samson, M., Poggi, M., Ailhaud, G., Alessi, M.-C., Dani, C., and Amri, E.-Z. (2008). Characterization of human mesenchymal stem cell secretome at early steps of adipocyte and osteoblast differentiation. *BMC Molecular Biology* 9, 26.

Childress, P., Philip, B.K., Robling, A.G., Bruzzaniti, A., Kacena, M.A., Bivi, N., Plotkin, L.I., Heller, A., and Bidwell, J.P. (2011). Nmp4/CIZ suppresses the response of bone to anabolic parathyroid hormone by regulating both osteoblasts and osteoclasts. *Calcified tissue international* 89, 74-89.

Childress, P., Stayrook, K.R., Alvarez, M.B., Wang, Z., Shao, Y., Hernandez-Buquer, S., Mack, J.K., Grese, Z.R., He, Y., Horan, D., *et al.* (2015). Genome-Wide Mapping and Interrogation of the Nmp4 Antianabolic Bone Axis. *Molecular Endocrinology* 29, 1269-1285.

Chuang, T.J., Lin, K.C., Chio, C.C., Wang, C.C., Chang, C.P., and Kuo, J.R. (2012). Effects of secretome obtained from normoxia-preconditioned human mesenchymal stem cells in traumatic brain injury rats. *The journal of trauma and acute care surgery* 73, 1161-1167.

Connor, J.H., Weiser, D.C., Li, S., Hallenbeck, J.M., and Shenolikar, S. (2001). Growth arrest and DNA damage-inducible protein GADD34 assembles a novel signaling complex containing protein phosphatase 1 and inhibitor 1. *Molecular and cellular biology* 21, 6841-6850.

Cordes, C., Baum, T., Dieckmeyer, M., Ruschke, S., Diefenbach, M.N., Hauner, H., Kirschke, J.S., and Karampinos, D.C. (2016). MR-Based Assessment of Bone Marrow Fat in Osteoporosis, Diabetes, and Obesity. *Frontiers in endocrinology* 7, 74.

Corrado, A., Neve, A., Maruotti, N., Gaudio, A., Marucci, A., and Cantatore, F.P. (2010). Dose-dependent metabolic effect of zoledronate on primary human osteoblastic cell cultures. *Clinical and experimental rheumatology* 28, 873-879.

Corselli, M., Chin, C.J., Parekh, C., Sahaghian, A., Wang, W., Ge, S., Evseenko, D., Wang, X., Montelatici, E., Lazzari, L., *et al.* (2013). Perivascular support of human hematopoietic stem/progenitor cells. *Blood* 121, 2891-2901.

Cosman, F. (2014). Combination therapy for osteoporosis: a reappraisal. *BoneKEy reports* 3, 518.

Cosman, F., Crittenden, D.B., Adachi, J.D., Binkley, N., Czerwinski, E., Ferrari, S., Hofbauer, L.C., Lau, E., Lewiecki, E.M., and Miyauchi, A. (2016a). Romosozumab treatment in postmenopausal women with osteoporosis. *New England Journal of Medicine* 375, 1532-1543.

Cosman, F., Eriksen, E.F., Recknor, C., Miller, P.D., Guanabens, N., Kasperk, C., Papanastasiou, P., Readie, A., Rao, H., Gasser, J.A., *et al.* (2011). Effects of intravenous zoledronic acid plus subcutaneous teriparatide [rhPTH(1-34)] in postmenopausal osteoporosis. *Journal of Bone and Mineral Research* 26, 503-511.

Cosman, F., Keaveny, T.M., Kopperdahl, D., Wermers, R.A., Wan, X., Krohn, K.D., and Krege, J.H. (2013). Hip and spine strength effects of adding versus switching to teriparatide in postmenopausal women with osteoporosis treated with prior alendronate or raloxifene. *Journal of bone and mineral research : the*

official journal of the American Society for Bone and Mineral Research 28, 1328-1336.

Cosman, F., Nieves, J.W., and Dempster, D. (2016b). Treatment Sequence Matters: Anabolic and Antiresorptive Therapy for Osteoporosis. *Journal of Bone and Mineral Research*.

Cosman, F., Wermers, R.A., Recknor, C., Mauck, K.F., Xie, L., Glass, E.V., and Krege, J.H. (2009). Effects of teriparatide in postmenopausal women with osteoporosis on prior alendronate or raloxifene: differences between stopping and continuing the antiresorptive agent. *The Journal of clinical endocrinology and metabolism* 94, 3772-3780.

Crane, J.L., Xian, L., and Cao, X. (2016). Role of TGF- β signaling in coupling bone remodeling. *TGF- β Signaling: Methods and Protocols*, 287-300.

Credle, J.J., Finer-Moore, J.S., Papa, F.R., Stroud, R.M., and Walter, P. (2005). On the mechanism of sensing unfolded protein in the endoplasmic reticulum. *Proceedings of the National Academy of Sciences of the United States of America* 102, 18773-18784.

Cryer, B., and Bauer, D.C. (2002). Oral bisphosphonates and upper gastrointestinal tract problems: what is the evidence? Paper presented at: Mayo Clinic Proceedings (Elsevier).

Cusano, N.E., and Bilezikian, J.P. (2013). Comparative effectiveness of combination osteoanabolic and antiresorptive therapy for osteoporosis: an update. *Journal of comparative effectiveness research* 2, 511-513.

Cusano, N.E., Costa, A.G., Silva, B.C., and Bilezikian, J.P. (2011). Therapy of osteoporosis in men with teriparatide. *Journal of osteoporosis* 2011, 463675.

da Silva Meirelles, L., Caplan, A.I., and Nardi, N.B. (2008). In search of the in vivo identity of mesenchymal stem cells. *Stem cells (Dayton, Ohio)* 26, 2287-2299.

Dai, J.C., He, P., Chen, X., and Greenfield, E.M. (2006). TNF α and PTH utilize distinct mechanisms to induce IL-6 and RANKL expression with markedly different kinetics. *Bone* 38, 509-520.

Damman, J., Bloks, V.W., Daha, M.R., van der Most, P.J., Sanjabi, B., van der Vlies, P., Snieder, H., Ploeg, R.J., Krikke, C., and Leuvenink, H.G. (2015). Hypoxia and complement-and-coagulation pathways in the deceased organ donor as the major target for intervention to improve renal allograft outcome. *Transplantation* 99, 1293-1300.

Dang, Z.C., van Bezooijen, R.L., Karperien, M., Papapoulos, S.E., and Lowik, C.W. (2002). Exposure of KS483 cells to estrogen enhances osteogenesis and inhibits adipogenesis. *Journal of bone and mineral research : the official journal of the American Society for Bone and Mineral Research* 17, 394-405.

Day, T.F., Guo, X., Garrett-Beal, L., and Yang, Y. (2005). Wnt/ β -catenin signaling in mesenchymal progenitors controls osteoblast and chondrocyte differentiation during vertebrate skeletogenesis. *Developmental cell* 8, 739-750.

Daye, D., and Wellen, K.E. (2012). Metabolic reprogramming in cancer: unraveling the role of glutamine in tumorigenesis. Paper presented at: Seminars in cell & developmental biology (Elsevier).

De Boer, J., Wang, H.J., and Van Blitterswijk, C. (2004). Effects of Wnt signaling on proliferation and differentiation of human mesenchymal stem cells. *Tissue engineering* 10, 393-401.

De Ugarte, D.A., Alfonso, Z., Zuk, P.A., Elbarbary, A., Zhu, M., Ashjian, P., Benhaim, P., Hedrick, M.H., and Fraser, J.K. (2003). Differential expression of stem cell mobilization-associated molecules on multi-lineage cells from adipose tissue and bone marrow. *Immunology letters* 89, 267-270.

Deal, C., Omizo, M., Schwartz, E.N., Eriksen, E.F., Cantor, P., Wang, J., Glass, E.V., Myers, S.L., and Kregge, J.H. (2005). Combination teriparatide and raloxifene therapy for postmenopausal osteoporosis: results from a 6-month double-blind placebo-controlled trial. *Journal of Bone and Mineral Research* 20, 1905-1911.

Delmas, P.D., Ensrud, K.E., Adachi, J.D., Harper, K.D., Sarkar, S., Gennari, C., Reginster, J.Y., Pols, H.A., Recker, R.R., Harris, S.T., *et al.* (2002). Efficacy of raloxifene on vertebral fracture risk reduction in postmenopausal women with osteoporosis: four-year results from a randomized clinical trial. *The Journal of clinical endocrinology and metabolism* 87, 3609-3617.

Dempster, D.W., Cosman, F., Parisien, M., Shen, V., and Lindsay, R. (1993). Anabolic actions of parathyroid hormone on bone. *Endocrine reviews* 14, 690-709.

Dey, S., Savant, S., Teske, B.F., Hatzoglou, M., Calkhoven, C.F., and Wek, R.C. (2012). Transcriptional repression of ATF4 gene by CCAAT/enhancer-binding protein beta (C/EBPbeta) differentially regulates integrated stress response. *Journal of Biological Chemistry* 287, 21936-21949.

Di Nicola, M., Carlo-Stella, C., Magni, M., Milanese, M., Longoni, P.D., Matteucci, P., Grisanti, S., and Gianni, A.M. (2002). Human bone marrow stromal cells suppress T-lymphocyte proliferation induced by cellular or nonspecific mitogenic stimuli. *Blood* 99, 3838-3843.

Digirolamo, C.M., Stokes, D., Colter, D., Phinney, D.G., Class, R., and Prockop, D.J. (1999). Propagation and senescence of human marrow stromal cells in culture: a simple colony-forming assay identifies samples with the greatest potential to propagate and differentiate. *British journal of haematology* 107, 275-281.

Diz, P., López-Cedrún, J.L., Arenaz, J., and Scully, C. (2012). Denosumab-related osteonecrosis of the jaw. *The Journal of the American Dental Association* 143, 981-984.

Dobin, A., Davis, C.A., Schlesinger, F., Drenkow, J., Zaleski, C., Jha, S., Batut, P., Chaisson, M., and Gingeras, T.R. (2013). STAR: ultrafast universal RNA-seq aligner. *Bioinformatics* 29, 15-21.

Dominici, M., Le Blanc, K., Mueller, I., Slaper-Cortenbach, I., Marini, F., Krause, D., Deans, R., Keating, A., Prockop, D., and Horwitz, E. (2006). Minimal criteria for defining multipotent mesenchymal stromal cells. The International Society for Cellular Therapy position statement. *Cytotherapy* 8, 315-317.

Duffy, M.M., Ritter, T., Ceredig, R., and Griffin, M.D. (2011). Mesenchymal stem cell effects on T-cell effector pathways. *Stem cell research & therapy* 2, 34.

English, K., French, A., and Wood, K.J. (2010). Mesenchymal stromal cells: facilitators of successful transplantation? *Cell Stem Cell* 7, 431-442.

Eriksen, E.F., and Brown, J.P. (2016). Commentary: Concurrent administration of PTH and antiresorptives: Additive effects or DXA cosmetics. *Bone* 86, 139-142.

Erlebacher, A., and Derynck, R. (1996). Increased expression of TGF-beta 2 in osteoblasts results in an osteoporosis-like phenotype. *Journal of cellular biochemistry* 132, 195-210.

Esen, E., Chen, J., Karner, C.M., Okunade, A.L., Patterson, B.W., and Long, F. (2013). WNT-LRP5 signaling induces Warburg effect through mTORC2 activation during osteoblast differentiation. *Cell Metabolism* 17, 745-755.

Esen, E., Lee, S.-Y., Wice, B.M., and Long, F. (2015). PTH Promotes Bone Anabolism by Stimulating Aerobic Glycolysis via IGF Signaling. *Journal of Bone and Mineral Research* 30, 1959-1968.

Estrada, R., Li, N., Sarojini, H., An, J., Lee, M.J., and Wang, E. (2009). Secretome from mesenchymal stem cells induces angiogenesis via Cyr61. *Journal of cellular physiology* 219, 563-571.

Ettinger, B., Black, D.M., Mitlak, B.H., Knickerbocker, R.K., Nickelsen, T., Genant, H.K., Christiansen, C., Delmas, P.D., Zanchetta, J.R., Stakkestad, J., *et al.* (1999). Reduction of vertebral fracture risk in postmenopausal women with osteoporosis treated with raloxifene: results from a 3-year randomized clinical trial. Multiple Outcomes of Raloxifene Evaluation (MORE) Investigators. *Jama* 282, 637-645.

Ettinger, B., San Martin, J., Crans, G., and Pavo, I. (2004). Differential effects of teriparatide on BMD after treatment with raloxifene or alendronate. *Journal of Bone and Mineral Research* 19, 745-751.

Everett, E. (2011). Fluoride's effects on the formation of teeth and bones, and the influence of genetics. *Journal of dental research* 90, 552-560.

Finkelstein, J.S., Wyland, J.J., Lee, H., and Neer, R.M. (2010). Effects of teriparatide, alendronate, or both in women with postmenopausal osteoporosis. *The Journal of Clinical Endocrinology & Metabolism* 95, 1838-1845.

Fox, J., Miller, M.A., Newman, M.K., Turner, C.H., Recker, R.R., and Smith, S.Y. (2007). Treatment of skeletally mature ovariectomized rhesus monkeys with PTH(1-84) for 16 months increases bone formation and density and improves trabecular architecture and biomechanical properties at the lumbar spine. *Journal of Bone and Mineral Research* 22, 260-273.

François, M., Romieu-Mourez, R., Li, M., and Galipeau, J. (2012). Human MSC suppression correlates with cytokine induction of indoleamine 2, 3-dioxygenase and bystander M2 macrophage differentiation. *Molecular Therapy* 20, 187-195.

Frenette, P.S., Pinho, S., Lucas, D., and Scheiermann, C. (2013). Mesenchymal stem cell: keystone of the hematopoietic stem cell niche and a stepping-stone for regenerative medicine. *Annual Review of Immunology* 31, 285-316.

Fujita, T., Azuma, Y., Fukuyama, R., Hattori, Y., Yoshida, C., Koida, M., Ogita, K., and Komori, T. (2004). Runx2 induces osteoblast and chondrocyte differentiation and enhances their migration by coupling with PI3K-Akt signaling. *Journal of Cell Biology* 166, 85-95.

Funes, J.M., Quintero, M., Henderson, S., Martinez, D., Qureshi, U., Westwood, C., Clements, M.O., Bourboulia, D., Pedley, R.B., and Moncada, S. (2007). Transformation of human mesenchymal stem cells increases their dependency on oxidative phosphorylation for energy production. *Proceedings of the National Academy of Sciences* 104, 6223-6228.

Fusakio, M.E., Willy, J.A., Wang, Y., Mirek, E.T., Al Baghdadi, R.J., Adams, C.M., Anthony, T.G., and Wek, R.C. (2016). Transcription factor ATF4 directs basal and stress-induced gene expression in the unfolded protein response and cholesterol metabolism in the liver. *Molecular biology of the cell* 27, 1536-1551.

Gerdoni, E., Gallo, B., Casazza, S., Musio, S., Bonanni, I., Pedemonte, E., Mantegazza, R., Frassoni, F., Mancardi, G., and Pedotti, R. (2007). Mesenchymal stem cells effectively modulate pathogenic immune response in experimental autoimmune encephalomyelitis. *Annals of Neurology* 61, 219-227.

Giner, M., Rios, M.J., Montoya, M.J., Vazquez, M.A., Miranda, C., and Perez-Cano, R. (2011). Alendronate and raloxifene affect the osteoprotegerin/RANKL system in human osteoblast primary cultures from patients with osteoporosis and osteoarthritis. *European journal of pharmacology* 650, 682-687.

Giunti, D., Parodi, B., Usai, C., Vergani, L., Casazza, S., Bruzzone, S., Mancardi, G., and Uccelli, A. (2012). Mesenchymal stem cells shape microglia effector functions through the release of CX3CL1. *Stem cells (Dayton, Ohio)* 30, 2044-2053.

Glaser, D.L., and Kaplan, F.S. (1997). Osteoporosis. Definition and clinical presentation. *Spine* 22, 12s-16s.

Grady, D., Gebretsadik, T., Kerlikowske, K., Ernster, V., and Petitti, D. (1995). Hormone replacement therapy and endometrial cancer risk: a meta-analysis. *Obstetrics and gynecology* 85, 304-313.

Greenbaum, A., Hsu, Y.M., Day, R.B., Schuettpelz, L.G., Christopher, M.J., Borgerding, J.N., Nagasawa, T., and Link, D.C. (2013). CXCL12 in early mesenchymal progenitors is required for haematopoietic stem-cell maintenance. *Nature* 495, 227-230.

Guntur, A.R., Le, P.T., Farber, C.R., and Rosen, C.J. (2014). Bioenergetics during calvarial osteoblast differentiation reflect strain differences in bone mass. *Endocrinology* 155, 1589-1595.

Guo, J., Liu, M., Yang, D., Bouxsein, M.L., Saito, H., Galvin, R.S., Kuhstoss, S.A., Thomas, C.C., Schipani, E., and Baron, R. (2010). Suppression of Wnt signaling by Dkk1 attenuates PTH-mediated stromal cell response and new bone formation. *Cell Metabolism* 11, 161-171.

Hamidouche, Z., Fromigué, O., Ringe, J., Häupl, T., and Marie, P.J. (2010). Crosstalks between integrin alpha 5 and IGF2/IGFBP2 signalling trigger human bone marrow-derived mesenchymal stromal osteogenic differentiation. *BMC Cell Biology* 11, 44.

Hansen, S., Hauge, E.M., Beck Jensen, J.E., and Brixen, K. (2013). Differing effects of PTH 1-34, PTH 1-84, and zoledronic acid on bone microarchitecture and estimated strength in postmenopausal women with osteoporosis: an 18-month open-labeled observational study using HR-pQCT. *Journal of Bone and Mineral Research* 28, 736-745.

Haze, K., Yoshida, H., Yanagi, H., Yura, T., and Mori, K. (1999). Mammalian transcription factor ATF6 is synthesized as a transmembrane protein and activated by proteolysis in response to endoplasmic reticulum stress. *Molecular biology of the cell* 10, 3787-3799.

He, Y., Childress, P., Hood, M., Jr., Alvarez, M., Kacena, M.A., Hanlon, M., McKee, B., Bidwell, J.P., and Yang, F.C. (2013). Nmp4/CIZ suppresses the parathyroid hormone anabolic window by restricting mesenchymal stem cell and osteoprogenitor frequency. *Stem Cells and Development* 22, 492-500.

Hetz, C., Chevet, E., and Harding, H.P. (2013). Targeting the unfolded protein response in disease. *Nature reviews Drug discovery* 12, 703-719.

Hernandez, C., Majeska, R., and Schaffler, M. (2004). Osteocyte density in woven bone. *Bone* 35, 1095-1099.

Hinnebusch, A.G. (2014). The scanning mechanism of eukaryotic translation initiation. *Annual review of biochemistry* 83, 779-812.

Hino, K., Nakamoto, T., Nifuji, A., Morinobu, M., Yamamoto, H., Ezura, Y., and Noda, M. (2007). Deficiency of ClZ, a nucleocytoplasmic shuttling protein, prevents unloading-induced bone loss through the enhancement of osteoblastic bone formation in vivo. *Bone* 40, 852-860.

Hollien, J., Lin, J.H., Li, H., Stevens, N., Walter, P., and Weissman, J.S. (2009). Regulated Ire1-dependent decay of messenger RNAs in mammalian cells. *Journal of Cell Biology* 186, 323-331.

Hsiao, E.C., Boudignon, B.M., Chang, W.C., Bencsik, M., Peng, J., Nguyen, T.D., Manalac, C., Halloran, B.P., Conklin, B.R., and Nissenson, R.A. (2008). Osteoblast expression of an engineered Gs-coupled receptor dramatically increases bone mass. *Proceedings of the National Academy of Sciences* 105, 1209-1214.

Hsu, P.P., and Sabatini, D.M. (2008). Cancer cell metabolism: Warburg and beyond. *Cell* 134, 703-707.

Huang, J.C., Sakata, T., Pflieger, L.L., Bencsik, M., Halloran, B.P., Bikle, D.D., and Nissenson, R.A. (2004). PTH differentially regulates expression of RANKL and OPG. *Journal of bone and mineral research : the official journal of the American Society for Bone and Mineral Research* 19, 235-244.

Hughes, D.E., Dai, A., Tiffée, J.C., Li, H.H., Mundy, G.R., and Boyce, B.F. (1996). Estrogen promotes apoptosis of murine osteoclasts mediated by TGF-beta. *Nature medicine* 2, 1132-1136.

Hughes-Fulford, M., and Li, C.-F. (2011). The role of FGF-2 and BMP-2 in regulation of gene induction, cell proliferation and mineralization. *Journal of Orthopaedic Surgery and Research* 6, 8.

Iida-Klein, A., Zhou, H., Lu, S.S., Levine, L.R., Ducayen-Knowles, M., Dempster, D.W., Nieves, J., and Lindsay, R. (2002). Anabolic action of parathyroid hormone is skeletal site specific at the tissue and cellular levels in mice. *Journal of Bone and Mineral Research* 17, 808-816.

Iurlaro, R., and Muñoz-Pinedo, C. (2015). Cell death induced by endoplasmic reticulum stress. *FEBS Journal*.

Janssen, H., and Marynen, P. (2006). Interaction partners for human ZNF384/CIZ/NMP4--zyxin as a mediator for p130CAS signaling? *Experimental cell research* 312, 1194-1204.

Jensen, A.R., Doster, D.L., Hunsberger, E.B., Manning, M.M., Stokes, S.M., Barwinska, D., March, K.L., Yoder, M.C., and Markel, T.A. (2016). Human Adipose Stromal Cells Increase Survival and Mesenteric Perfusion Following Intestinal Ischemia and Reperfusion Injury. *Shock (Augusta, Ga)* 46, 75-82.

Jia, D., and Heersche, J. (2000). Insulin-like growth factor-1 and-2 stimulate osteoprogenitor proliferation and differentiation and adipocyte formation in cell populations derived from adult rat bone. *Bone* 27, 785-794.

Jiang, D., Muschhammer, J., Qi, Y., Kügler, A., De Vries, J.C., Saffarzadeh, M., Sindrilaru, A., Beken, S.V., Wlaschek, M., and Kluth, M.A. (2016). Suppression of Neutrophil-Mediated Tissue Damage-A Novel Skill of Mesenchymal Stem Cells. *Stem Cells* 34, 2393-2406.

Jilka, R.L. (2009). Inhibiting the inhibitor: a new route to bone anabolism. *Journal of Bone and Mineral Research* 24, 575-577.

Jilka, R.L. (2013). The relevance of mouse models for investigating age-related bone loss in humans. *The journals of gerontology Series A, Biological sciences and medical sciences* 68, 1209-1217.

Jilka, R.L., Weinstein, R.S., Bellido, T., Parfitt, A.M., and Manolagas, S.C. (1998). Osteoblast programmed cell death (apoptosis): modulation by growth factors and cytokines. *Journal of bone and mineral research : the official journal of the American Society for Bone and Mineral Research* 13, 793-802.

Jung, Y., Song, J., Shiozawa, Y., Wang, J., Wang, Z., Williams, B., Havens, A., Schneider, A., Ge, C., Franceschi, R.T., *et al.* (2008). Hematopoietic stem cells regulate mesenchymal stromal cell induction into osteoblasts thereby participating in the formation of the stem cell niche. *Stem cells (Dayton, Ohio)* 26, 2042-2051.

Jurkin, J., Henkel, T., Nielsen, A.F., Minnich, M., Popow, J., Kaufmann, T., Heindl, K., Hoffmann, T., Busslinger, M., and Martinez, J. (2014). The mammalian tRNA ligase complex mediates splicing of XBP1 mRNA and controls antibody secretion in plasma cells. *EMBO Journal* 33, 2922-2936.

Kalbasi Anaraki, P., Patecki, M., Larmann, J., Tkachuk, S., Jurk, K., Haller, H., Theilmeier, G., and Dumler, I. (2013). Urokinase receptor mediates osteogenic differentiation of mesenchymal stem cells and vascular calcification via the complement C5a receptor. *Stem Cells and Development* 23, 352-362.

Kamiya, N., Kobayashi, T., Mochida, Y., Yu, P.B., Yamauchi, M., Kronenberg, H.M., and Mishina, Y. (2010). Wnt inhibitors Dkk1 and Sost are downstream

targets of BMP signaling through the type IA receptor (BMPRIA) in osteoblasts. *Journal of Bone and Mineral Research* 25, 200-210.

Kapinas, K., and Delany, A.M. (2011). MicroRNA biogenesis and regulation of bone remodeling. *Arthritis research & therapy* 13, 220.

Keaveny, T.M., Hoffmann, P.F., Singh, M., Palermo, L., Bilezikian, J.P., Greenspan, S.L., and Black, D.M. (2008). Femoral bone strength and its relation to cortical and trabecular changes after treatment with PTH, alendronate, and their combination as assessed by finite element analysis of quantitative CT scans. *Journal of Bone and Mineral Research* 23, 1974-1982.

Kent, D., Copley, M., Benz, C., Dykstra, B., Bowie, M., and Eaves, C. (2008). Regulation of hematopoietic stem cells by the steel factor/KIT signaling pathway. *Clinical cancer research : an official journal of the American Association for Cancer Research* 14, 1926-1930.

Kim, J.M., Kim, J., Kim, Y.H., Kim, K.T., Ryu, S.H., Lee, T.G., and Suh, P.G. (2013). Comparative secretome analysis of human bone marrow-derived mesenchymal stem cells during osteogenesis. *Journal of Cellular Physiology* 228, 216-224.

Kim, S.W., Pajevic, P.D., Selig, M., Barry, K.J., Yang, J.Y., Shin, C.S., Baek, W.Y., Kim, J.E., and Kronenberg, H.M. (2012). Intermittent parathyroid hormone administration converts quiescent lining cells to active osteoblasts. *Journal of bone and mineral research : the official journal of the American Society for Bone and Mineral Research* 27, 2075-2084.

Kokabu, S., Gamer, L., Cox, K., Lowery, J., Tsuji, K., Raz, R., Economides, A., Katagiri, T., and Rosen, V. (2012). BMP3 suppresses osteoblast differentiation of

bone marrow stromal cells via interaction with Acvr2b. *Molecular Endocrinology* 26, 87-94.

Kostenuik, P.J., Harris, J., Halloran, B.P., Turner, R.T., Morey-Holton, E.R., and Bikle, D.D. (1999). Skeletal unloading causes resistance of osteoprogenitor cells to parathyroid hormone and to insulin-like growth factor-I. *Journal of bone and mineral research : the official journal of the American Society for Bone and Mineral Research* 14, 21-31.

Kulkarni, N.H., Wei, T., Kumar, A., Dow, E.R., Stewart, T.R., Shou, J., N'Cho, M., Sterchi, D.L., Gitter, B.D., Higgs, R.E., *et al.* (2007). Changes in osteoblast, chondrocyte, and adipocyte lineages mediate the bone anabolic actions of PTH and small molecule GSK-3 inhibitor. *Journal of Cellular Biochemistry* 102, 1504-1518.

Le Blanc, K., Frassoni, F., Ball, L., Locatelli, F., Roelofs, H., Lewis, I., Lanino, E., Sundberg, B., Bernardo, M.E., and Remberger, M. (2008). Mesenchymal stem cells for treatment of steroid-resistant, severe, acute graft-versus-host disease: a phase II study. *The Lancet* 371, 1579-1586.

Leder, B.Z., Tsai, J.N., Uihlein, A.V., Wallace, P.M., Lee, H., Neer, R.M., and Burnett-Bowie, S.A. (2015). Denosumab and teriparatide transitions in postmenopausal osteoporosis (the DATA-Switch study): extension of a randomised controlled trial. *Lancet* 386, 1147-1155.

Lewiecki, E.M., Miller, P.D., McClung, M.R., Cohen, S.B., Bolognese, M.A., Liu, Y., Wang, A., Siddhanti, S., and Fitzpatrick, L.A. (2007). Two-year treatment with denosumab (AMG 162) in a randomized phase 2 study of postmenopausal women with low BMD. *Journal of bone and mineral research : the official journal of the American Society for Bone and Mineral Research* 22, 1832-1841.

Lezcano, V., Bellido, T., Plotkin, L.I., Boland, R., and Morelli, S. (2014). Osteoblastic protein tyrosine phosphatases inhibition and connexin 43 phosphorylation by alendronate. *Experimental cell research* 324, 30-39.

Li, E. (2002). Chromatin modification and epigenetic reprogramming in mammalian development. *Nature Reviews Genetics* 3, 662-673.

Li, Y.F., Zhou, C.C., Li, J.H., Luo, E., Zhu, S.S., Feng, G., and Hu, J. (2012). The effects of combined human parathyroid hormone (1-34) and zoledronic acid treatment on fracture healing in osteoporotic rats. *Osteoporosis International* 23, 1463-1474.

Liao, Y., Smyth, G.K., and Shi, W. (2014). featureCounts: an efficient general purpose program for assigning sequence reads to genomic features. *Bioinformatics* 30, 923-930.

Lin, K.-L., Chou, C.-H., Hsieh, S.-C., Hwa, S.-Y., Lee, M.-T., and Wang, F.-F. (2010). Transcriptional upregulation of DDR2 by ATF4 facilitates osteoblastic differentiation through p38 MAPK-mediated Runx2 activation. *Journal of Bone and Mineral Research* 25, 2489-2503.

Lin, Y., Liu, L.J., Murray, T., Sodek, J., and Rao, L. (2004). Effect of raloxifene and its interaction with human PTH on bone formation. *Journal of endocrinological investigation* 27, 416-423.

Liotta, F., Angeli, R., Cosmi, L., Fili, L., Manuelli, C., Frosali, F., Mazzinghi, B., Maggi, L., Pasini, A., and Lisi, V. (2008). Toll-like receptors 3 and 4 are expressed by human bone marrow-derived mesenchymal stem cells and can inhibit their T-cell modulatory activity by impairing Notch signaling. *Stem Cells* 26, 279-289.

Liu, Z., Graff, E., and Benayahu, D. (2000). Effect of raloxifene-analog (LY 117018-Hcl) on the bone marrow of ovariectomized mice. *Journal of Cellular Biochemistry* 76, 509-517.

Lui, P.P., Lee, Y.W., Mok, T.Y., Cheuk, Y.C., and Chan, K.M. (2013). Alendronate reduced peri-tunnel bone loss and enhanced tendon graft to bone tunnel healing in anterior cruciate ligament reconstruction. *European cells & materials* 25, 78-96.

Martini, A., La Starza, R., Janssen, H., Bilhou-Nabera, C., Corveleyn, A., Somers, R., Aventin, A., Foa, R., Hagemeyer, A., Mecucci, C., *et al.* (2002). Recurrent rearrangement of the Ewing's sarcoma gene, EWSR1, or its homologue, TAF15, with the transcription factor CIZ/NMP4 in acute leukemia. *Cancer research* 62, 5408-5412.

Martino, S., Cauley, J.A., Barrett-Connor, E., Powles, T.J., Mershon, J., Disch, D., Secret, R.J., and Cummings, S.R. (2004). Continuing outcomes relevant to Evista: breast cancer incidence in postmenopausal osteoporotic women in a randomized trial of raloxifene. *Journal of the National Cancer Institute* 96, 1751-1761.

Matsumori, H., Hattori, K., Ohgushi, H., Dohi, Y., Ueda, Y., Shigematsu, H., Satoh, N., Yajima, H., and Takakura, Y. (2009). Raloxifene: its ossification-promoting effect on female mesenchymal stem cells. *Journal of orthopaedic science : official journal of the Japanese Orthopaedic Association* 14, 640-645.

Matsunobu, T., Torigoe, K., Ishikawa, M., De Vega, S., Kulkarni, A.B., Iwamoto, Y., and Yamada, Y. (2009). Critical roles of the TGF- β type I receptor ALK5 in perichondrial formation and function, cartilage integrity, and osteoblast differentiation during growth plate development. *Developmental Biology* 332, 325-338.

Matsuzaki, Y., Mabuchi, Y., and Okano, H. (2014). Leptin receptor makes its mark on MSCs. *Cell Stem Cell* 15, 112-114.

Mbalaviele, G., Sheikh, S., Stains, J.P., Salazar, V.S., Cheng, S.L., Chen, D., and Civitelli, R. (2005). β -Catenin and BMP-2 synergize to promote osteoblast differentiation and new bone formation. *Journal of Cellular Biochemistry* 94, 403-418.

McBride, S.H., and Silva, M.J. (2012). Adaptive and injury response of bone to mechanical loading. *BoneKEY reports* 1.

McCormick, B.B., Davis, J., and Burns, K.D. (2012). Severe hypocalcemia following denosumab injection in a hemodialysis patient. *American Journal of Kidney Diseases* 60, 626-628.

McCullough, K.D., Martindale, J.L., Klotz, L.-O., Aw, T.-Y., and Holbrook, N.J. (2001). Gadd153 sensitizes cells to endoplasmic reticulum stress by down-regulating Bcl2 and perturbing the cellular redox state. *Molecular and cellular biology* 21, 1249-1259.

Melief, S.M., Geutskens, S.B., Fibbe, W.E., and Roelofs, H. (2013). Multipotent stromal cells skew monocytes towards an anti-inflammatory interleukin-10-producing phenotype by production of interleukin-6. *Haematologica* 98, 888-895.

Mendez-Ferrer, S., Michurina, T.V., Ferraro, F., Mazloom, A.R., Macarthur, B.D., Lira, S.A., Scadden, D.T., Ma'ayan, A., Enikolopov, G.N., and Frenette, P.S. (2010). Mesenchymal and haematopoietic stem cells form a unique bone marrow niche. *Nature* 466, 829-834.

Michaelson, M.D., Kaufman, D.S., Lee, H., McGovern, F.J., Kantoff, P.W., Fallon, M.A., Finkelstein, J.S., and Smith, M.R. (2007). Randomized controlled trial of annual zoledronic acid to prevent gonadotropin-releasing hormone agonist-induced bone loss in men with prostate cancer. *Journal of clinical oncology : official journal of the American Society of Clinical Oncology* 25, 1038-1042.

Miki, Y., Suzuki, T., Nagasaki, S., Hata, S., Akahira, J., and Sasano, H. (2009). Comparative effects of raloxifene, tamoxifen and estradiol on human osteoblasts in vitro: estrogen receptor dependent or independent pathways of raloxifene. *The Journal of steroid biochemistry and molecular biology* 113, 281-289.

Mizoguchi, T., Pinho, S., Ahmed, J., Kunisaki, Y., Hanoun, M., Mendelson, A., Ono, N., Kronenberg, H.M., and Frenette, P.S. (2014). Osterix marks distinct waves of primitive and definitive stromal progenitors during bone marrow development. *Developmental Cell* 29, 340-349.

Moore DS, M.G. (2003). *Introduction to the Practice of Statistics*, 4th edn (New York, NY: W.H. Freeman and Co).

Morgan, S., Poundarik, A.A., and Vashishth, D. (2015). Do Non-collagenous Proteins Affect Skeletal Mechanical Properties? *Calcified tissue international* 97, 281-291.

Morikawa, S., Mabuchi, Y., Kubota, Y., Nagai, Y., Niibe, K., Hiratsu, E., Suzuki, S., Miyauchi-Hara, C., Nagoshi, N., Sunabori, T., *et al.* (2009). Prospective identification, isolation, and systemic transplantation of multipotent mesenchymal stem cells in murine bone marrow. *The Journal of experimental medicine* 206, 2483-2496.

Morinobu, M., Nakamoto, T., Hino, K., Tsuji, K., Shen, Z.J., Nakashima, K., Nifuji, A., Yamamoto, H., Hirai, H., and Noda, M. (2005). The nucleocytoplasmic shuttling protein CIZ reduces adult bone mass by inhibiting bone morphogenetic protein-induced bone formation. *The Journal of experimental medicine* 201, 961-970.

Mosna, F., Sensebe, L., and Krampera, M. (2010). Human bone marrow and adipose tissue mesenchymal stem cells: a user's guide. *Stem cells and development* 19, 1449-1470.

Muraglia, A., Cancedda, R., and Quarto, R. (2000). Clonal mesenchymal progenitors from human bone marrow differentiate in vitro according to a hierarchical model. *Journal of cell science* 113 (Pt 7), 1161-1166.

Muschitz, C., Kocijan, R., Fahrleitner-Pammer, A., Lung, S., and Resch, H. (2013). Antiresorptives overlapping ongoing teriparatide treatment result in additional increases in bone mineral density. *Journal of Bone and Mineral Research* 28, 196-205.

Mylotte, L.A., Duffy, A.M., Murphy, M., O'Brien, T., Samali, A., Barry, F., and Szegezdi, E. (2008). Metabolic flexibility permits mesenchymal stem cell survival in an ischemic environment. *Stem Cells* 26, 1325-1336.

Nakamoto, T., Izu, Y., Kawasaki, M., Notomi, T., Hayata, T., Noda, M., and Ezura, Y. (2016). Mice Deficient in CIZ/NMP4 Develop an Attenuated Form of K/BxN-Serum Induced Arthritis. *Journal of Cellular Biochemistry* 117, 970-977.

Nakamoto, T., Shiratsuchi, A., Oda, H., Inoue, K., Matsumura, T., Ichikawa, M., Saito, T., Seo, S., Maki, K., Asai, T., *et al.* (2004). Impaired spermatogenesis and male fertility defects in CIZ/Nmp4-disrupted mice. *Genes to cells : devoted to molecular & cellular mechanisms* 9, 575-589.

Nakamoto, T., Yamagata, T., Sakai, R., Ogawa, S., Honda, H., Ueno, H., Hirano, N., Yazaki, Y., and Hirai, H. (2000). CIZ, a zinc finger protein that interacts with p130(cas) and activates the expression of matrix metalloproteinases. *Molecular and Cellular Biology* 20, 1649-1658.

Nakashima, K., Zhou, X., Kunkel, G., Zhang, Z., Deng, J.M., Behringer, R.R., and de Crombrughe, B. (2002). The novel zinc finger-containing transcription factor osterix is required for osteoblast differentiation and bone formation. *Cell* 108, 17-29.

Newman, C.L., Chen, N.X., Smith, E., Smith, M., Brown, D., Moe, S.M., and Allen, M.R. (2015). Compromised vertebral structural and mechanical properties associated with progressive kidney disease and the effects of traditional pharmacological interventions. *Bone* 77, 50-56.

Nikel, O., Laurencin, D., McCallum, S.A., Gundberg, C.M., and Vashishth, D. (2013). NMR investigation of the role of osteocalcin and osteopontin at the organic-inorganic interface in bone. *Langmuir* 29, 13873-13882.

Nilsson, S.K., Johnston, H.M., Whitty, G.A., Williams, B., Webb, R.J., Denhardt, D.T., Bertonecello, I., Bendall, L.J., Simmons, P.J., and Haylock, D.N. (2005). Osteopontin, a key component of the hematopoietic stem cell niche and regulator of primitive hematopoietic progenitor cells. *Blood* 106, 1232-1239.

Ochiai, H., Okada, S., Saito, A., Hoshi, K., Yamashita, H., Takato, T., and Azuma, T. (2012). Inhibition of insulin-like growth factor-1 (IGF-1) expression by prolonged transforming growth factor- β 1 (TGF- β 1) administration suppresses osteoblast differentiation. *Journal of Biological Chemistry* 287, 22654-22661.

Ohoka, N., Yoshii, S., Hattori, T., Onozaki, K., and Hayashi, H. (2005). TRB3, a novel ER stress-inducible gene, is induced via ATF4-CHOP pathway and is involved in cell death. *Embo j* 24, 1243-1255.

Okada, N., Kawazoe, K., Teraoka, K., Kujime, T., Abe, M., Shinohara, Y., and Minakuchi, K. (2013). Identification of the risk factors associated with hypocalcemia induced by denosumab. *Biological and Pharmaceutical Bulletin* 36, 1622-1626.

Okada, T., Haze, K., Nadanaka, S., Yoshida, H., Seidah, N.G., Hirano, Y., Sato, R., Negishi, M., and Mori, K. (2003). A serine protease inhibitor prevents endoplasmic reticulum stress-induced cleavage but not transport of the membrane-bound transcription factor ATF6. *The Journal of biological chemistry* 278, 31024-31032.

Okazaki, R., Durham, S.K., Riggs, B.L., and Conover, C.A. (1995). Transforming growth factor- β and forskolin increase all classes of insulin-like growth factor-I transcripts in normal human osteoblast-like cells. *Biochemical and biophysical research communications* 207, 963-970.

Olate, S., Uribe, F., Martinez, F., Almeida, A., and Unibazo, A. (2014). Osteonecrosis of the jaw in patient with denosumab therapy. *International journal of clinical and experimental medicine* 7, 3707.

Ortiz, L.A., DuTreil, M., Fattman, C., Pandey, A.C., Torres, G., Go, K., and Phinney, D.G. (2007). Interleukin 1 receptor antagonist mediates the antiinflammatory and antifibrotic effect of mesenchymal stem cells during lung injury. *Proceedings of the National Academy of Sciences* 104, 11002-11007.

Pan, B., To, L.B., Farrugia, A.N., Findlay, D.M., Green, J., Gronthos, S., Evdokiou, A., Lynch, K., Atkins, G.J., and Zannettino, A.C. (2004). The nitrogen-containing bisphosphonate, zoledronic acid, increases mineralisation of human bone-derived cells in vitro. *Bone* 34, 112-123.

Papapoulos, S., Chapurlat, R., Libanati, C., Brandi, M.L., Brown, J.P., Czerwinski, E., Krieg, M.A., Man, Z., Mellstrom, D., Radominski, S.C., *et al.* (2012). Five years of denosumab exposure in women with postmenopausal osteoporosis: results from the first two years of the FREEDOM extension. *Journal of bone and mineral research : the official journal of the American Society for Bone and Mineral Research* 27, 694-701.

Papayannopoulou, T., Craddock, C., Nakamoto, B., Priestley, G.V., and Wolf, N.S. (1995). The VLA4/VCAM-1 adhesion pathway defines contrasting mechanisms of lodgement of transplanted murine hemopoietic progenitors between bone marrow and spleen. *Proc Natl Acad Sci U S A* 92, 9647-9651.

Park, S.J., Kim, S.H., Choi, H.S., Rhee, Y., and Lim, S.-K. (2009). Fibroblast growth factor 2-induced cytoplasmic asparaginyl-tRNA synthetase promotes survival of osteoblasts by regulating anti-apoptotic PI3K/Akt signaling. *Bone* 45, 994-1003.

Pereira, R.C., Delany, A.M., and Canalis, E. (2004). CCAAT/enhancer binding protein homologous protein (DDIT3) induces osteoblastic cell differentiation. *Endocrinology* 145, 1952-1960.

Pettway, G.J., Meganck, J.A., Koh, A.J., Keller, E.T., Goldstein, S.A., and McCauley, L.K. (2008). Parathyroid hormone mediates bone growth through the regulation of osteoblast proliferation and differentiation. *Bone* 42, 806-818.

Pettway, G.J., Schneider, A., Koh, A.J., Widjaja, E., Morris, M.D., Meganck, J.A., Goldstein, S.A., and McCauley, L.K. (2005). Anabolic actions of PTH (1-34): use of a novel tissue engineering model to investigate temporal effects on bone. *Bone* 36, 959-970.

Piek, E., Sleumer, L.S., van Someren, E.P., Heuver, L., de Haan, J.R., de Grijs, I., Gilissen, C., Hendriks, J.M., van Ravestein-van Os, R.I., and Bauerschmidt, S. (2010). Osteo-transcriptomics of human mesenchymal stem cells: accelerated gene expression and osteoblast differentiation induced by vitamin D reveals c-MYC as an enhancer of BMP2-induced osteogenesis. *Bone* 46, 613-627.

Pincus, D., Chevalier, M.W., Aragón, T., Van Anken, E., Vidal, S.E., El-Samad, H., and Walter, P. (2010). BiP binding to the ER-stress sensor Ire1 tunes the homeostatic behavior of the unfolded protein response. *PLoS biology* 8, e1000415.

Pinkerton, J.V., and Dalkin, A.C. (2007). Combination therapy for treatment of osteoporosis: A review. *American journal of obstetrics and gynecology* 197, 559-565.

Plotkin, L.I., Weinstein, R.S., Parfitt, A.M., Roberson, P.K., Manolagas, S.C., and Bellido, T. (1999). Prevention of osteocyte and osteoblast apoptosis by bisphosphonates and calcitonin. *The Journal of clinical investigation* 104, 1363-1374.

Poundarik, A.A., Diab, T., Sroga, G.E., Ural, A., Boskey, A.L., Gundberg, C.M., and Vashishth, D. (2012). Dilatational band formation in bone. *Proceedings of the National Academy of Sciences* 109, 19178-19183.

Pozzi, S., Vallet, S., Mukherjee, S., Cirstea, D., Vaghela, N., Santo, L., Rosen, E., Ikeda, H., Okawa, Y., Kiziltepe, T., *et al.* (2009). High-dose zoledronic acid impacts bone remodeling with effects on osteoblastic lineage and bone mechanical properties. *Clinical cancer research : an official journal of the American Association for Cancer Research* 15, 5829-5839.

Prince, R., Sipos, A., Hossain, A., Syversen, U., Ish-Shalom, S., Marcinowska, E., Halse, J., Lindsay, R., Dalsky, G.P., and Mitlak, B.H. (2005). Sustained nonvertebral fragility fracture risk reduction after discontinuation of teriparatide treatment. *Journal of bone and mineral research : the official journal of the American Society for Bone and Mineral Research* 20, 1507-1513.

Puthalakath, H., O'Reilly, L.A., Gunn, P., Lee, L., Kelly, P.N., Huntington, N.D., Hughes, P.D., Michalak, E.M., McKimm-Breschkin, J., Motoyama, N., *et al.* (2007). ER stress triggers apoptosis by activating BH3-only protein Bim. *Cell* 129, 1337-1349.

Qian, H., Buza-Vidas, N., Hyland, C.D., Jensen, C.T., Antonchuk, J., Mansson, R., Thoren, L.A., Ekblom, M., Alexander, W.S., and Jacobsen, S.E. (2007). Critical role of thrombopoietin in maintaining adult quiescent hematopoietic stem cells. *Cell Stem Cell* 1, 671-684.

Qian, H., Le Blanc, K., and Sigvardsson, M. (2012). Primary mesenchymal stem and progenitor cells from bone marrow lack expression of CD44 protein. *The Journal of biological chemistry* 287, 25795-25807.

Raggatt, L.J., and Partridge, N.C. (2010). Cellular and molecular mechanisms of bone remodeling. *Journal of Biological Chemistry* 285, 25103-25108.

Rajashekhar, G., Ramadan, A., Abburi, C., Callaghan, B., Traktuev, D.O., Evans-Molina, C., Maturi, R., Harris, A., Kern, T.S., and March, K.L. (2014). Regenerative therapeutic potential of adipose stromal cells in early stage diabetic retinopathy. *PloS one* 9, e84671.

Rasini, V., Dominici, M., Kluba, T., Siegel, G., Lusenti, G., Northoff, H., Horwitz, E.M., and Schafer, R. (2013). Mesenchymal stromal/stem cells markers in the human bone marrow. *Cytotherapy* 15, 292-306.

Rauci, A., Bellosta, P., Grassi, R., Basilico, C., and Mansukhani, A. (2008). Osteoblast proliferation or differentiation is regulated by relative strengths of opposing signaling pathways. *Journal of Cellular Physiology* 215, 442-451.

Rawadi, G., Vayssiere, B., Dunn, F., Baron, R., and Roman-Roman, S. (2003). BMP-2 controls alkaline phosphatase expression and osteoblast mineralization by a Wnt autocrine loop. *Journal of Bone and Mineral Research* 18, 1842-1853.

Reid, I.R., Miller, P.D., Brown, J.P., Kendler, D.L., Fahrleitner-Pammer, A., Valter, I., Maasalu, K., Bolognese, M.A., Woodson, G., Bone, H., *et al.* (2010). Effects of denosumab on bone histomorphometry: the FREEDOM and STAND studies. *Journal of bone and mineral research : the official journal of the American Society for Bone and Mineral Research* 25, 2256-2265.

Reimold, A.M., Iwakoshi, N.N., Manis, J., Vallabhajosyula, P., Szomolanyi-Tsuda, E., Gravallese, E.M., Friend, D., Grusby, M.J., Alt, F., and Glimcher, L.H. (2001). Plasma cell differentiation requires the transcription factor XBP-1. *Nature* 412, 300-307.

Rickard, D.J., Wang, F.L., Rodriguez-Rojas, A.M., Wu, Z., Trice, W.J., Hoffman, S.J., Votta, B., Stroup, G.B., Kumar, S., and Nuttall, M.E. (2006). Intermittent treatment with parathyroid hormone (PTH) as well as a non-peptide small

molecule agonist of the PTH1 receptor inhibits adipocyte differentiation in human bone marrow stromal cells. *Bone* 39, 1361-1372.

Riggs, B.L., Hodgson, S.F., O'fallon, W.M., Chao, E.Y., Wahner, H.W., Muhs, J.M., Cedel, S.L., and Melon III, L.J. (1990). Effect of fluoride treatment on the fracture rate in postmenopausal women with osteoporosis. *New England journal of medicine* 322, 802-809.

Robey, P.G., and Boskey, A.L. (2009). The composition of bone. *Primer on the bone metabolic diseases and disorders of mineral metabolism Seventh ed Official publication of the American Society for Bone and Mineral Research*, 32-38.

Robinson, M.D., McCarthy, D.J., and Smyth, G.K. (2010). edgeR: a Bioconductor package for differential expression analysis of digital gene expression data. *Bioinformatics* 26, 139-140.

Robling, A.G., Childress, P., Yu, J., Cotte, J., Heller, A., Philip, B.K., and Bidwell, J.P. (2009). Nmp4/CIZ suppresses parathyroid hormone-induced increases in trabecular bone. *Journal of Cellular Physiology* 219, 734-743.

Romanello, M., Piatkowska, E., Antoniali, G., Cesaratto, L., Vascotto, C., Iozzo, R.V., Delneri, D., and Brancia, F.L. (2014). Osteoblastic cell secretome: A novel role for progranulin during risedronate treatment. *Bone* 58, 81-91.

Ruggiero, S.L., Mehrotra, B., Rosenberg, T.J., and Engroff, S.L. (2004). Osteonecrosis of the jaws associated with the use of bisphosphonates: a review of 63 cases. *Journal of Oral and Maxillofacial Surgery* 62, 527-534.

Russell, R., Watts, N., Ebetino, F., and Rogers, M. (2008). Mechanisms of action of bisphosphonates: similarities and differences and their potential influence on clinical efficacy. *Osteoporosis International* 19, 733-759.

Sacchetti, B., Funari, A., Michienzi, S., Di Cesare, S., Piersanti, S., Saggio, I., Tagliafico, E., Ferrari, S., Robey, P.G., Riminucci, M., *et al.* (2007). Self-renewing osteoprogenitors in bone marrow sinusoids can organize a hematopoietic microenvironment. *Cell* 131, 324-336.

Saito, A., Ochiai, K., Kondo, S., Tsumagari, K., Murakami, T., Cavener, D.R., and Imaizumi, K. (2011). Endoplasmic reticulum stress response mediated by the PERK-eIF2 α -ATF4 pathway is involved in osteoblast differentiation induced by BMP2. *Journal of Biological Chemistry* 286, 4809-4818.

Samadfam, R., Xia, Q., and Goltzman, D. (2007). Pretreatment with anticatabolic agents blunts but does not eliminate the skeletal anabolic response to parathyroid hormone in oophorectomized mice. *Endocrinology* 148, 2778-2787.

Sato, K., Ozaki, K., Oh, I., Meguro, A., Hatanaka, K., Nagai, T., Muroi, K., and Ozawa, K. (2007). Nitric oxide plays a critical role in suppression of T-cell proliferation by mesenchymal stem cells. *Blood* 109, 228-234.

Schena, F., Gambini, C., Gregorio, A., Mosconi, M., Reverberi, D., Gattorno, M., Casazza, S., Uccelli, A., Moretta, L., and Martini, A. (2010). Interferon- γ -dependent inhibition of B cell activation by bone marrow-derived mesenchymal stem cells in a murine model of systemic lupus erythematosus. *Arthritis and rheumatism* 62, 2776-2786.

Schindler, A.J., and Schekman, R. (2009). In vitro reconstitution of ER-stress induced ATF6 transport in COPII vesicles. *Proc Natl Acad Sci U S A* 106, 17775-17780.

Schweitzer, K.S., Johnstone, B.H., Garrison, J., Rush, N.I., Cooper, S., Traktuev, D.O., Feng, D., Adamowicz, J.J., Van Demark, M., Fisher, A.J., *et al.* (2011). Adipose stem cell treatment in mice attenuates lung and systemic injury induced by cigarette smoking. *American journal of respiratory and critical care medicine* 183, 215-225.

Selmani, Z., Naji, A., Zidi, I., Favier, B., Gaiffe, E., Obert, L., Borg, C., Saas, P., Tiberghien, P., and Rouas-Freiss, N. (2008). Human leukocyte antigen- G5 secretion by human mesenchymal stem cells is required to suppress T lymphocyte and natural killer function and to induce CD4⁺ CD25^{high}FOXP3⁺ regulatory T cells. *Stem Cells* 26, 212-222.

Shah, N.R., and Wong, T. (2006). Current breast cancer risks of hormone replacement therapy in postmenopausal women. *Expert opinion on pharmacotherapy* 7, 2455-2463.

Shah, R., Alvarez, M., Jones, D.R., Torrungruang, K., Watt, A.J., Selvamurugan, N., Partridge, N.C., Quinn, C.O., Pavalko, F.M., Rhodes, S.J., *et al.* (2004). Nmp4/CIZ regulation of matrix metalloproteinase 13 (MMP-13) response to parathyroid hormone in osteoblasts. *American journal of physiology Endocrinology and metabolism* 287, E289-296.

Shen, J., Chen, X., Hendershot, L., and Prywes, R. (2002). ER stress regulation of ATF6 localization by dissociation of BiP/GRP78 binding and unmasking of Golgi localization signals. *Developmental Cell* 3, 99-111.

Sheng, Z.F., Xu, K., Ma, Y.L., Liu, J.H., Dai, R.C., Zhang, Y.H., Jiang, Y.B., and Liao, E.Y. (2009). Zoledronate reverses mandibular bone loss in osteoprotegerin-deficient mice. *Osteoporosis International* 20, 151-159.

Shi, S., and Gronthos, S. (2003). Perivascular niche of postnatal mesenchymal stem cells in human bone marrow and dental pulp. *Journal of bone and mineral research : the official journal of the American Society for Bone and Mineral Research* 18, 696-704.

Shim, H., Dolde, C., Lewis, B.C., Wu, C.-S., Dang, G., Jungmann, R.A., Dalla-Favera, R., and Dang, C.V. (1997). c-Myc transactivation of LDH-A: implications for tumor metabolism and growth. *Proceedings of the National Academy of Sciences* 94, 6658-6663.

Silvestrini, G., Ballanti, P., Leopizzi, M., Sebastiani, M., Berni, S., Di Vito, M., and Bonucci, E. (2007). Effects of intermittent parathyroid hormone (PTH) administration on SOST mRNA and protein in rat bone. *Journal of molecular histology* 38, 261-269.

Simmons, P.J., Masinovsky, B., Longenecker, B.M., Berenson, R., Torok-Storb, B., and Gallatin, W.M. (1992). Vascular cell adhesion molecule-1 expressed by bone marrow stromal cells mediates the binding of hematopoietic progenitor cells. *Blood* 80, 388-395.

Søgaard, C., Mosekilde, L., Richards, A., and Mosekilde, L. (1994). Marked decrease in trabecular bone quality after five years of sodium fluoride therapy; assessed by biomechanical testing of iliac crest bone biopsies in osteoporotic patients. *Bone* 15, 393-399.

Soltysova, A., Breza, J., Takacova, M., Feruszova, J., Hudecova, S., Novotna, B., Rozborilova, E., Pastorekova, S., Kadasi, L., and Krizanova, O. (2015). Deregulation of energetic metabolism in the clear cell renal cell carcinoma: A multiple pathway analysis based on microarray profiling. *International Journal of Oncology* 47, 287-295.

Somjen, D., Katzburg, S., Sharon, O., Knoll, E., Hendel, D., and Stern, N. (2011). Sex specific response of cultured human bone cells to ERalpha and ERbeta specific agonists by modulation of cell proliferation and creatine kinase specific activity. *The Journal of steroid biochemistry and molecular biology* 125, 226-230.

Soung, D.Y., Dong, Y., Wang, Y.J., Zuscik, M.J., Schwarz, E.M., O'Keefe, R.J., and Drissi, H. (2007). Runx3/AML2/Cbfa3 regulates early and late chondrocyte differentiation. *Journal of Bone and Mineral Research* 22, 1260-1270.

Stevenson, J.C., Lees, B., Devenport, M., Cust, M.P., and Ganger, K.F. (1989). Determinants of bone density in normal women: risk factors for future osteoporosis? *BMJ (Clinical research ed)* 298, 924-928.

Stewart, A.J., Roberts, S.J., Seawright, E., Davey, M.G., Fleming, R.H., and Farquharson, C. (2006). The presence of PHOSPHO1 in matrix vesicles and its developmental expression prior to skeletal mineralization. *Bone* 39, 1000-1007.

Suzuki, E., Ochiai-Shino, H., Aoki, H., Onodera, S., Saito, A., Saito, A., and Azuma, T. (2014). Akt activation is required for TGF- β 1-induced osteoblast differentiation of MC3T3-E1 pre-osteoblasts. *PloS One* 9, e112566.

Tae, S.K., Lee, S.H., Park, J.S., and Im, G.I. (2006). Mesenchymal stem cells for tissue engineering and regenerative medicine. *Biomedical materials (Bristol, England)* 1, 63-71.

Tang, Y., Wu, X., Lei, W., Pang, L., Wan, C., Shi, Z., Zhao, L., Nagy, T.R., Peng, X., and Hu, J. (2009). TGF- β 1-induced migration of bone mesenchymal stem cells couples bone resorption with formation. *Nature Medicine* 15, 757-765.

Taranta, A., Brama, M., Teti, A., De luca, V., Scandurra, R., Spera, G., Agnusdei, D., Termine, J.D., and Migliaccio, S. (2002). The selective estrogen receptor modulator raloxifene regulates osteoclast and osteoblast activity in vitro. *Bone* 30, 368-376.

Terauchi, M., Li, J.-Y., Bedi, B., Baek, K.-H., Tawfeek, H., Galley, S., Gilbert, L., Nanes, M.S., Zayzafoon, M., and Guldborg, R. (2009). T lymphocytes amplify the anabolic activity of parathyroid hormone through Wnt10b signaling. *Cell Metabolism* 10, 229-240.

Thunyakitpisal, P., Alvarez, M., Tokunaga, K., Onyia, J.E., Hock, J., Ohashi, N., Feister, H., Rhodes, S.J., and Bidwell, J.P. (2001). Cloning and functional analysis of a family of nuclear matrix transcription factors (NP/NMP4) that regulate type I collagen expression in osteoblasts. *Journal of Bone and Mineral Research* 16, 10-23.

Tonna, S., Takyar, F.M., Vrahnas, C., Crimeen-Irwin, B., Ho, P.W., Poulton, I.J., Brennan, H.J., McGregor, N.E., Allan, E.H., and Nguyen, H. (2014). EphrinB2 signaling in osteoblasts promotes bone mineralization by preventing apoptosis. *The FASEB Journal* 28, 4482-4496.

Tormin, A., Li, O., Brune, J.C., Walsh, S., Schutz, B., Ehinger, M., Ditzel, N., Kassem, M., and Scheduling, S. (2011). CD146 expression on primary nonhematopoietic bone marrow stem cells is correlated with in situ localization. *Blood* 117, 5067-5077.

Torrunguang, K., Alvarez, M., Shah, R., Onyia, J.E., Rhodes, S.J., and Bidwell, J.P. (2002). DNA binding and gene activation properties of the Nmp4 nuclear matrix transcription factors. *Journal of Biological Chemistry* 277, 16153-16159.

Tu, X., Chen, J., Lim, J., Karner, C.M., Lee, S.-Y., Heisig, J., Wiese, C., Surendran, K., Kopan, R., and Gessler, M. (2012). Physiological notch signaling maintains bone homeostasis via RBPjk and Hey upstream of NFATc1. *PLoS genetics* 8, e1002577.

Tucker, K.L. (2009). Osteoporosis prevention and nutrition. *Current Osteoporosis Reports* 7, 111.

van Anken, E., Romijn, E.P., Maggioni, C., Mezghrani, A., Sitia, R., Braakman, I., and Heck, A.J. (2003). Sequential waves of functionally related proteins are expressed when B cells prepare for antibody secretion. *Immunity* 18, 243-253.

Van Riggelen, J., Yetil, A., and Felsher, D.W. (2010). MYC as a regulator of ribosome biogenesis and protein synthesis. *Nature Reviews Cancer* 10, 301-309.

Viereck, V., Grundker, C., Blaschke, S., Niederkleine, B., Siggelkow, H., Frosch, K.H., Raddatz, D., Emons, G., and Hofbauer, L.C. (2003). Raloxifene concurrently stimulates osteoprotegerin and inhibits interleukin-6 production by human trabecular osteoblasts. *The Journal of clinical endocrinology and metabolism* 88, 4206-4213.

Wagner, W., Horn, P., Castoldi, M., Diehlmann, A., Bork, S., Saffrich, R., Benes, V., Blake, J., Pfister, S., Eckstein, V., *et al.* (2008). Replicative senescence of mesenchymal stem cells: a continuous and organized process. *PloS one* 3, e2213.

Walter, P., and Ron, D. (2011). The unfolded protein response: from stress pathway to homeostatic regulation. *Science* 334, 1081-1086.

Wang, B.L., Dai, C.L., Quan, J.X., Zhu, Z.F., Zheng, F., Zhang, H.X., Guo, S.Y., Guo, G., Zhang, J.Y., and Qiu, M.C. (2006). Parathyroid hormone regulates osterix and Runx2 mRNA expression predominantly through protein kinase A signaling in osteoblast-like cells. *Journal of endocrinological investigation* 29, 101-108.

Wang, C., Zhang, G., Gu, M., Fan, J., Chen, J., Zhang, G., and Li, B. (2015). Parathyroid Hormone Plus Alendronate in Osteoporosis: A Meta-Analysis of Randomized Controlled Trials. *Journal of investigative surgery : the official journal of the Academy of Surgical Research* 28, 309-316.

Wattanachanya, L., Wang, L., Millard, S.M., Lu, W.D., O'Carroll, D., Hsiao, E.C., Conklin, B.R., and Nissenson, R.A. (2015). Assessing the osteoblast transcriptome in a model of enhanced bone formation due to constitutive Gs-G protein signaling in osteoblasts. *Experimental cell research* 333, 289-302.

Wei, J., Sheng, X., Feng, D., McGrath, B., and Cavener, D.R. (2008). PERK is essential for neonatal skeletal development to regulate osteoblast proliferation and differentiation. *Journal of Cellular Physiology* 217, 693-707.

Weinstein, R.S., Roberson, P.K., and Manolagas, S.C. (2009). Giant osteoclast formation and long-term oral bisphosphonate therapy. *New England Journal of Medicine* 360, 53-62.

Willy, J.A., Young, S.K., Stevens, J.L., Masuoka, H.C., and Wek, R.C. (2015). CHOP links endoplasmic reticulum stress to NF-kappaB activation in the pathogenesis of nonalcoholic steatohepatitis. *Molecular biology of the cell* 26, 2190-2204.

Wise, D.R., and Thompson, C.B. (2010). Glutamine addiction: a new therapeutic target in cancer. *Trends in biochemical sciences* 35, 427-433.

Wislet-Gendebien, S., Bruyère, F., Hans, G., Leprince, P., Moonen, G., and Rogister, B. (2004). Nestin-positive mesenchymal stem cells favour the astroglial lineage in neural progenitors and stem cells by releasing active BMP4. *BMC Neuroscience* 5, 33.

Wu, J., Rutkowski, D.T., Dubois, M., Swathirajan, J., Saunders, T., Wang, J., Song, B., Yau, G.D., and Kaufman, R.J. (2007). ATF6alpha optimizes long-term endoplasmic reticulum function to protect cells from chronic stress. *Dev Cell* 13, 351-364.

Wu, X., Estwick, S.A., Chen, S., Yu, M., Ming, W., Nebesio, T.D., Li, Y., Yuan, J., Kapur, R., Ingram, D., *et al.* (2006). Neurofibromin plays a critical role in modulating osteoblast differentiation of mesenchymal stem/progenitor cells. *Human molecular genetics* 15, 2837-2845.

Wu, X., Pang, L., Lei, W., Lu, W., Li, J., Li, Z., Frassica, F.J., Chen, X., Wan, M., and Cao, X. (2010). Inhibition of Sca-1-positive skeletal stem cell recruitment by alendronate blunts the anabolic effects of parathyroid hormone on bone remodeling. *Cell Stem Cell* 7, 571-580.

Xing, W., Kim, J., Wergedal, J., Chen, S.-T., and Mohan, S. (2010). Ephrin B1 regulates bone marrow stromal cell differentiation and bone formation by influencing TAZ transactivation via complex formation with NHERF1. *Molecular and Cellular Biology* 30, 711-721.

Yadav, M.C., Simao, A.M.S., Narisawa, S., Huesa, C., McKee, M.D., Farquharson, C., and Millán, J.L. (2011). Loss of skeletal mineralization by the simultaneous ablation of PHOSPHO1 and alkaline phosphatase function: a unified model of the mechanisms of initiation of skeletal calcification. *Journal of Bone and Mineral Research* 26, 286-297.

Yamaguchi, H., and Wang, H.G. (2004). CHOP is involved in endoplasmic reticulum stress-induced apoptosis by enhancing DR5 expression in human carcinoma cells. *The Journal of biological chemistry* 279, 45495-45502.

Yamaguchi, M., and Sugimoto, E. (2000). Stimulatory effect of genistein and daidzein on protein synthesis in osteoblastic MC3T3-E1 cells: activation of aminoacyl-tRNA synthetase. *Molecular and Cellular Biochemistry* 214, 97-102.

Yamamoto, K., Sato, T., Matsui, T., Sato, M., Okada, T., Yoshida, H., Harada, A., and Mori, K. (2007). Transcriptional induction of mammalian ER quality control proteins is mediated by single or combined action of ATF6alpha and XBP1. *Dev Cell* 13, 365-376.

Yang, Y., Luo, X., Xie, X., Yan, F., Chen, G., Zhao, W., Jiang, Z., Fang, C., and Shen, J. (2016). Influences of teriparatide administration on marrow fat content in postmenopausal osteopenic women using MR spectroscopy. *Climacteric* 19, 285-291.

Yang, Z., Bidwell, J.P., Young, S.R., Gerard-O'Riley, R., Wang, H., and Pavalko, F.M. (2010). Nmp4/CIZ inhibits mechanically induced beta-catenin signaling activity in osteoblasts. *Journal of Cellular Physiology* 223, 435-441.

Yoshida, C.A., Yamamoto, H., Fujita, T., Furuichi, T., Ito, K., Inoue, K.-i., Yamana, K., Zanma, A., Takada, K., and Ito, Y. (2004). Runx2 and Runx3 are essential for chondrocyte maturation, and Runx2 regulates limb growth through induction of Indian hedgehog. *Genes & Development* 18, 952-963.

Yoshihara, H., Arai, F., Hosokawa, K., Hagiwara, T., Takubo, K., Nakamura, Y., Gomei, Y., Iwasaki, H., Matsuoka, S., Miyamoto, K., *et al.* (2007). Thrombopoietin/MPL signaling regulates hematopoietic stem cell quiescence and interaction with the osteoblastic niche. *Cell Stem Cell* 1, 685-697.

Young, S.K., Shao, Y., Bidwell, J.P., and Wek, R.C. (2016). Nuclear Matrix Protein 4 Is a Novel Regulator of Ribosome Biogenesis and Controls the Unfolded Protein Response via Repression of Gadd34 Expression. *Journal of Biological Chemistry* 291, 13780-13788.

Yu, S., Zhu, K., Lai, Y., Zhao, Z., Fan, J., Im, H.J., Chen, D., and Xiao, G. (2013). Atf4 promotes beta-catenin expression and osteoblastic differentiation of bone marrow mesenchymal stem cells. *International journal of biological sciences* 9, 256-266.

Yu Shao, S.H.-B., Paul Childress, Keith R. Stayrook, Marta B Alvarez, Hannah Davis, Lilian Plotkin, Yongzheng He, Keith W. Condon, David B. Burr, Stuart J Warden, Alexander G Robling, Feng-Chun Yang, Ronald C Wek, Matthew R Allen, Joseph P Bidwell (2017). Improving Combination Osteoporosis Therapy in a Preclinical Model of Heightened Osteoanabolism. *Endocrinology In Press*.

Yue, R., Zhou, B.O., Shimada, I.S., Zhao, Z., and Morrison, S.J. (2016). Leptin Receptor Promotes Adipogenesis and Reduces Osteogenesis by Regulating Mesenchymal Stromal Cells in Adult Bone Marrow. *Cell Stem Cell* 18, 782-796.

Zhang, M., Xuan, S., Bouxsein, M.L., von Stechow, D., Akeno, N., Faugere, M.C., Malluche, H., Zhao, G., Rosen, C.J., and Efstratiadis, A. (2002). Osteoblast-specific knockout of the insulin-like growth factor (IGF) receptor gene reveals an essential role of IGF signaling in bone matrix mineralization. *Journal of Biological Chemistry* 277, 44005-44012.

Zhang, R., Oyajobi, B.O., Harris, S.E., Chen, D., Tsao, C., Deng, H.-W., and Zhao, M. (2013). Wnt/ β -catenin signaling activates bone morphogenetic protein 2 expression in osteoblasts. *Bone* 52, 145-156.

Zhang, Z.L., Tong, J., Lu, R.N., Scutt, A.M., Goltzman, D., and Miao, D.S. (2009). Therapeutic potential of non-adherent BM-derived mesenchymal stem cells in tissue regeneration. *Bone marrow transplantation* 43, 69-81.

Zhou, B.O., Yue, R., Murphy, M.M., Peyer, J.G., and Morrison, S.J. (2014). Leptin-receptor-expressing mesenchymal stromal cells represent the main source of bone formed by adult bone marrow. *Cell Stem Cell* 15, 154-168.

CURRICULUM VITAE

Yu Shao

Education:

2012-2017 Ph.D. Indiana University
Department of Medical and Molecular Genetics
IUPUI, Indianapolis, USA, 46202

2005-2009 B.S. Nanyang Technological University
School of Biological Sciences
Singapore, Singapore, 639798

Research Experience:

September 2013-August 2017 PhD candidate

Working in Dr. Joseph Bidwell's lab. Major focus is on determining the role of mesenchymal stem cells in the elevated anabolic window displayed by *Nmp4* knockout mice upon PTH treatment as well as other osteoporosis therapies and the potential molecular mechanisms that drive it.

October 2009-May 2012 Research Technician

Worked in Dr. Lifeng Zhang's lab as a research technician:

Involving Projects:

1. Screening of male ES cell lines with transgenic *Xist* gene expression
2. Fluorescence labeling of *Xist* probe via PCR method
3. Determination of the cellular localization of *Hoxd4* P1 transcript
4. Construction of a gene-targeting vector
5. *Xist* cDNA cloning
6. Supervision of Ms. Xueting Yong's final year project "Testing new antibodies of epigenetic modifications on the inactive X chromosome"

December 2008-April 2009

Final Year Project

Worked in Dr. Zhiwei Feng's lab to carry out my final year project which involved screening and identification of novel genes responsible for NG2⁺ neural precursor cell differentiation into glial/neuronal cells.

August 2008-November 2008

Worked in Dr. Klaus Heese's lab. Learned various basic techniques, such as gel electrophoresis, western blot, mouse injection, brain dissection, cell culture, tissue and cell imaging etc.

Conferences Attended:

Anatomy Fall Forum

Indianapolis IN-Poster Presentation, 2016

Publications:

1. **Yu Shao**, Selene Hernandez-Buquer, Paul Childress, Keith R. Stayrook, Marta B Alvarez, Hannah Davis, Lilian Plotkin, Yongzheng He, Keith W. Condon, David B. Burr, Stuart J Warden, Alexander G Robling, Feng-Chun Yang, Ronald C Wek, Matthew R Allen, Joseph P Bidwell. (In Press) "Improving Combination Osteoporosis Therapy in a Preclinical Model of Heightened Osteoanabolism." *Endocrinology*.
2. Sara K. Young, **Yu Shao**, Joseph P. Bidwell, and Ronald C. Wek. "Nuclear Matrix Protein 4 Is a Novel Regulator of Ribosome Biogenesis and Controls the Unfolded Protein Response Via Repression of Gadd34 Expression." *Journal of biological chemistry* 291, no. 26 (2016): 13780-88.
3. Paul Childress, Keith R. Stayrook, Marta B. Alvarez, Zhiping Wang, **Yu Shao**, Selene Hernandez-Buquer, Justin K. Mack, Zachary R. Grese, Yongzheng He, Daniel Horan, Fredrick M. Pavalko, Stuart J. Warden, Alexander G. Robling, Feng-Chun Yang, Matthew R. Allen, Venkatesh Krishnan, Yunlong Liu, and Joseph P. Bidwell. "Genome-wide mapping and interrogation of the Nmp4 antianabolic bone axis." *Molecular*

Endocrinology 29, no. 9 (2015): 1269-1285.

4. Phua, Sze Lynn Calista, V Sivakamasundari, **Yu Shao**, Xiaohan Cai, Li-Feng Zhang, Thomas Lufkin, and Mark Featherstone. "Nuclear Accumulation of an Uncapped Rna Produced by Drosha Cleavage of a Transcript Encoding Mir-10b and Hoxd4." *PloS one* 6, no. 10 (2011): e25689.